Photoelectron Spectroscopy of Nitroalkane Anions

By

Christopher Lynn Adams

B.S. Adams State College, 2006

A thesis submitted to the

Faculty of the Graduate School of the

University of Colorado in partial fulfillment

of the requirement for the degree of

Doctor of Philosophy

2011

This thesis entitled:

Photoelectron Spectroscopy of Nitroalkane Anions

written by Christopher Lynn Adams

has been approved for the Chemical Physics program by

_____

J. Mathias Weber

_____

Veronica Bierbaum

Date:_____

The final copy of this thesis has been examined by the signatories, and we find that both the content and the form meet acceptable presentation standards of scholarly work in the above mentioned discipline.

Adams, Christopher L. (Ph.D. Chemical Physics)

Photoelectron Spectroscopy of Nitroalkane Anions

Thesis directed by Professor J. Mathias Weber

This thesis describes research on the electronic properties of nitroalkane anions, $CH_3(CH_2)_nNO_2^-$ (where $n = 0, 1, 2, \text{and } 3$), using a newly built velocity-map imaging photoelectron spectrometer. The nitroalkanes are an intriguing class of molecules that possess many similarities owing to the dominating presence of the nitro group. They all possess relatively low adiabatic electron affinities, large dipole moments, and undergo similar distortions (largely localized within the nitro group) upon electron attachment. The focus of the studies presented in this thesis is quantitatively characterizing the anion and neutral states, determining fundamental molecular properties (i.e., adiabatic electron affinities, bond dissociation energies, vertical detachment energies, etc.), and highlighting some of the interesting dynamics that the nitroalkane anions can exhibit using photoelectron spectroscopy.

The first two studies present the photoelectron spectra of nitromethane and nitroethane anions. As these molecules are small enough to be tractable by a more involved theoretical analysis, *ab initio* theory and Franck-Condon simulations were utilized to simulate and interpret the photoelectron spectra. In order for the simulations to achieve good agreement with the experimental spectra, additional efforts were directed at characterizing the torsional potentials of the methyl and ethyl groups and predicting the contribution of torsional motion to the photoelectron spectra. These investigations led to new assignments for the adiabatic electron affinities, the first observation of their dipole-bound states in photoelectron spectra, and

determinations of the $C\text{-}NO_2$ bond dissociation energies for the nitromethane and nitroethane anion.

The third study presents the photoelectron spectra of nitropropane and nitrobutane anions. Each of these molecules possesses a number of stable anion and neutral conformers. *Ab initio* theory and Franck-Condon simulations were employed to identify possible conformations responsible for the dominant features in the photoelectron spectra. Finally, an anomalous feature belonging to a separate photoelectron emission pathway was identified in the photoelectron spectrum using spectra obtained at different photon energies and through an analysis of the angular distributions.

The nitroalkane anions possess adiabatic electron affinities that are smaller than the transition energies of their fundamental CH stretching modes. As a consequence, excitation of one of these modes will lead to vibrational autodetachment that is facilitated by intramolecular vibrational excitation. The last study presents vibrational autodetachment photoelectron spectra of the nitromethane anion. The spectra were analyzed using several simple models to extract some of the important underlying information regarding the intramolecular vibrational relaxation occurring prior to vibrational autodetachment.

Dedication

To my parents. For giving me the confidence to aspire, but more importantly, the humility to learn from my mistakes.

Acknowledgements

Over the last five years, graduate school has demanded a great deal of my time, energy and focus. It wasn't uncommon that I would gauge my commitment to work by the likelihood of attempting to enter my house using my lab key. Fortunately, I have been surrounded by a strong cast of friends, family, and coworkers who have helped me accomplish this work. I must first thank my advisor, Mathias Weber. As the third graduate student to join Mathias' research group, I was given a wonderful opportunity to contribute to the first generation of instruments in the lab, which proved to be an invaluable personal and scientific learning experience. During this time, I got to know Mathias as both a mentor and a friend and I am grateful for all that he has done for me.

I have been fortunate to work with a number of outstanding coworkers over the last several years. When I joined the lab, I got the opportunity to work with Holger Schneider. Holger was the senior graduate student on the instrument I worked on. He was not only a great mentor, who would go above and beyond to help, but he also became a great friend. While Jesse Marcum and I never worked on the same instrument during my time in Mathias' lab, he has become a good friend and a great resource in just about any scientific discussion. I know I can count on an engaging and active dialogue anytime I present him with a problem. I can only hope that he didn't mind being my Litmus test for stupid ideas on more than one occasion. Sydney Kaufman joined the lab two years after me. While we have not had the opportunity to do much science together, she has become a good friend and has been a great addition to the lab. I wish her all the luck in taming the temperamental ESI. Recently, I have had the privilege of passing the torch to Ben Knurr. Over the last year, Ben has almost taken full charge over the instrument I toiled on for so many years. In this time, he has seen it through three self-guided

studies! I'm glad to see I'll be leaving it in capable hands. I wish him the best of luck and I hope, for his sake, that it keeps behaving. I must also thank one of our undergraduates, Eric Pozzi. Eric has been doing research with us over the last two years. I had the privilege to teach him in a general chemistry lab and later the opportunity to work with him on a failed Raman shifter. He has been a good friend and as he continues to graduate school at Northwestern University, I wish him the best of luck.

I also would like to thank the people in the negative ion super group from the labs of Carl Lineberger, Barney Ellison, and Veronica Bierbaum. Having the opportunity to be surrounded by a great number of pioneering researchers in the field on anion chemistry has produced numerous discussions and been a great resource. I must also thank the amazing people staffing the electronic and machine shops of JILA. Their patience and expertise has saved us countless hours.

Lastly, I must thank my friends and family. In my first year of graduate school, I met Marta Maron, Meghan Dunn, and Danny Bell. Over the last several years, we became great friends and have shared a great deal of laughs. I wish them the best of luck in their careers after graduate school and I hope we can stay in touch. My family has helped me and my wife so much in the last several years. I cannot thank them enough for their love and support. Finally, I must thank my wife. Lil, has supported me through undergraduate and now through graduate school, she has been a wonderful mother to our child, and she has remained my best friend. I am truly thankful that I have her in my life.

Contents

1 Introduction 1

1.1 References for Chapter 1 4

2 Anion Photoelectron Spectroscopy 6

2.2 Selection Rules 7

2.3 Threshold Laws 8

2.4 Anisotropy Parameters 10

2.5 Franck-Condon Factors 11

2.6 References for Chapter 1 15

3 Experimental Apparatus 17

3.1 Overview 17

3.2 Ion Source 18

3.2.1 Implementation 20

3.3 Time-of-Flight Mass Spectrometer 22

3.4 Laser System 24

3.6 Velocity Map Imaging Photoelectron Spectrometer 28

3.6.1 Photoelectron Image Acquisition 28

3.6.2 Data Analysis 31

3.7 Using Argon Solvation for Accurate Adiabatic Electron Affinity Determinations 37

3.8 References for Chapter 3 38

4 Photoelectron Spectroscopy of Nitromethane Anion 40

4.1 Introduction 40

4.2 Computational Details 42

4.2.1 *Ab Initio* Calculations 42

4.2.2 Franck-Condon Analysis 43

4.3 Results and Analysis 50

4.3.1 Interpretation of the photoelectron spectrum: the adiabatic electron affinity and the dipole-bound state 50

4.3.2 Photoelectron Angular Distributions 55

4.3.3 Franck-Condon Simulation 58

4.3.4 CN bond energy 68

4.4 Summary and Conclusions 69

4.5 References for Chapter 3 70

5 The Photoelectron Spectroscopy of Nitroethane Anions 75

5.1 Introduction 75

5.2 Computational Details 77

5.2.1 *Ab Initio* Calculations 77

5.2.2 Franck-Condon Analysis 79

5.4 Results and Discussion 87

5.4.1 Experimental Results 87

5.4.2 Threshold Effects and Angular Distributions 93

5.4.3 Franck-Condon Simulations 96

5.5 Summary 101

5.6 References for Chapter 5 102

6 Photoelectron Spectroscopy of 1-Nitropropane and 1-Nitrobutane anions 105

6.1 Introduction 105

6.2 Computational Details 106

6.2.1 *Ab Initio* Calculations 106

6.4 Results and Discussion 108

6.4.1 Experimental Photoelectron Spectra 108

6.4.3 Stable Anionic Conformers 119

6.4.4 Franck-Condon Simulations 122

6.4.5 Angular Distributions 128

6.4.6 Remarks on the Anomalous Feature in Photodetachment from 1-nitropropane and 1-nitrobutane anions 131

6.5 Summary 131

6.6 References for Chapter 6 132

7 Vibrational Autodetachment Photoelectron Spectroscopy of Nitromethane Anion 135

7.1 Overview of Vibrational Autodetachment 135

7.2 Vibrational Autodetachment of Nitromethane Anion: General Considerations 141

7.3 Photoelectron Imaging Results 144

7.4 Modeling 146

7.4.1 “No Torsion” Model 148

7.4.2 Energy Randomization Model 150

7.4.3 Partial Randomization Model 153

7.4.4 Application to VAD PE for the Symmetric and Antisymmetric Methylene Stretching Modes 156

7.4.5 Critical Discussion of the Modeling 158

7.5 Open Questions and Future Challenges 160

7.6 References 162

8 Bibliography 173

List of Tables

Table 4.1 – Frequencies (cm^{-1}) and geometry displacements. 45

Table 4.2 – Lowest Free and Hindered Internal Rotor States 49

Table 5.1 – Dipole Moments and AEA's of Nitromethane and Nitroethane 76

Table 5.2 - Frequencies (cm^{-1}) and geometry displacements. 80

Table 5.3 – Lowest Hindered Internal Rotor States 86

List of Figures

Figure 2.1 – A representation of two scenarios. The scenario on the left involves photodetachment in which there is no displacement but the force constant changes. The scenario on the right depicts a displacement without a change in the force constant. 13

Figure 3.1 – Schematic diagram of the instrument used for a photoelectron spectroscopy study.18

Figure 3.2 – Schematic diagram of the entrainment ion source. The source has the capability to entrain two gases. However, all of the studies within this thesis utilize only one entrainment valve. 21

Figure 3.3 - Overview of the IR OPO/OPA tunable light source. 27

Figure 3.4 – Schematic diagram of velocity map imaging photoelectron spectrometer. 29

Figure 3.5 – Shown on the right is a photoelectron image of S^- taken at 532 nm. The left half illustrates the raw image. The right half illustrates the BASEX reconstructed equatorial slice through the original three-dimensional photoelectron distribution. On the left side of the figure is the photoelectron spectrum generated from the reconstructed image. The transitions are labeled to illustrate corresponding features. 33

Figure 4.1 – Geometries of $CH_3NO_2^-$ and CH_3NO_2; α denotes the angle between the ONO plane and the CN bond axis from DFT calculations; results from the CCSD(T) calculations are in parentheses. 42

Figure 4.2 – PE spectra of $CH_3NO_2^-$ at 322 meV (2600 cm^{-1}, lower trace), 397 meV (3200 cm^{-1}) and from Ref. 1 (inset, abscissa is in units of eV); the circles are data points, the full lines are five point adjacent averages to guide the eye; the arrow denotes the peak corresponding to the vibrational ground state of the neutral molecule AEA=(168 ± 6) meV; D is the signature of the dipole-bound state. 51

Figure 4.3 – PE image of $CH_3NO_2^-$ at 322 meV (2600 cm^{-1}) photon energy, based on one quadrant of the raw PE image. The left half of the figure contains the raw PE image with the intensity in the upper portion doubled to better show the dynamic range of the image without saturating the gray scale. The right half of the figure shows the BASEX transformed image with the "center-line artifact" from the BASEX transformed image removed. The signature belonging to the dipole-bound state has been labeled "D." 52

Figure 4.4 – PE spectra of $CH_3NO_2^-$ (upper trace) and $CH_3NO_2^-\cdot Ar$ (lower trace) at 397 meV (3200 cm^{-1}) photon energy. The dashed lines and arrows show how the vibrational progression of the neutral molecule shifts by 63 meV toward higher binding energies upon solvation by one Ar atom. 54

Figure 4.5 – Anisotropy parameters are presented as a function of electron kinetic energy for different photon energies. Squares, circles, triangles, and stars correspond to data taken at 285 meV (2300 cm^{-1}), 310 meV (2500 cm^{-1}), 322 meV (2600 cm^{-1}), and 397 meV (3200 cm^{-1}), respectively. Filled symbols correspond to the valence electronic state, while the open symbols belong to the dipole-bound state. The data points marked with larger circles belong to the hot bands at binding energies of 77 and 122 meV. Error bars have been conservatively estimated to be ±0.1, except in cases where fits of the angular distributions resulted in larger error bars because of poorer signal-to-noise ratios. The dashed line shows the theoretical maximum value for the anisotropy parameter ($\beta = 2$). 57

Figure 4.6 – Comparison of the torsional Franck-Condon simulation (vertical sticks) at 100 K temperature and the experimental results for $CH_3NO_2^-$·Ar, shifted by the EA of the Ar complex (full line). 59

Figure 4.7 – Comparison of the experimental PE spectrum by Compton et al. (Ref 1) with a fitted Franck-Condon simulation (see text). 61

Figure 4.8 – HOMO of $CH_3NO_2^-$. The HOMO is mainly localized on the nitro group, but small parts also penetrate into the rest of the molecule, notably the σ^* antibonding orbital of the CH group *syn* to the nitro group. 63

Figure 4.9 – Franck-Condon fits to the experimental PE spectrum of $CH_3NO_2^-$ (open circles) at 397 meV (3200 cm^{-1}) with no velocity scaling (dotted line), scaled with $E_K^{1/2}$ (pure *s*-wave, full line), and scaled with $E_K^{3/2}$ (pure *p*-wave, dashed line); see text for details. The sequences marked in the spectrum are based on the NO_2 wagging mode ν_1 with transitions $n \leftarrow 0$ (series I) and $n \leftarrow 1$ (series II). The asterisk marks the $0 \leftarrow 2$ hot band of the NO_2 wagging mode. Note that the top scale shows the electron kinetic energy while the bottom scale gives the electron binding energy. 67

Figure 4.10 – Thermochemical cycle for the determination of the BDE_{CN} in nitromethane anion. 69

Figure 5.1 - Geometries of $CH_3CH_2NO_2^-$ and $CH_3CH_2NO_2$; θ denotes the angle between the ONO plane and the CN bond axis, which is the most salient geometry change upon electron loss. 78

Figure 5.3 - Calculated potential energy curves (circles) generated by rotation about the CN bond in the nitroethane anion (lower curve) and neutral (upper curve). The black line illustrates the fit to each calculated potential (see text). The filled blue circles represent points calculated using a relaxed-geometry scan while the filled red circles are points generated by a fixed-geometry scan (see text). The different nitroethane anion conformers are illustrated above their respective positions along the potential energy curve. The anion has two isoenergetic conformers separated by a 660 cm^{-1} barrier and flanked by a higher energy conformer with a large barrier to

isomerization. The neutral has a relatively flat potential nearly coinciding with that of a free internal rotor..... 83

Figure 5.4 - PE spectra of $CH_3CH_2NO_2^-$ at 389 meV (upper trace), 347 meV (center trace), and 322 meV (lower trace) photon energy. The dashed line denotes the (0←0) transition corresponding to an AEA of (191 ± 6) meV..... 88

Figure 5.5 – PE image obtained at a photon energy of 389 meV (3140 cm^{-1}). The left half of the image is the raw PE image. The right half is the BASEX reconstructed image..... 89

Figure 5.6 - PE spectra of $CH_3CH_2NO_2^-$ (upper curve) and $CH_3CH_2NO_2^-$·Ar (lower curve) taken at 389 meV photon energy. The arrows and drop lines illustrate the shift of the spectrum upon Ar solvation by (61 ±7) meV..... 91

Figure 5.7 - PE spectrum of $CH_3CH_2NO_2^-$ taken at a photon energy of 322 meV. The spectrum is plotted as a function of electron speed to best illustrate the dipole-bound state; the inset shows the PE spectrum as a function of binding energy. In each spectrum the dipole-bound state is labeled "D"..... 92

Figure 5.8 - Thermochemical cycle for the determination of the C-NO_2 bond dissociation energy, $BDE_{C\text{-}NO_2}$, in nitroethane anion..... 93

Figure 5.9 - Anisotropy parameters as a function of electron kinetic energy obtained at different photon energies where solid circles, hollow circles, and triangles represent parameters from images taken at photon energies of 389 meV, 347 meV, and 322 meV, respectively. The error bars are conservatively estimated to be ± 0.1..... 95

Figure 5.10 - Experimental PE spectrum taken at a photon energy of 389 meV (open circles) along with Franck-Condon simulations performed with the inclusion of the hindered-to-free internal rotor transitions (solid line) and in their absence (dotted line). The inset is centered about the (0←0) transition and includes a stick spectrum of the individual calculated transitions to emphasize the contribution of the hindered-to-free CN rotor transitions to the peak profile... 97

Figure 5.11 - Experimental PE spectra taken at a photon energy of 389 meV (open circles) along with the Franck-Condon simulations performed without threshold scaling (dash-dotted line), scaled by $E^{3/2}$ (dotted line) and scaled by $E^{1/2}$ (solid line). The sequences marked in the spectrum are based on the nitro wagging mode ν_{22} with transitions n←0 (series A) and n←1 (series B). 100

Figure 6.1 – Photoelectron spectrum of 1-NP anion obtained at a photon energy of 2.331 eV. 109

Figure 6.2 – Photoelectron image of 1-NP taken at a photon energy of 329 meV (2650 cm^{-1}). The labels "A" and "B" denote two features that are consistently observed at the same binding energy. The label "F" denotes a prominent feature found at a fixed kinetic energy in the spectra

taken at photon energies of 329 meV (2650 cm^{-1}) and 368 meV (2968 cm^{-1}). See text for more details. 110

Figure 6.3 - Photoelectron spectra of 1-NP anion taken at photon energies of 393 meV (3170 cm^{-1}), 368 meV (2968 cm^{-1}), 329 meV (2650 cm^{-1}), and 273 meV (2200 cm^{-1}), from top to bottom. The spectra on the left are presented as a function of binding energy while the spectra on the right are graphed as a function of kinetic energy. The labels "A" and "B" denote two features that are consistently observed at the same binding energy. The label "F" denotes a prominent feature found at a "fixed" kinetic energy in the spectra taken at photon energies of 329 meV (2650 cm^{-1}) and 368 meV (2968 cm^{-1}). The dotted line in the spectra on the right indicates a kinetic energy of 165 meV (see text for further details). 111

Figure 6.4 – Photoelectron spectra of bare 1-NP anion (upper curve) as well as argon-solvated 1-NP anion (lower curve) taken at a photon energy of 393 meV. The arrows represent the shift of the spectrum by an energy of (56 ± 7) meV upon argon solvation. The labels "A" and "B" denote two features that are consistently observed at the same binding energy in the bare 1-NP anion spectra. 113

Figure 6.5 – Photoelectron spectra of 1-NB anion, obtained at a photon energy of 2.331 eV... 114

Figure 6.6 - Photoelectron spectra of 1-NB anion at photon energies of 444 meV (3580cm^{-1}), 424 meV (3420 cm^{-1}), 404 meV (3260 cm^{-1}), 384 meV (3100 cm^{-1}), 329 meV (2650 cm^{-1}), from top to bottom. The spectra on the left are presented as a function of binding energy while the spectra on the right are graphed as a function of kinetic energy. The labels "A" and "B" denote two features that are consistently observed at the same binding energy. The label "F" denotes a prominent feature found at a "fixed" kinetic energy in the spectra. The dotted line in the spectra on the right indicates a kinetic energy of 165 meV (see text for further details). 116

Figure 6.7 - – Photoelectron image of 1-NB taken at a photon energy of 384 meV (3100 cm^{-1}). The labels "A" and "B" denote two features that are consistently observed at the same binding energy. The label "F" denotes a prominent feature found at a fixed kinetic energy in the spectra. See text for more details. 117

Figure 6.8 – The photoelectron spectrum of bare 1-NB anion (top curve) and argon-solvated 1-NB anion (bottom curve), taken at a photon energy of 384 meV. The arrow is used to illustrate the shift of the 0←0 feature. A "F" is placed above the anomalous feature and an "A" is placed above the feature corresponding to the 0←0 transition. 118

Figure 6.9 - Illustration of the various conformers of the 1-NP anion generated from rotations about the CN or central CC bond, their relative energies, and their population relative to the lowest energy conformer, according to a Boltzmann distribution. H1 and H2 are consistently defined but arbitrary designations to distinguish the hydrogens. The key at the top denotes the atoms H1 and H2. The conformers outlined in red are excluded in the Franck-Condon simulations, see discussion for more details. 119

Figure 6.10 - Diagram of the stable conformers along with their relative energies, excluding the conformations in which the CC bond is *syn* to the NO_2 group. Their population relative to the lowest energy conformer, according to a Boltzmann distribution, is denoted in the parentheses. H1 and H2 are consistently defined but arbitrary designations to distinguish the hydrogens. The key at the top denotes the atoms H1 and H2. The conformers outlined in red are excluded in the Franck-Condon simulations, see discussion for more details. 122

Figure 6.11 – The Franck-Condon simulations of the two lowest energy conformers of 1-NP anion, using an anion temperature of 250 K. An inset in each graph illustrates the 1-NP anion conformer along with its relative energy. The open circles, solid lines, and bars represent the observed, simulated curve, and the individual transitions. 125

Figure 6.12 - The Franck-Condon simulations of the three lowest energy conformers of 1-NB anion, using an anion temperature of 250 K. An inset in each graph illustrates the 1-NP anion conformer along with its relative energy. The open circles, solid lines, and bars represent the observed, simulated curve, and the individual transitions. 127

Figure 6.13 – Plot of the fitted anisotropy parameters, β, as a function of kinetic energy for the four different lower-energy photon wavelengths used in the study of 1-NP anion (gray lines) as well as their average (dark black line). The dashed line is located at a kinetic energy of 166 meV. 129

Figure 6.14 - Plot of the fitted anisotropy parameters, β, as a function of kinetic energy for the five different lower-energy photon wavelengths used in the study of 1-NB anion (gray lines) as well as their average (dark black line). The dashed line is located at a kinetic energy of 166 meV. 130

Figure 7.1 – Schematic drawing of the diabatic anionic and neutral potential energy surfaces of nitromethane. The anionic surface is connected to that of the neutral along the detachment coordinate *Q*. In contrast, the CH stretching modes are not connecting the two surfaces and excitation of one quantum of a CH stretching vibration will not lead to immediate detachment. VAD will only occur after sufficient energy has been redistributed into *Q*. 142

Figure 7.2 – Highest occupied molecular orbital (HOMO) of the nitromethane valence anion. 143

Figure 7.3 – Comparison of BASEX transformed photoelectron images of $CH_3NO_2^-$. The image on the left panel is taken off-resonance at an energy of 3200 cm^{-1}. The image on the right panel is taken on the vibrational resonance of the totally symmetric $\nu_s(CH_3)$ at 2777 cm^{-1}. 144

Figure 7.4 – Comparison of the experimental VAD spectrum (connected open circles) of $CH_3NO_2^-$ on the $\nu_s(CH_3)$ resonance (symmetric methyl stretch) with the "no torsion" model (full line, see text). The contribution of each vibrational state was weighted to yield the best fit of the model to the experimental data. 150

Figure 7.5 – Comparison of the experimental VAD spectrum (solid black line) of $CH_3NO_2^-$ on the $\nu_s(CH_3)$ resonance (symmetric methyl stretch) with the energy randomization model (solid red line, see text). The model has been normalized to the experimental data at the 0-eV feature. 151

Figure 7.6 – Comparison of the experimental VAD spectrum (connected open circles) of $CH_3NO_2^-$ on the $\nu_s(CH_3)$ resonance (symmetric methyl stretch) with the density of states (full line) in neutral CH_3NO_2. The DOS has been normalized to the experimental data at the 0-eV feature. 153

Figure 7.7 – Comparison of the experimental VAD spectrum (solid black line) of $CH_3NO_2^-$ on the $\nu_s(CH_3)$ resonance (symmetric methyl stretch) with the partial randomization model (solid red line). The model has been normalized to the experimental data at the 0-eV feature..... 155

Figure 7.8 – Comparison of the experimental VAD photoelectron spectra (connected open circles) belonging to the $\nu'_s(CH_3)$ (symmetric methylene stretch, left panel) and $\nu_a(CH_3)$ (antisymmetric methylene stretch, right panel) modes of $CH_3NO_2^-$ with the partial randomization model (full lines). The dashed line in both spectra is a representation of the full energy randomization model. The models have been normalized to the experimental data at the 0-eV feature for each spectrum. 157

1 Introduction

It has been almost forty years since the first laser photodetachment study of a molecular anion was performed.[1] Since that time, the field of gas-phase anion research has expanded immensely. The relative ease with which anions can be controlled in electric fields, the increasing sophistication of laser technology, and the advances in producing gas-phase anions have made the molecular anion an ideal molecular laboratory that has been used with great success to elevate our understanding of chemical phenomena.

In the field of gas-phase anion chemistry, it would be difficult to overstate the importance of photoelectron spectroscopy. Its relatively simple premise has lent itself to constant adaptation and improvement which have allowed this technique to stay relevant as one of the best means of investigating anions. Photoelectron spectroscopy provides a sensitive probe of the geometries and the electronic structure of the anions and their neutral counterparts and can yield fundamental properties such as the molecular adiabatic electron affinity, which in turn can be used to find bond energies (provided the other relevant thermochemical data are known).[2] Beyond this, many other interesting facts can be learned about unstable neutral molecules or clusters if they are stabilized as anions. In this vein, photoelectron spectroscopy has served as a powerful technique to study radicals,[3-5] which often form stable anions, or to study transition states on the neutral potential energy surface which are accessible from an anion or anionic cluster.[6-8]

In the work presented here, we employ a newly built velocity-map imaging photoelectron spectrometer to investigate nitroalkane anions, $CH_3(CH_2)_nNO_2^-$ where $n = 0, 1, 2,$ and 3. The nitroalkanes are all colorless oily liquids under standard conditions which are primarily used as

fuel additives (all of the species are known explosives), solvents, or as pharmaceutical precursors. The similarities in their structures and properties stems from the dominating presence of the NO_2 group. In the neutral species, the nitro group gives rise to a large dipole moment, which has been shown using Rydberg electron transfer studies[9, 10] to support a dipole bound state for the lower nitroalkanes, nitromethane and nitroethane. Additionally, the nitroalkanes have generated interest since the barrier to rotation for the methyl and ethyl group of the lower order nitroalkanes is negligible, leading to sufficient motion in this mode at moderate temperatures.[11, 12] This has led to several studies that have focused on the manner in which the orientation of the nitro group, relative to the alkyl group, affects the vibrations of the molecule and subsequently influences vibrational energy redistribution[11] in these known explosives. In regards to the anions, all of the species adopt a similar geometry about the nitrogen as the excess electron is largely localized on the lowest unoccupied molecular orbital centered on the p-orbital of the nitrogen atom which drives the planar geometry into a trigonal pyramidal configuration. In turn, the localization of the electron makes the adiabatic electron affinity relatively invariant to the size of the alkyl chain. Vibrational spectroscopy studies performed by Schneider *et al.*[13] have indicated that the electron affinity is less than 2500 cm^{-1} for the different alkyl chain lengths. This property leads to an uncommon situation in which the fundamental CH stretching modes have energies in excess of the adiabatic electron affinity. Excitation within the mid-infrared region can lead to two distinctly different processes governing the photodetachment. If a photon interacts with the anion at a non-resonant frequency the electron can be photodetached immediately as an electronic excitation of the detaching electron. But if the anion interacts with a photon at a vibrationally resonant frequency, this can lead to a vibrational transition which will be followed by electron emission facilitated by intramolecular vibrational relaxation. Each of

these processes will leave distinct “footprints” on the photoelectron spectrum. The former will yield a conventional photoelectron spectrum while the latter will leave a signature of the intramolecular vibrational relaxation occurring prior to photoemission.

This thesis discusses photoelectron spectra of the nitroalkane anions obtained at photon energies away from the influence of any vibrational frequencies (conventional photoelectron spectroscopy) and at vibrationally resonant frequencies. Chapter 2 will provide an overview of the theory governing photodetachment and the information that can be acquired from photoelectron spectroscopy as these ideas form the foundation of any analysis. Chapter 3 will describe the instrument used to create the anions, isolate the anions of interest and acquire the photoelectron spectra. Chapters 4, 5, and 6 will discuss conventional photoelectron spectra obtained for the nitroalkane anions. Chapter 4 gives an account of the studies and simulations performed on the nitromethane anion that have led to the determination of the electron affinity, the observance of a dipole bound state and identification of much of the vibrational structure within the spectrum. Chapter 5 focuses on the photoelectron spectra and simulations of nitroethane anion that also yielded the adiabatic electron affinity and the observance of the dipole bound state. Chapter 6 concentrates on the spectra of nitropropane and nitrobutane anions as well as the simulations performed to identify the conformers yielding the experimentally determined electron affinity. Chapter 7 will focus on the photoelectron spectra obtained at vibrationally resonant photon energies of the nitromethane anion and present some simple models to describe the results.

1.1 References for Chapter 1

1. M. W. Siegel, R. J. Celotta, J. L. Hall, J. Levine and R. A. Bennett,"Molecular Photodetachment Spectrometry. I. The Electron Affinity of Nitric Oxide and the Molecular Constants of NO." *Physical Review A* **6** (2), 607 (1972).

2. S. J. Blanksby and G. B. Ellison,"Bond dissociation energies of organic molecules." *Accounts of Chemical Research* **36** (4), 255-263 (2003).

3. K. M. Ervin, T. M. Ramond, G. E. Davico, R. L. Schwartz, S. M. Casey and W. C. Lineberger,"Naphthyl radical: Negative ion photoelectron spectroscopy, Franck-Condon simulation, and thermochemistry." *Journal of Physical Chemistry A* **105** (48), 10822-10831 (2001).

4. T. Ichino, S. W. Wren, K. M. Vogelhuber, A. J. Gianola, W. C. Lineberger and J. F. Stanton,"The vibronic level structure of the cyclopentadienyl radical." *Journal of Chemical Physics* **129** (8) (2008).

5. P. G. Wenthold and W. C. Lineberger,"Negative ion photoelectron spectroscopy studies of organic reactive intermediates." *Accounts of Chemical Research* **32** (7), 597-604 (1999).

6. P. G. Wenthold, D. A. Hrovat, W. T. Borden and W. C. Lineberger,"Transition-state spectroscopy of cyclooctatetraene." *Science* **272** (5267), 1456-1459 (1996).

7. S. N. Eustis, D. Radisic, K. H. Bowen, R. A. Bachorz, M. Haranczyk, G. K. Schenter and M. Gutowski,"Electron-driven acid-base chemistry: Proton transfer from hydrogen chloride to ammonia." *Science* **319** (5865), 936-939 (2008).

8. E. Garand, J. Zhou, D. E. Manolopoulos, M. H. Alexander and D. M. Neumark,"Nonadiabatic interactions in the $Cl+H_2$reaction probed by ClH_2^- and ClD_2^- photoelectron imaging." *Science* **319** (5859), 72-75 (2008).

9. R. N. Compton, H. S. Carman, C. Desfrancois, H. Abdoul-Carmine, J. P. Schermann, J. H. Hendricks, S. A. Lyapustina and K. H. Bowen,"On the binding of electrons to nitromethane: Dipole and valence bound anions." *Journal of Chemical Physics* **105** (9), 3472-3478 (1996).

10. S. T. Stokes, K. H. Bowen, T. Sommerfeld, S. Ard, N. Mirsaleh-Kohan, J. D. Steill and R. N. Compton,"Negative ions of nitroethane and its clusters." *Journal of Chemical Physics* **129** (6) (2008).

11. D. Gorse, D. Cavagnat, M. Pesquer and C. Lapouge,"Theoretical and Spectroscopic Study of Asymmetric Methyl Rotor Dynamics in Gaseous Partially Deuterated Nitromethanes." *Journal of Physical Chemistry* **97** (17), 4262-4269 (1993).

12. P. Groner, R. Meyer, A. Günter, H. Kühne and H. H. Günthard,"Far Infrared Spectrum of Nitroethane." *Chemical Physics* **5** (1), 136-141 (1974).

13. H. Schneider, K. M. Vogelhuber, F. Schinle, J. F. Stanton and J. M. Weber,"Vibrational spectroscopy of nitroalkane chains using electron autodetachment and Ar predissociation." *Journal of Physical Chemistry A* **112** (33), 7498-7506 (2008).

2 Anion Photoelectron Spectroscopy

If an anion interacts with a photon with energy in excess of the binding energy of the electron, photoelectron emission can occur. The conservation of energy requires that the emitted photoelectron has an energy that can be written as

Equation 2.1

$$E_{KE} = \hbar\omega - E_{BE}$$

where E_{KE} represents the photoelectron's kinetic energy, E_{BE} represents the binding energy of the electron or □ more accurately □ the energy difference between the initial and final molecular states, and $\hbar\omega$ is the energy of the photodetaching radiation. As the neutral molecule remaining after photoemission is much heavier than the emitted electron, it is a good approximation to neglect the kinetic energy imparted to the neutral.[1] As a consequence, the photoelectrons can be analyzed as a function of kinetic energy, at a fixed photon energy, and a photoelectron spectrum may be constructed as a function of the electron binding energy. The photoelectron spectrum encodes a wealth of information pertaining to the neutral or parent states, such as geometrical changes that the molecular frame undergoes upon photoemission, the energies of the electronics states of the neutral, the vibrational spacing within each electronic band, and the adiabatic electron affinity of the neutral.[2, 3] In addition to the kinetic energy of the emitted electron, the angular distribution for photoemission can be obtained as a function of the kinetic energy. The photoelectron angular distribution is primarily used to extract information about the nature of the detaching orbital of the anion. The following sections will highlight the principles that govern the shape of a photoelectron spectrum and as a consequence, form the foundation for its analysis.

2.2 Selection Rules

The selection rules for photodetachment govern what electronic states of the neutral can be accessed, the acceptable orbital angular momenta of the outgoing photoelectron, and the manner in which the overlap of the vibrational wavefunctions modulate the intensity within a particular electronic transition. As the final state in photodetachment involves an unbound electron, the selection rules are slightly different from other electronic spectroscopic methods. The following rules are for single photon photodetachment involving one electron within the electric dipole approximation.

The spin selection rules require that the total spin of the system is conserved. As the electron will carry away its spin angular momentum the spin of the resulting neutral must differ from that of the parent anion by $\Delta S = \pm 1/2$ upon electron loss. This offers the perfect complementary tool to optical electronic spectroscopy, in which the spin selection rule strictly forbids a change in multiplicity. This is one example of many, in which photoelectron spectroscopy provides a valuable means of investigating the properties of a neutral molecule that are difficult to attain otherwise.

The orbital selection rules specify the allowed outgoing waves for the photodetached electron. As in electronic spectroscopy, the photon will impart one unit of angular momentum to the electron resulting in a selection rule of $\Delta \ell = \pm 1$ relative to the initial orbital for the outgoing wave.[4, 5] In atomic systems this leads to a situation in which detachment from a p orbital results in outgoing s- and d-waves. For molecular systems, in which the electronic orbital angular momentum is no longer a good quantum number, the outgoing electron wavefunction is assumed to transform like a member of the irreducible representation of the symmetry group of the anion and the allowed symmetries of the outgoing electron may be determined by the direct product of

the irreducible representations of ψ_f, $\hat{\mu}$, and ψ_i, which represent the outgoing electron's wavefunction, the dipole moment operator, and the wavefunction of the parent orbital in the anion, respectively.[5] The allowed symmetries of the outgoing electron will yield a direct product which contains the totally symmetric representation. The orbital selection rules will be revisited later, as the weighting of the outgoing waves is strongly modified by threshold laws.

An analysis of the transition moment integral, which leads to the selection rules presented above, does not yield vibrational selection rules.[6] Rather, it leads to the term, $\langle\psi_{v'}|\psi_{v''}\rangle$, where $\psi_{v'}$ represents the vibrational wavefunction of the neutral and $\psi_{v''}$ represents the vibrational wavefunction of the anion. This term serves to strongly modify the intensity profile of an allowed electronic transition as a function of the overlap of the vibrational wavefunction of the anion and the neutral molecule. The absolute square of this term, $|\langle\psi_{v'}|\psi_{v''}\rangle|^2$, is called the Franck-Condon factor. Since it plays an important role in understanding any photoelectron spectrum, a more complete discussion of its ramifications will be given below.

2.3 Threshold Laws

The intensity profile of photoelectron spectra acquired at photon energies just above electron detachment threshold are strongly modified by threshold laws. Wigner[7] first illustrated the generality of the threshold rules, in which the longest-range interaction of two reacting particles dictates the energy dependence of the cross-section. In photodetachment from singly charged anions, the reacting particles are the neutral core and the detached electron, and the longest range interaction is either the anisotropic $1/r^2$ potential of a molecular dipole or the $\ell(\ell+1)/r^2$ centrifugal potential.[8]

Considering the simplest case of an atomic anion first, in which the longest range interaction is the centrifugal potential, Wigner's laws[7] show that the near-threshold cross section for photodetachment is given by

Equation 2.2

$$\sigma(E_{KE}) \propto E_{KE}^{\ell+1/2}$$

where E_{KE} is the kinetic energy of the photoelectron and ℓ is the angular momentum of the outgoing electron. Wigner's threshold law is exact at the limit of threshold but for larger kinetic energies a power series expansion in E_{KE} is necessary to account for the shorter-range interactions. The dependence of the cross section on the angular momentum of the outgoing electron is a consequence of the centrifugal barrier. An electron near threshold will have to tunnel through this barrier which is larger for electrons with larger angular momentum. This, in turn, favors the production of electrons with the lowest angular momentum near threshold.[8] As was discussed earlier, photodetachment from a p orbital results in an outgoing s- or d-wave. However, if the photodetachment is performed near threshold the d-wave will be strongly suppressed resulting in an almost pure s-wave detachment with a cross-section at threshold proportional to $E_{KE}^{1/2}$.

An extension of Wigner's threshold law for molecules (without a dipole moment) was derived by Reed et al.,[5] who outlined a procedure to determine the leading term for the cross section. The procedure begins with determining the allowed symmetries of the outgoing electrons, as outlined above for the orbital selection rules. Since the spherical waves of a given angular momentum can be assigned to irreducible representations, the symmetry corresponding to the spherical wave with the lowest angular momentum is expected to give the leading term in

the cross section. This is a very powerful approach in molecules with higher symmetry; unfortunately, there is no simple way to accurately predict the cross section at threshold for systems of low symmetry, as there are very few symmetry restrictions on the nature of the outgoing wave.

Further complications exist when a dipole is present. In this case, the long-range interaction will be the sum of the centrifugal and dipolar potential and as a result, the leading term of the near-threshold expansion of the cross section will be modified. The manner in which the dipole modifies the leading term is difficult to predict, as the orientation relative to the emitted electron becomes important. In addition, near threshold the electron will depart on time scales comparable to the rotational period of the molecule, which will make the cross section sensitive to the rotational motion perpendicular to the dipole moment.[8] Analyses of the near-threshold cross section of the nitroalkane anions discussed in this thesis are difficult, since they all have significant dipoles and are of low symmetry.

2.4 Anisotropy Parameters

The anisotropy characteristics of the photodetachment offer insight into the symmetry of the parent orbital in the anion. The photoelectron angular distributions for a one-photon process with linearly polarized light are described by the function,[9]

Equation 2.3

$$I(E,\theta) = \frac{\sigma(E)}{4\pi}[1 + \beta(E)P_2(\cos\theta)]$$

where θ is the angle between the laser polarization and the emission angle, σ is the total detachment cross section, β is the anisotropy parameter and varies within the limits of -1 to 2, and $P_2(\cos\theta) = 1/2(3\cos^2\theta - 1)$ is the second-order Legendre polynomial. The anisotropy parameter completely defines the angular distribution and is a function of the angular momentum of the contributing partial waves and the interference that occurs between them. Given the low symmetry of the nitroalkane anions it is difficult to extract detailed information regarding the parent orbital or identify the interfering partial waves yielding a particular β. But despite these limitations, the anisotropy parameter can still provide useful information. At very low kinetic energies, the threshold analysis of Reed *et al.*[5] indicates that one partial wave will dominate over the contributions of others. Consequently, the beta parameter at low kinetic energies can be used to get a sense of the identity of the leading term governing the threshold law. Finally, large or abrupt changes in the beta parameter can be used to identify photoelectrons originating from different electronic states since the variation of the anisotropy parameter should be smooth for a given parent state.

2.5 Franck-Condon Factors

The Franck-Condon factors are given by,

Equation 2.4

$$FCF = |\langle \psi_{v'} | \psi_{v''} \rangle|^2$$

where $\psi_{v'}$ represents the vibrational wavefunction of the neutral and $\psi_{v''}$ represents the vibrational wavefunction of the anion. The validity of the Franck-Condon factors is based on

several approximations. The first approximation is that the electronic transition probability is not a function of the nuclear coordinates. This is typically a good approximation since the transition probability is a slowly varying function of the nuclear coordinates. Second, within the Born-Oppenheimer approximation it is expected that the electronic transition happens on a much faster time scale than the nuclear motion. As the nuclei are effectively frozen, the most probable vibronic transition will occur between the two states in which the overlap of the vibrational wavefunctions is greatest.

The effect of the Franck-Condon principle is most easily seen in the example of photoemission from a diatomic anion approximated as a harmonic oscillator, as it has only one vibrational mode. In an effort to highlight the impact of certain parameters on the photoelectron spectrum, several scenarios are discussed. In the first example, the shape of the neutral potential (i.e., force constant) is varied relative to the anion potential. The second example discusses the effect of changing the equilibrium displacement of the neutral relative to the anion, and lastly, the significance of including vibrationally excited anion states (hot bands) is considered. Figure 2.1 illustrates the effects of the first two scenarios. If the equilibrium distance of both potential energy curves is the same, the overlap of the initial and final vibrational wavefunctions will be greatest for the transition to the ground state of the neutral since the vibrational wavefunctions are very similar. In this scenario (i.e., no displacement), transitions to the other vibrational states ($\nu_n' \leftarrow \nu_0''$) only occur if the force constant (i.e., shape) of the neutral curve is different from that of the anion. If this is the case, the $2n \leftarrow 0$ transitions may become active in the spectrum, given the overlap of the even wavefunctions. The $n \leftarrow 0$ transitions can only become possible if the potential curve is anharmonic.

Displacement of the neutral potential energy curve leads to substantial activity in transitions to higher-lying vibrations as the anion vibrational ground state wavefunction begins to achieve the greatest overlap in the classical turning points of the excited vibrational states. Additionally, it is important to note the diminished intensity of the $0 \leftarrow 0$ transition, corresponding to the adiabatic electron affinity. If there is a substantial difference in the equilibrium distance of the anion and neutral molecules, this will lead to substantial difficulties in identifying the adiabatic electron affinity. If the temperature of the system is sufficiently high, excited vibrational states of the anion will be populated. The excited states will create additional progressions or hot bands that are interspersed in the progression created from the ground state. This gives rise to great difficulty in locating the $0 \leftarrow 0$ transition, as it is necessary to identify the contributions from the hot band and the ground state before an accurate assignment can be made.

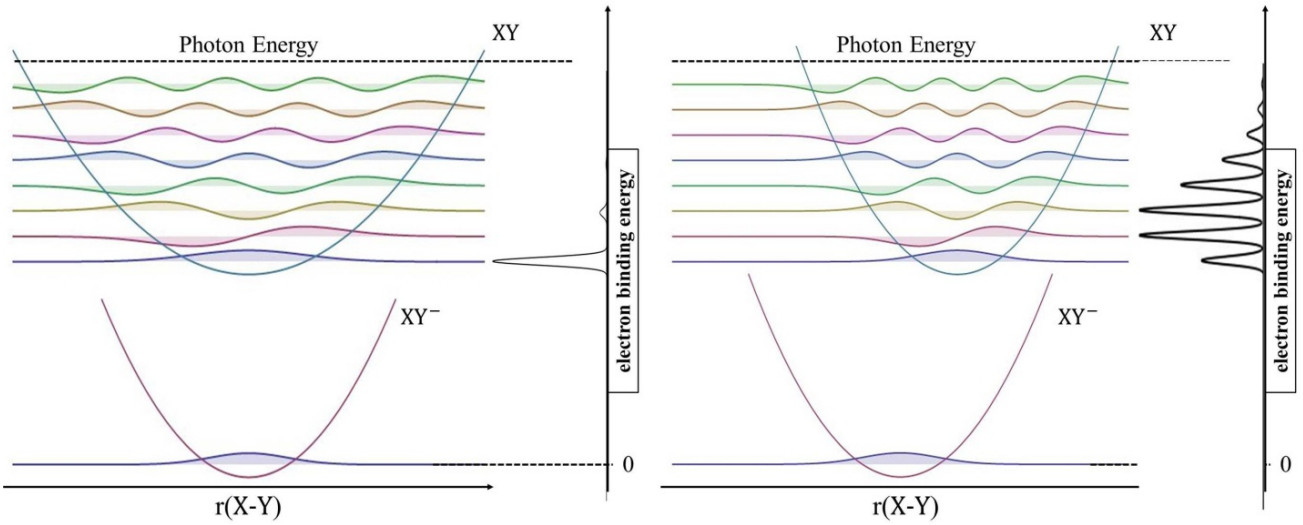

Figure 2.1 – A representation of two scenarios. The scenario on the left involves photodetachment in which there is no displacement but the force constant changes. The scenario on the right depicts a displacement without a change in the force constant.

In a polyatomic system, the difficulty in interpreting the spectrum is compounded by the large number of vibrational modes. For a molecule with N atoms, which is not linear, there will

be $3N-6$ vibrational modes. If the vibrational modes are well represented as uncoupled, harmonic oscillators the vibrational wavefunction can be written as,

Equation 2.5

$$\psi_v = \psi_{v_1}(Q_1) \cdot \psi_{v_2}(Q_2) \cdots \psi_{v_{3N-6}}(Q_{3N-6}),$$

where Q_n represents the normal coordinate of the n^{th} normal mode.[10] If the vibrational normal modes are preserved in the photoelectron emission, the Franck-Condon factors can be expressed as a product of the overlap of each normal mode since the vibrational wave functions will still be orthogonal. However, the geometry changes that occur during photoelectron emission are typically accompanied by a change in the normal coordinates. This phenomenon was first noted by Duschinsky;[11] he suggested the transformation could be described according to the following equation,

Equation 2.6

$$Q'' = \mathrm{J}''Q' + K''$$

where K'' is the normal coordinate displacement vector in the basis of the normal coordinates of the anion and J'' is the Duschinsky rotation matrix which describes the mixing of the normal coordinates.[10] Additionally, Duschinsky outlined some general conclusions that are a consequence of symmetry considerations.[11] First, a common symmetry group is found to describe both the anion and the neutral. If a normal coordinate is antisymmetric with respect to some symmetry element, then the displacement of that mode is zero. This leads to little activity in the nontotally symmetric modes since, with no displacement, the active transitions must be even transitions of $2n \leftarrow 0$ or facilitated by anharmonicity. The second result is that only normal modes that behave identically under all symmetry operations will mix. As a consequence,

normal modes belonging to the totally symmetric group will mix, as will the nontotally symmetric normal modes belonging to the same symmetry groups.

2.6 References for Chapter 1

1. J. H. D. Eland,"Molecular Photoelectron Spectroscopy." *Journal of Physics E-Scientific Instruments* **11** (10), 969-977 (1978).

2. K. M. Ervin and W. C. Lineberger, in *Advances in Gas Phase Ion Chemistry*, edited by N. G. Adams and L. M. Babcock (JAI, Greenwich, CT, 1992), pp. 121.

3. P. Chen, in *Unimolecular and Bimolecular Reaction Dynamics*, edited by C.-Y. Ng, T. Baer and I. Powis (John Wiley & Sons, Chichester, 1994), pp. 371.

4. R. Mabbs, E. R. Grumbling, K. Pichugin and A. Sanov,"Photoelectron imaging: an experimental window into electronic structure." *Chemical Society Reviews* **38** (8), 2169-2177 (2009).

5. K. J. Reed, A. H. Zimmerman, H. C. Andersen and J. I. Brauman,"Cross-Sections for Photodetachment of Electrons from Negative-Ions near Threshold." *Journal of Chemical Physics* **64** (4), 1368-1375 (1976).

6. D. C. Harris, & Bertolucci, M.D., *Symmetry and Spectroscopy: An Introduction to Vibrational and Electronic Spectroscopy*. (New York: Oxford University Press, 1978).

7. E. P. Wigner,"On the Behavior of Cross Sections near Thresholds." *Phys. Rev.* **73** (9), 1002-1009 (1948).

8. J. R. Smith, J. B. Kim and W. C. Lineberger,"High-resolution threshold photodetachment spectroscopy of OH." *Phys. Rev. A* **55** (3), 2036-2043 (1997).

9. J. Cooper and R. N. Zare,"Angular Distribution of Photoelectrons." *Journal of Chemical Physics* **48** (2), 942-943 (1968).

10. K. M. Ervin, J. Ho and W. C. Lineberger,"Ultraviolet Photoelectron Spectrum of NO_2." *J. Phys. Chem.* **92** (19), 5405-5412 (1988).

11. F. Duschinsky,"The importance of the electron spectrum in multi atomic molecules. concerning the Franck-Condon principle." *Acta Physicochimica URSS* **7** (4), 551-566 (1937).

3 Experimental Apparatus

3.1 Overview

The experimental apparatus may be divided into four parts: ion source, time-of-flight mass spectrometer, light source, and photoelectron spectrometer. Ions are created in a pulsed supersonic entrainment ion source and directed into the acceleration region of a time-of-flight mass spectrometer. The ions are mass-selected within the time-of-flight mass spectrometer and injected into the interaction region of a velocity-map-imaging photoelectron spectrometer. The mass-selected ion beam is intersected with either the tunable output of an infrared optical parameter converter or 532 nm radiation generated from the second-harmonic of a Nd:YAG laser. The nascent photoelectrons are then accelerated into the flight tube of the photoelectron spectrometer and mapped onto a position sensitive imaging detector. Each image is digitized by a CCD camera and collected until a sufficient signal-to-noise ratio is achieved for a photoelectron image. Each part of the instrument will be described in more detail in the following sections, see Figure 3.1 below for a schematic overview of the instrument.

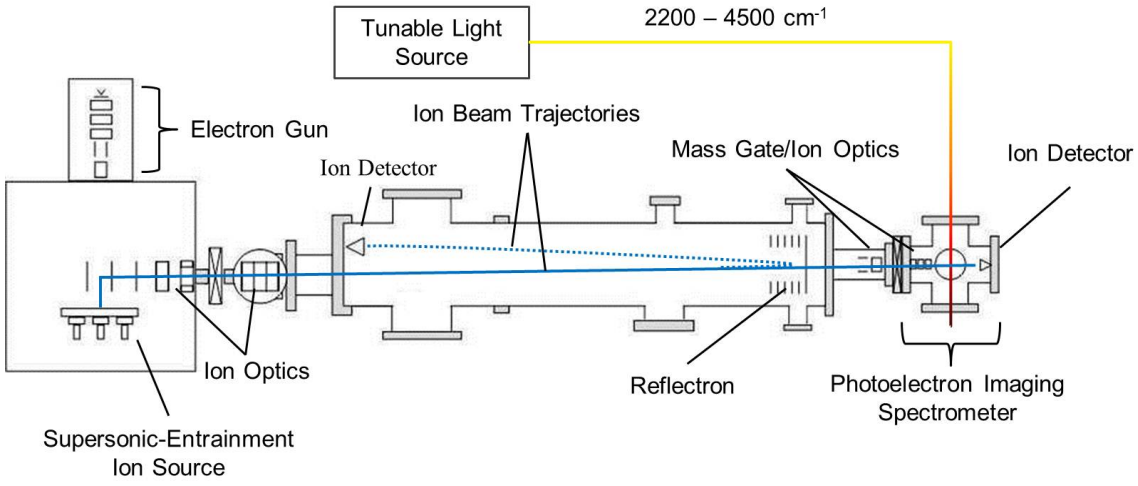

Figure 3.1 – Schematic diagram of the instrument used for a photoelectron spectroscopy study.

3.2 Ion Source

Anions are created in an electron impact plasma generated in a pulsed supersonic expansion. Over the last two decades, this type of ion source has proven a successful and reliable way to create molecular anions.[1, 2] Central to the success of this technique, is the efficient attachment of slow electrons to many neutral molecules.[1] Slow-secondary electrons are produced from the injection of high energy electrons (~ 1 kV) into the high density region of a supersonic expansion of an inert gas, such as argon. The ionization of argon produces slow-secondary electrons that will remain in the expansion while the high-energy electrons continue through the expansion, leaving a trail of slow-secondary electrons. This technique produces a sufficient density of slow secondary electrons in the expansion and yields a neutral plasma that circumvents issues arising from space-charge limits associated with charged beams.[2]

The electron bombardment of a supersonic expansion serves as a well-suited environment for anion formation; however, there are several approaches to introducing the anion precursors of

interest into the expansion. Perhaps the most obvious means of introducing a neutral molecule (or anion precursor) into the expansion is by expanding a gas mixture. This approach can be used, but the composition of the expansion mixture is difficult to control as many molecular precursors readily adsorb onto the walls of the gas lines.[2] A more precise means of introducing the anion precursor and controlling the nature of the expansion is realized using supersonic entrainment.[2]

Supersonic entrainment is a hydrodynamic process, first characterized and extensively studied by Campargue,[3] in which a gas in the vicinity of the high density region of an expansion efficiently penetrates the boundary of the expansion and is readily incorporated into the supersonic flow. Practically, this is achieved by admitting the anion precursor, prior to the creation of the supersonic expansion, into an entrainment reactor that serves as a "holding area" which allows sufficient gas densities to build up in the vicinity of the main expansion nozzle.[2] When the supersonic expansion is created, the anion precursor is entrained in the expansion where it may cluster with the argon gas and subsequently form temporary negative ions:

Equation 3.1

$$XY \bullet \mathrm{Ar}_n + e^- \rightarrow [XY^- \bullet \mathrm{Ar}_n]^*$$

The transient negative anion may undergo simple autodetachment, but more interestingly it may be stabilized by dissociative electron attachment, evaporation of the argon atoms, or collisions with background molecules (M):

Equation 3.2

$$[XY^- \bullet \mathrm{Ar}_n]^* \rightarrow X^- \bullet \mathrm{Ar}_m + Y + (n-m)\mathrm{Ar}$$

Equation 3.3

$$[XY^- \bullet \mathrm{Ar}_n]^* \rightarrow XY^- \bullet \mathrm{Ar}_m + (n-m)\mathrm{Ar}$$

Equation 3.4

$$[XY^- \bullet \mathrm{Ar}_n]^* + \mathrm{M} \rightarrow XY^- \bullet \mathrm{Ar}_n + \mathrm{M}$$

While the supersonic expansion provides cooling, particularly in the rotational degrees of freedom, numerous studies have revealed that the vibrational temperature of the anions formed within the expansion is governed primarily by evaporation. As a consequence, the binding energy of the most weakly bound species will dictate the upper limit for the internal energy of a cluster.[2, 4, 5] Cooler ion temperatures can be achieved by optimizing source conditions to favor the production of target anions solvated by moderately large clusters of argon atoms, which have binding energies of ~500 cm^{-1}/Ar. This is accomplished using relatively low pressures of the anion precursors to ensure that most collisions are between molecules and argon atoms.

3.2.1 Implementation

A schematic diagram illustrating the supersonic entrainment ion source is shown in Figure 3.2. The entrainment ion source is located within the a large chamber pumped by a 2000 L/s diffusion pump (BOC Edwards Diffstak) and a 1000 L/s turbomolecular pump (Turbovac, 1000C, Leybold) that maintain a background pressure of several 10^{-7} mbar. The source consists of three independently controlled solenoid valves, an entrainment reactor, and an electron gun.

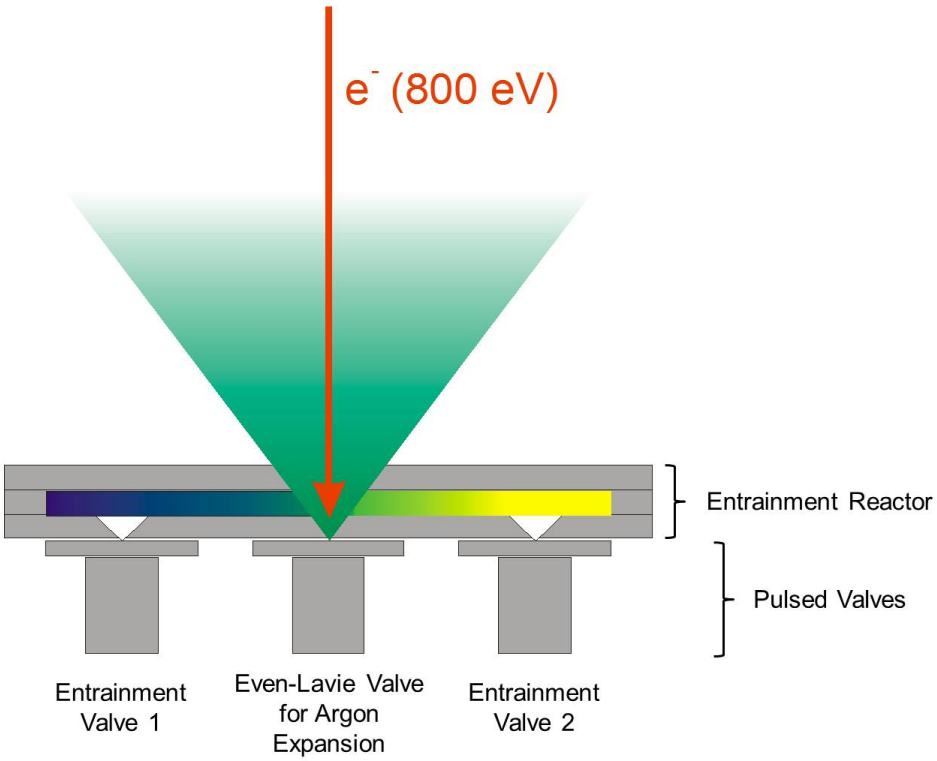

Figure 3.2 – Schematic diagram of the entrainment ion source. The source has the capability to entrain two gases. However, all of the studies within this thesis utilize only one entrainment valve.

The electron gun continuously produces a beam of high-energy electrons, typically accelerated to a kinetic energy of 800 eV. The beam is counter-propagating to the main expansion and is directed by several electron optics elements to the high-density region of the expansion. The experiment is operated at 20 Hz repetition rate. The sequence begins when the pulsed solenoid-actuated valves flanking the main expansion (Series 9, Parker Hannifin Corporation, General Valve Division) admits the anion precursors of interest into the entrainment reactor. Following this, a supersonic expansion of neat argon (99.9999%) is generated. As the argon jet dictates the character of the expansion, a more precise valve is desirable. To achieve these ends, we employ an Even-Lavie valve capable of a backing pressure of up to 100 bar (typically operated at 14 bar) and very short opening times (~25 μs). The large backing pressure allows us to maximize cooling from the supersonic expansion while the short

opening times make it possible to maintain a relatively low background pressure during operation (around several 10^{-6} to 10^{-5} mbar). The neutral plasma that is generated expands freely between the repeller and extractor of our Wiley-McLaren[6] time-of-flight mass spectrometer which is oriented perpendicularly to the expansion. The source conditions are optimized for cold-anion creation through varying the amplitude of each gas pulse, the relative timing of each gas pulse, the path and intensity of the electron beam, and the timing of the mass spectrometer's extraction pulse.

3.3 Time-of-Flight Mass Spectrometer

The instrument is equipped with a Wiley-McLaren[6] time-of-flight mass spectrometer. The plasma created in the ion source is injected directly into the acceleration region of the mass spectrometer. A high voltage pulse is applied to the repeller, extractor, and ground electrodes, accelerating the anions to a kinetic energy of ~ 3.5 keV. The beam is guided by xy-deflectors into a differentially pumped stage pumped by a 230 L/s turbomolecular pump (Pfeiffer TMU 261 P) with an operating pressure of several 10^{-7} mbar. The differentially pumped stage is equipped with an additional pair of xy-deflectors and an Einzel lens that serve to direct and focus the beam through the time-of-flight. The flight tube is pumped by a 520 L/s turbomolecular pump (Pfeiffer TMU 521 YP) and kept at an operating pressure of several 10^{-8} mbar.

The anions will separate during the flight as a function of their mass-to-charge (m/q) ratio.

Equation 3.5

$$t \propto \sqrt{\frac{m}{q}}$$

Due to the finite volume of the anions in the acceleration region, ions of the same mass will be accelerated to slightly different kinetic energies. All ions of the same mass-to-charge ratio will arrive at the same time at one point in the flight path; this point defines the space focus of the mass spectrometer. The ratio of the accelerating electric fields in the Wiley-McLaren[6] setup determines the position of the space focus.

The instrument currently has two operational modes: one is used to characterize the ion source and perform infrared photodissociation spectroscopy studies while the other is used for photoelectron spectroscopy. In the first mode, the anions are directed into a two-stage reflectron (R.M. Jordan Company); the space focus of the reflectron is centered on a dual microchannel plate detector in a chevron configuration coupled to a conical anode for ion detection. The detector output is monitored as a function of time to obtain a mass spectrum. The reflectron nearly doubles the flight path and serves as an energy focusing device which substantially increases the resolution of the mass spectrometer, defined as

Equation 3.6

$$R = \frac{m}{\Delta m} = \frac{t}{2\Delta t}.$$

For this mode, the resolution is R~800. Procedurally, ion source optimization is achieved by adjusting source conditions in order to maximize the intensity of large, argon solvated clusters containing the anion of interest, ensuring that the overall temperature of the expansion is low.

Once the source has been optimized for the production of relatively cold ions, the second mode is used. The beam is directed through the electrically grounded reflectron, at which point a pulsed mass gate can be used to transmit only the ions of interest. The mass gate is operated by applying ± 150 V across a deflection electrode, a voltage sufficient to deflect the ion beam into the chamber walls. When the anion of interest is in the vicinity of the mass gate the voltage is pulsed to 0 V allowing an unimpeded flight into the photoelectron spectrometer. The mass-selected beam is passed through a 5 mm aperture as it crosses the threshold into the photoelectron spectrometer chamber. The beam is then passed through an Einzel lens that serves to focus the anion beam to several millimeters within the photodetachment region of the photoelectron spectrometer. The mass resolution in this mode is R~150. As the photoelectron spectrometer is oriented perpendicular to the path of the ion beam, the anions continue and impinge on a dual microchannel plate in the chevron configuration coupled to an anode. The detector signal can be measured on a digital oscilloscope to acquire a mass spectrum. Alternatively, a retarding voltage may be applied to a grid directly in front of the detector such that photoneutrals generated in the photoelectron spectrometer may be monitored; this detection scheme is important for maximizing the signal in the photoelectron spectrometer.

3.4 Laser System

Near-threshold photodetachment experiments are performed with the tunable output of an optical parametric converter (LaserVision). A schematic diagram of the light source is displayed in Figure 3.3. The system consists of a Nd:YAG pump laser, an optical parametric oscillator (OPO), and an optical parametric amplifier (OPA). The Nd:YAG pump laser (Innolas Spitlight 600) produces a linearly polarized, ~7 ns pulse with a typical output power of 475 mJ/ pulse at a

wavelength of 1064 nm. The pump beam is directed by a series of steering optics and through a beam splitter; one-third of the beam is frequency-doubled in a potassium titanyl phosphate (KTP) crystal while the remaining two-thirds is directed through a delay before being used to pump the OPA. After the OPA, the residual 1064 nm radiation is removed by a longpass dichroic mirror while the 532 nm radiation is used to pump the two KTP crystals within the linear cavity of the OPO. Conservation of energy requires,

Equation 3.7

$$2\omega_P = \omega_S + \omega_I,$$

where ω_P, ω_S, and ω_I are the frequencies of the pump, signal and idler, respectively. Angle-tuning of the KTP crystals is used to modulate phasematching conditions for the desired output wavelengths. The current setup allows for continuous tuning of the signal wave from $710 - 885$ nm, corresponding to a range between $1330 - 2120$ nm for the idler wave. At the present time, a polarizer is used to filter out the signal wave within the OPO cavity. After this stage, as a safety precaution the idler wave is passed through a half-waveplate such that the polarization is rotated to permit angle-tuning of the OPA crystals within the horizontal plane. The OPA consists of four potassium titanyl phosphate (KTP) crystals; the idler and the 1064 nm radiation are superimposed and directed through the KTP chain. Difference frequency mixing generates mid-infrared radiation from $2200 - 4500$ cm^{-1} according to,

Equation 3.8

$$\omega_{\text{Mid-IR}} = \omega_P - \omega_I.$$

Following the OPA, a dichroic mirror is used to remove the residual 1064 nm radiation. Of the co-propagating vertically-polarized mid-infrared radiation and horizontally-polarized idler radiation, a beam is chosen using a polarizer.

The vertically-polarized mid-infrared radiation is directed towards a twisted periscope which flips the radiation to a horizontal polarization. Before the beam is admitted into the photodetachment region, a Brewster "stack of plates" polarizer is used to ensure a clean, horizontal polarization. Following this, a lens focuses the beam into the photodetachment region of the photoelectron spectrometer. Irises are placed at the entrance and exit of the photoelectron spectrometer chamber. The beam is centered on each iris to ensure reproducible alignment of the laser beam in the photoelectron spectrometer, as the focus of the imaging spectrometer is sensitive to the vertical (as defined by the imaging spectrometer's flight tube) position of the detachment region. The optical parametric converter is calibrated by analysis of the signal wave with a fiber optic spectrometer (Ocean Optics), which is calibrated to the emission spectrum of an argon discharge. As the bandwidth of the fiber optic spectrometer is 2 cm^{-1} and the bandwidth of the optical parametric converter is 2 cm^{-1} we estimate a 3 cm^{-1} resolution of the system.

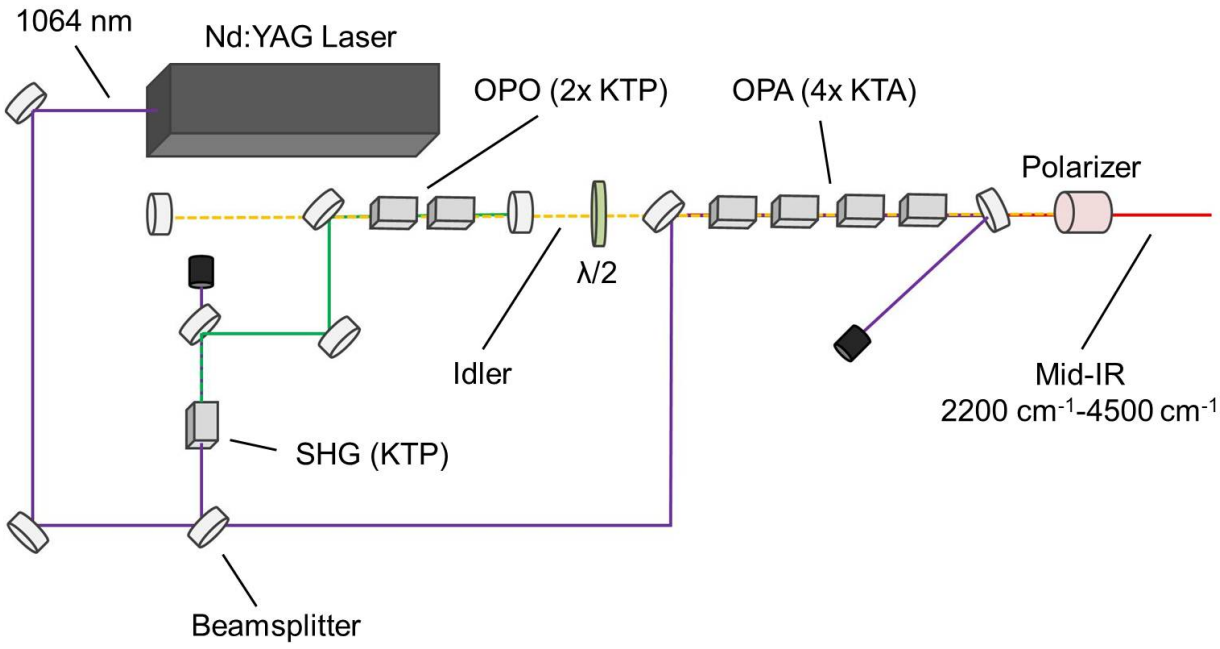

Figure 3.3 - Overview of the IR OPO/OPA tunable light source.

Higher-energy photoelectron studies are performed using the radiation generated from the second-harmonic of the Nd:YAG laser. In this case, the beam is directed by steering optics and frequency doubled within a KTP crystal. The co-propagating 532 nm and 1064 nm radiation is directed into a Pellin-Broca prism, where the angle of incidence is adjusted to select the wavelength that is transmitted to the photoelectron spectrometer. The beam is then directed through several prisms before reaching a half-waveplate used to rotate the polarization to the horizontal plane, as is required by the photoelectron experiment. Finally, the beam is passed through a converging lens which focuses the light into the photodetachment region of the photoelectron spectrometer. The beam is aligned within the photoelectron spectrometer using irises (mentioned above).

3.6 Velocity Map Imaging Photoelectron Spectrometer

3.6.1 Photoelectron Image Acquisition

The photoelectron imaging spectrometer is based on the design of the Lineberger and Sanov[7, 8] groups and utilizes the velocity-map imaging technique pioneered by Eppink and Parker.[9, 10] The details of the photoelectron spectrometer are as follows. The spectrometer is housed within an 8″ six-way chamber and oriented perpendicularly to the plane defined by the ion and laser beams. The chamber maintains a typical operating pressure of several 10^{-8} mbar and is pumped by a 520 L/s turbomolecular pump (Pfeiffer TMU 521 YP). The photoelectron spectrometer consists of a set of imaging optics and a drift region terminated by a position sensitive detector. The imaging optics consist of three, 1 mm thick, oxygen-free-high-conductivity (OFHC) copper plate electrodes with diameters of 108 mm, which are evenly spaced by 25 mm and coated with a thin surface of colloidal graphite. The three electrodes are designated the repeller (V_R), the extractor (V_E), and ground (V_G), where $V_R < V_E < V_G$. The extractor and ground electrodes each have 20 mm diameter holes, while the repeller electrode is a solid plate. The stack of imaging optics is encapsulated by two concentric µ-metal cylindrical cups (1 mm thick) with four 25 mm apertures permitting the passage of the ion and laser beams through the interaction region of the photoelectron spectrometer. The annealed µ-metal is a soft magnetic material that provides shielding from stray magnetic fields. The boundary between the imaging optics and the drift region is defined by the grounded electrode. The drift region is a 150 mm field-free flight tube (as defined from the ground electrode to the face of the microchannel plate) shielded by two concentric, 1 mm thick µ-metal cylinders. The drift region is terminated by a position sensitive detector. A schematic representation of the spectrometer is given in Figure 3.4 below.

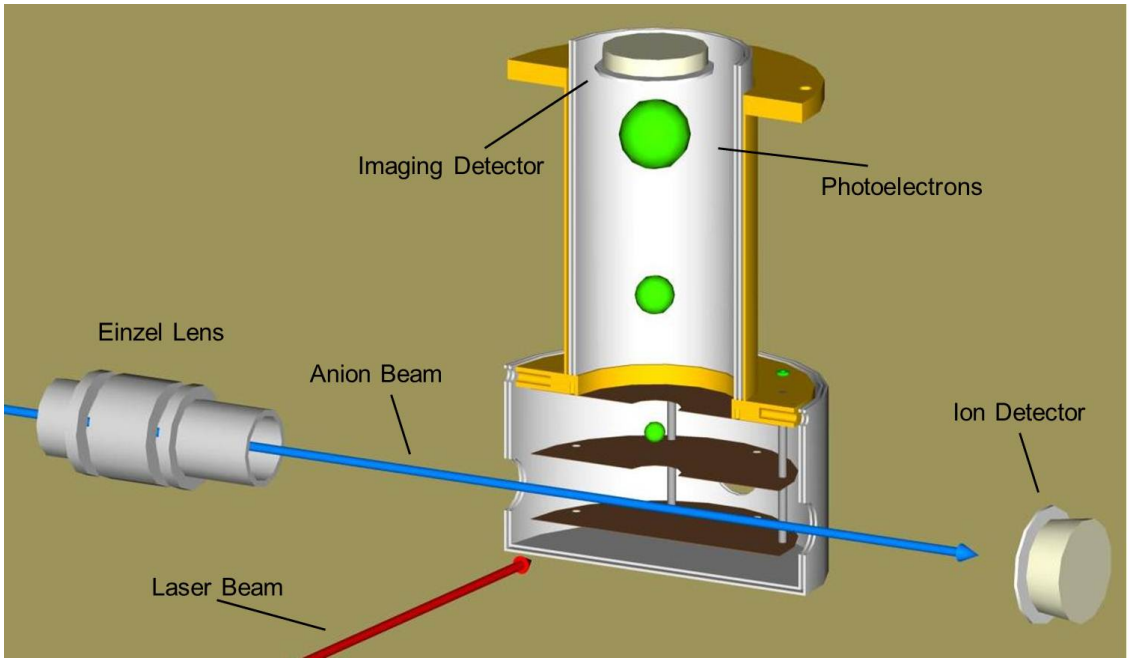

Figure 3.4 – Schematic diagram of velocity map imaging photoelectron spectrometer.

The mass-selected anion beam is collimated by a 5 mm aperture and focused by an Einzel lens into the detachment region. The photodetachment region is defined by the overlapping volume of the mass-selected anion beam with the laser beam which is located between the repeller and extractor electrodes. The overlap of the two beams is monitored by the generation of the photoneutrals as described at the end of section 3.3. The signal is optimized by adjusting the focus of the Einzel lens and steering optics directing the beam into the photoelectron spectrometer; additionally, the timing of the laser beam pulse is adjusted to ensure overlap with the most intense part of the anion bunch. The simple geometry defined by the imaging optics creates an inhomogeneous field within the photodetachment region. The field acts to focus all nascent photoelectrons with the same initial velocity, irrespective of their initial position within the detachment plane, to the same location on the position sensitive detector. The large insensitivity of the origin of the photoelectron within the detachment plane is what defines this as velocity map imaging.[9, 10] The location of the imaging-optics' focal plane is determined by the

ratio of the repeller to extractor voltages, V_R/V_E. This plane must be empirically optimized to coincide with the face of the detector. This is achieved in a brute-force optimization, in which an initial estimate of the V_R/V_E ratio is obtained from a simulation (performed with the Simion charged particle optics simulator, Version 7) and fine adjustments to the ratio are inferred from the peak width of well-defined transitions in an atomic photoelectron spectrum, typically S^-, as iterative adjustments are made. In the current setup, the ratio is

Equation 3.9

$$\frac{V_R}{V_E} = 0.721;$$

however, if any adjustments are made in the laser beam height, the ratio will have to be adjusted.

The photoelectrons are accelerated by the electric fields at the detachment region into the field-free drift tube and are projected onto the front face of a position sensitive detector. The position sensitive detector consists of two microchannel plates, with an active area of 40 mm, in a chevron configuration followed by a fiber optic P-47 type phosphor screen (Burle Electro-Optics, Inc.). The front face of the detector, i.e., the face of the first michrochannel plate, is kept at ground. The back face of the second microchannel plate is pulsed from a voltage of 1100 V to 2000 V in a 5 μs window centered on the photodetachment event; since the gain is only appreciable at the greater voltage, the noise in the photoelectron image is greatly reduced. The front face of the phosphor screen is held at a voltage of 5000 V. The phosphorescence is digitized by a charge coupled device (CCD) camera (UNIQ UP-610CL, 659x694) mounted just above the phosphor screen and housed in a shroud to eliminate any ambient light.

Each image is acquired and analyzed in real-time using the centroiding (WenImaging) program developed by Suits and coworkers.[11] The centroiding algorithm performs a center-of-

mass calculation on each event spot (caused by a single detected electron), achieving sub-pixel resolution. This approach permits the use of a relatively inexpensive camera that is not cooled, possesses a comparatively small CCD array, and has a lower intrinsic signal-to-noise ratio. The data coordinates of each analyzed event are stored in an output file which is updated with every cycle of the experiment (at a rate of 20 Hz). Each photoelectron image is typically an accumulation of several 10^6 events. It should be noted that the number of photoelectrons in each shot has to be low enough to prevent overlapping electron spots. The centroiding algorithm partitions the image into smaller arrays to perform the center-of-mass calculation. When several event spots are spread over the partitioned array the program produces an artifact located in the upper left corner of the images, after some time the shape of the artifact takes the form of a "jet" pattern in one corner of the image. This issue usually manifests itself in near-threshold photoelectron studies, as the intensity at very low kinetic energies is often very large. Problems arising from this issue are alleviated by adjusting the photodetachment yield to an intensity that significantly reduces the chance of nearly overlapping events.

3.6.2 Data Analysis

The acquired photoelectron image is a two-dimensional projection of the initial three-dimensional photoelectron distribution. The laser is polarized in the direction of the ion beam (i.e., in the detector plane); this serves to define an axis of cylindrical symmetry for the system. This property allows the initial three-dimensional distribution to be reconstructed by an inverse Abel transformation as implemented by the BASEX program developed by Reisler and coworkers.[12] The centroided image is imported into BASEX. The center of the image must be defined. This may be performed manually or by using the center-finding algorithm within the

program (discussed in more detail below). The program performs the reconstruction, returns an equatorial slice through the three-dimensional distribution, and then integrates over all emission angles at each radius to obtain the photoelectron yield as a function of electron velocity. At this point, the spectrum is calibrated (see discussion below) to a well-known photoelectron spectrum and recast as a function of the kinetic energy according to the Jacobian transformation,

Equation 3.10

$$I(E_{KE}) \propto \frac{I(v)}{v}.$$

Additionally, the BASEX program can calculate anisotropy parameters by fitting the intensity profile as a function of radius using

Equation 3.11

$$I(r,\theta) = C[1 + \beta(r)P_2(\cos\theta)]$$

where $I(r,\theta)$ is the well-known function governing a one-photon process, θ is the angle between the laser polarization and the emission angle, C is a constant, and β is the anisotropy parameter that completely characterizes the angular distribution (see chapter 2 for a detailed discussion of the anisotropy parameter). Figure 3.5 illustrates a composite of a raw photoelectron image (left half) and a reconstructed image (right half) from a photoelectron study of S^-.

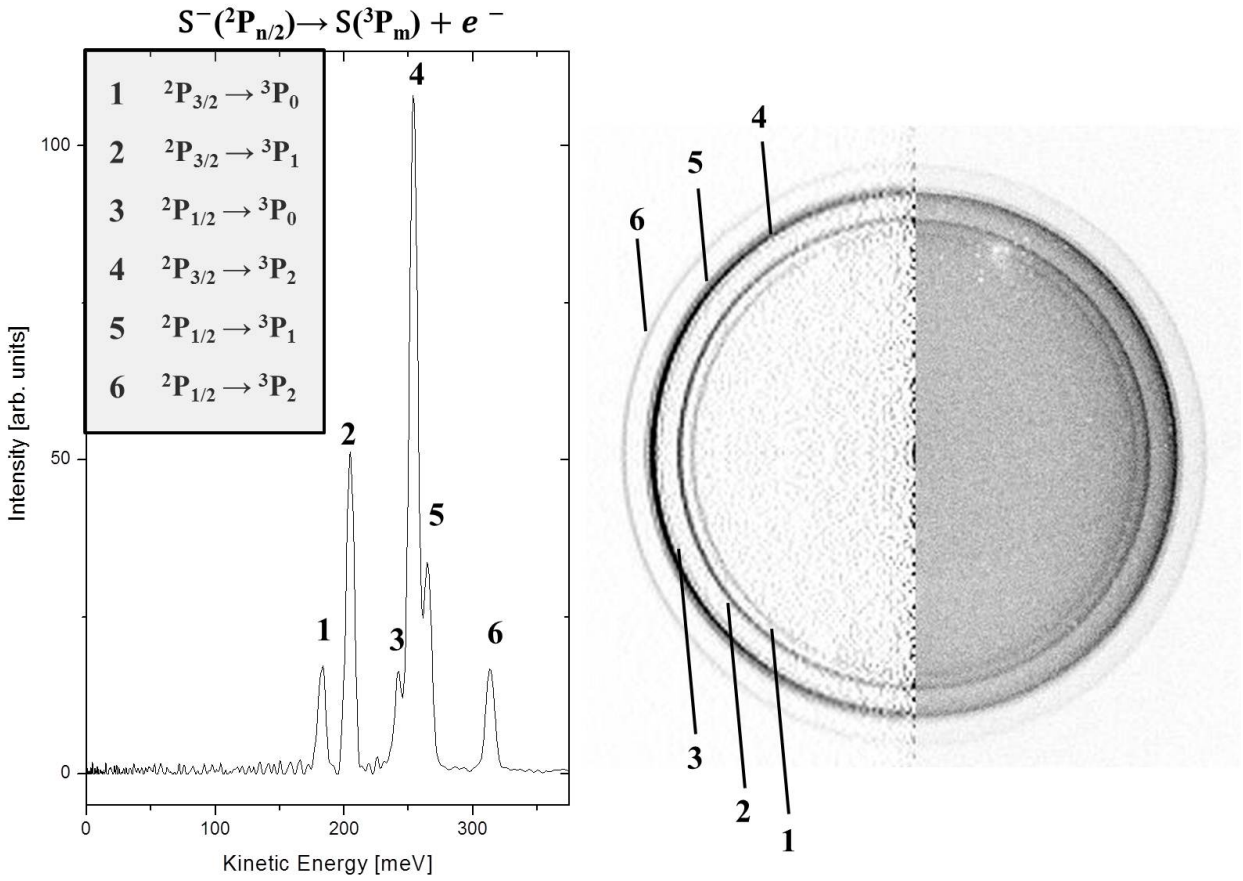

Figure 3.5 – Shown on the right is a photoelectron image of S^- taken at 532 nm. The left half illustrates the raw image. The right half illustrates the BASEX reconstructed equatorial slice through the original three-dimensional photoelectron distribution. On the left side of the figure is the photoelectron spectrum generated from the reconstructed image. The transitions are labeled to illustrate corresponding features.

Each photoelectron spectrum is calibrated to the well-known photoelectron spectra of S^- or O_2^-.[13, 14] Calibrations are performed with the output of the second harmonic of the Nd:YAG laser at a photon energy of 2.331 eV. The S^- photoelectron spectrum is used to calibrate the low-energy photoelectron spectra which use the output of the tunable optical parametric converter. The S^- ions are created within the source by dissociative electron attachment to CS_2 vapor, entrained in the argon expansion. The O_2^- photoelectron spectrum is used to calibrate the higher energy photoelectron spectrum taken at a wavelength of 532 nm; the anions are created by electron attachment to molecular oxygen entrained in the argon expansion. The resolution of the

spectrometer is determined by fitting the width of the features in these well-characterized spectra as a function of kinetic energy; results indicate a resolution of $\Delta v = (5800 \pm 1000)$ m/s for the spectrometer.

The microchannel plates utilized in the imaging experiment suffer from several inhomogeneities over the detector surface, leading to uneven amplification across the detector. This introduces two complications in the reconstruction of the photoelectron image. First, the center of the image becomes difficult to accurately find, either by the algorithm or by eye. Second, the inhomogeneities decrease the signal-to-noise ratio of the image.

As a consequence of the first issue, a procedure has been developed for accurately determining the image center. The idea is to process the image, eliminate the inhomogeneities, and make a "dummy" image that has the same center as the centroiding photoelectron image but has an easily identifiable center. The centroided images are processed in a Java-based image processing program (ImageJ 1.43u). The image is first subjected to an edge finding algorithm, converted to binary, and finally a "fill holes" algorithm is used to create a large circle. The center for this image is then easily found using the BASEX center-finding algorithm. For very anisotropic images, it is often better to only perform the edge finding algorithm. In the event, the photoelectron image has no sharp features it is necessary to use a time-consuming iterative procedure, in which an estimate of the image center is given by the center finding algorithm or by eye and as many as sixteen or twenty-five images with different centers are reconstructed to find the best center.

Regarding the second issue, the inhomogeneities decrease the signal-to-noise ratio in particular regions of the image. Due to symmetry arguments, all of the information is contained

within a quadrant of the photoelectron image. If the inhomogeneities are localized within one half of the image, it is often advantageous (i.e., increases the signal-to-noise) to construct a raw image from one half of the centroided image prior to reconstruction. This is performed in ImageJ by locating the center of the image according to the procedures outlined above. Then one half of the image is mirrored along the center line, imported into BASEX and reconstructed.

As described above, in the current setup the photoelectron imaging spectrometer is oriented perpendicularly to the ion beam. This leads to several important ramifications in the operation of the spectrometer. The first issue arises from the photodetachment of an anion moving with ~ 3.5 keV of kinetic energy. When the electron is emitted, its velocity will be the vector sum of the anion velocity and the velocity imparted from photodetachment. As a result, the image is displaced from the center of the phosphor screen and the useable area of the microchannel plate is reduced. The displacement is given by the product of the velocity imparted from the ion beam and the flight time of the photoelectron, this is limited to an acceptable distance by increasing the magnitude of the repeller voltage (while maintaining the ratio $\frac{V_R}{V_E}$). The most consequential effect of the imaging spectrometer's orientation comes from the nature of the space focus of the time-of-flight spectrometer. The space focus is typically located at the photodetachment region in order to get the largest photodetachment signal. Unfortunately, this is associated with a large uncertainty in the ion kinetic energy commensurate with the spread of the plasma within the acceleration region of the time-of-flight mass spectrometer. The uncertainty in the velocity of the anion beam will contribute to an uncertainty in the velocity of the photodetached electrons along the time-of-flight axis, deteriorating the resolution of the spectrometer. The argument can be made more quantitative if we look at the mathematical relations. Let us first consider a collection of anions, with the same mass, spread

along the time-of-flight axis within the acceleration region of the mass spectrometer. These anions will have an associated intensity profile, $I(z)$, where z is the coordinate along the time-of-flight axis. This intensity profile will also have some finite uncertainty, Δz. Since the time-of-flight acceleration region produces a linear potential gradient between the repeller and extractor electrodes, $\Delta z \propto \Delta E_A$, where E_A is the initial kinetic energy of the anions in the acceleration region of the mass spectrometer. The initial kinetic energy spread is given by

Equation 3.12

$$\Delta E_A = m_A v_A \Delta v_A,$$

where m_A, v_A and E_A represent the anion's mass, velocity and kinetic energy, respectively. It can be shown that this will lead to a kinetic energy spread along the time-of-flight axis of

Equation 3.13

$$\Delta E_e = \frac{m_e}{m_A} \Delta E_A,$$

where m_e and E_e represent the mass and kinetic energy of the photodetached electrons. If we consider some typical parameters in our experiment, the plasma is freely expanded between the repeller and extractor (separated by 30 mm). For this setup, a fair estimate of ΔE_A is ~ 400 V. This indicates that for an anion with a 50 amu mass, the uncertainty introduced to the photoelectron, in the direction of the anion beam, is ~ 4 meV. This introduces a large part of the uncertainty present in every photoelectron spectrum and is particularly harmful to spectra in which β approaches 2 (a parallel transition). We attempt to abate the effect of this inherent problem by lowering the magnitude of the ion acceleration voltages while maintaining the TOF space focus, resulting in a reduction of ΔE_A.

3.7 Using Argon Solvation for Accurate Adiabatic Electron Affinity Determinations

One of the primary goals of many photoelectron studies is to accurately determine the adiabatic electron affinity of the molecule under study. This is often complicated by small Franck-Condon factors for the origin of the vibrational progression of the electronic ground state of the neutral, which must be resolved for to determine the adiabatic electron affinity, or by the finite temperature of the ions prepared for photodetachment, which leads to multiple progressions that make the identity of the adiabatic electron affinity unclear. The Franck-Condon factors obviously cannot be modified, as they are a property of the system; however, the temperature of the ions may be reduced using several experimental approaches.

The first approach to reducing the temperature of the ions has been outlined above in section 3.3, in which the source conditions are optimized to produce the anions of interest solvated in large argon clusters. This technique serves to moderately cool the bare anions and, as suggested from Franck-Condon simulations, yields an anion temperature of ~ 250 K. At this temperature, especially in molecules with many energetically low-lying vibrations, the adiabatic electron affinity remains difficult to assign as many of the progressions arising from hot bands still have appreciable intensity.

The photoelectron spectra of the anions solvated with argon atoms provide one of the most effective means of eliminating hot bands and correctly identifying the adiabatic electron affinity. The presence of the argon ensures that the ions have temperatures of only a few tens of K, since the argon binding energies to most anions are only a few tens of meV. Additionally, the very weak binding energy of the argon to the neutral molecule is expected to have a negligible effect on the neutral vibrational modes. The relatively cool argon-solvated anion will yield a

photoelectron spectrum that is shifted relative to the spectrum of the unsolvated anion by the argon solvation energy, but more importantly the hot bands will be strongly suppressed or eliminated. This often allows for an unambiguous assignment of the features that correspond to the $n \leftarrow 0$ transitions in the photoelectron spectrum.

3.8 References for Chapter 3

1. M. A. Johnson and W. C. Lineberger, in *Techniques for the Study of Gas-Phase Ion Molecule Reactions*, edited by J. M. Farrar and W. Saunders (Wiley, New York, 1988), pp. 591.

2. W. H. Robertson, J. A. Kelley and M. A. Johnson,"A pulsed supersonic entrainment reactor for the rational preparation of cold ionic complexes." *Review of Scientific Instruments* **71** (12), 4431-4434 (2000).

3. R. Campargue,"Aerodynamic Separation Effect on Gas and Isotope Mixtures Induced by Invasion of Free Jet Shock Wave Structure." *Journal of Chemical Physics* **52** (4), 1795 (1970).

4. C. E. Klots,"Evaporative Cooling." *Journal of Chemical Physics* **83** (11), 5854-5860 (1985).

5. C. E. Klots,"The evaporative ensemble." *Zeitschrift für Physik D Atoms, Molecules and Clusters* **5** (1), 83-89 (1987).

6. W. C. Wiley and I. H. McLaren,"Time-of-Flight Mass Spectrometer with Improved Resolution." *Review of Scientific Instruments* **26** (12), 1150-1157 (1955).

7. A. Sanov and W. C. Lineberger,"Dynamics of cluster anions: a detailed look at condensed-phase interactions." *Physchemcomm*, 165-177 (2002).

8. A. Sanov and W. C. Lineberger,"Cluster anions: Structure, interactions, and dynamics in the sub-nanoscale regime." *Physical Chemistry Chemical Physics* **6** (9), 2018-2032 (2004).

9. A. Eppink and D. H. Parker,"Velocity map imaging of ions and electrons using electrostatic lenses: Application in photoelectron and photofragment ion imaging of molecular oxygen." *Review of Scientific Instruments* **68** (9), 3477-3484 (1997).

10. D. H. Parker and A. Eppink,"Photoelectron and photofragment velocity map imaging of state-selected molecular oxygen dissociation/ionization dynamics." *Journal of Chemical Physics* **107** (7), 2357-2362 (1997).

11. W. Li, S. D. Chambreau, S. A. Lahankar and A. G. Suits,"Megapixel ion imaging with standard video." *Review of Scientific Instruments* **76** (6) (2005).

12. V. Dribinski, A. Ossadtchi, V. A. Mandelshtam and H. Reisler,"Reconstruction of abel-transformable images: The Gaussian basis-set expansion abel transform method." *Review of Scientific Instruments* **73** (7), 2634-2642 (2002).

13. H. Hotop and W. C. Lineberger,"Binding-Energies in Atomic Negative-Ions .2." *Journal of Physical and Chemical Reference Data* **14** (3), 731-750 (1985).

14. K. M. Ervin, I. Anusiewicz, P. Skurski, J. Simons and W. C. Lineberger,"The Only Stable State of O_2^- Is the X $^2\Pi_g$ Ground State and It (Still!) Has an Adiabatic Electron Detachment Energy of 0.45 eV." *The Journal of Physical Chemistry A* **107** (41), 8521-8529 (2003).

4 Photoelectron Spectroscopy of Nitromethane Anion

This chapter has been reproduced in part with permission from Adams, C.L., Schneider, H., Ervin, K.M., and Weber, J.M., "Low-energy photoelectron imaging spectroscopy of nitromethane anions: Electron affinity, vibrational features, anisotropies, and the dipole-bound state." *Journal of Chemical Physics*, 2009. **130**: 074307.

4.1 Introduction

The interaction of nitromethane (CH_3NO_2) with low-energy electrons and the properties of the $CH_3NO_2^-$ anion have been the subject of many studies, both experimentally[1-10] and theoretically.[11-13] One remarkable feature of CH_3NO_2 is that it has a sufficiently large dipole moment ($\mu = 3.46$ D) to bind an excess electron not only in a valence-like state but also in a state more accurately described as a dipole-bound state.[1-3, 11, 12] Interestingly, the signature of the dipole-bound state has not been observed in photoelectron (PE) spectroscopy. The binding energy of the valence-like state is small[1] relative to several of the fundamental vibrational transitions in the anion, making it an ideal molecular system for the investigation of the interaction of vibrational excitation and electron emission.[4, 10]

The adiabatic electron affinity (AEA) of CH_3NO_2 has been determined to be (260 ± 80) meV by Compton *et al.*[1] by using the last discernible peaks on a very extended and congested vibrational progression as bracketing features. The error bars were intended to cover the range of possible origin assignments of a vibrational progression with (80 ± 9) meV or (645 ± 56) cm^{-1} spacing, yielding possible electron affinities of about 180, 260, or 340 meV. In light of the

interest in the interaction of CH_3NO_2 with low-energy electrons and investigation of vibration-electron interaction, a more accurate and precise determination of the AEA is desirable.

The extended and congested vibrational progressions that made earlier AEA measurements difficult is based on the large differences in the geometry of the nitro group between the anion and the neutral molecule. In the neutral molecule, the CN bond lies in the ONO plane, while the nitro group is strongly angled away from the CN bond in the anion geometry (see Figure 4.1). The vibrational spacing found in the PE spectrum reported by Compton *et al.*[1] is consistent with both the NO_2 bending mode and the NO_2 wagging mode of the neutral molecule.

In this chapter, low-energy PE imaging results for $CH_3NO_2^-$ and cold $CH_3NO_2^- \bullet Ar$ are presented along with simulations of the PE spectrum. The feature corresponding to the vibrational ground state in the PE spectrum is unambiguously determined by comparison of the bare (and relatively warm) $CH_3NO_2^-$ with that of cold $CH_3NO_2^- \bullet Ar$, resulting in a value for the AEA of CH_3NO_2 of (168 ± 6) meV. A weak signature in the PE spectrum is tentatively assigned as the dipole-bound state. Finally, the angular distributions of the observed features are discussed in the context of the threshold laws for photodetachment and assignments of the vibrational structure in the spectra are made, based on the simulations.

4.2 Computational Details

4.2.1 *Ab Initio* Calculations

Computational chemistry calculations were performed using the GAUSSIAN03 program.[14] Geometries and frequencies for (^{2}A′) $CH_3NO_2^-$ and (^{1}A′) CH_3NO_2 were calculated using density functional theory (DFT) with the Becke-3-Lee-Yang-Parr (B3LYP) hybrid functional[15, 16] and the 6-311++G(2*df*,2*p*) basis set.[17, 18] Geometries were also calculated using coupled-cluster theory with single and double excitations and perturbative inclusion of triples (CCSD(T)) (Ref. 19) with the aug-cc-PVTZ basis set.[20] The anion and neutral geometries for the two levels of theory are shown in Figure 4.1. The most significant geometry deviation between the DFT and coupled-cluster calculations is in the angle α between the plane of the NO_2 group and the CN bond.

Figure 4.1 – Geometries of $CH_3NO_2^-$ and CH_3NO_2; α denotes the angle between the ONO plane and the CN bond axis from DFT calculations; results from the CCSD(T) calculations are in parentheses.

Calculated DFT frequencies are provided in Table 4.1. The calculated electron affinity is $EA_0(CH_3NO_2)$ = 0.162 eV at the CCSD(T)/aug-cc-pVTZ level with vibrational zero-point energy corrections from the B3LYP/6-311++G(2*df*,2*p*) harmonic frequencies.

4.2.3 Franck-Condon Analysis

Nitromethane has fifteen vibrational modes. Fourteen of these modes are well described as harmonic oscillators; for these modes, the calculated vibrational normal modes from the DFT calculations were employed to simulate the Franck-Condon profiles using the PESCAL program developed by Ervin and coworkers.[21, 22] The remaining mode corresponds to the torsional vibration for internal rotation about the CN bond. This mode was treated independently and later incorporated into the final Franck-Condon simulations; this will be discussed in more detail below. The Franck-Condon factors were calculated in the independent harmonic oscillator approximation with full treatment of Duschinsky rotation[23] of the normal mode eigenvectors between the anion and neutral, using the Sharp-Rosenstock-Chen recursion method.[21, 24, 25]

The vibrational frequencies for neutral CH_3NO_2, excluding the torsion, were taken from the experimental Infrared/Raman fundamental frequencies[26] and substituted for the calculated values. The three CH stretch fundamental frequencies for the anions were taken from infrared spectroscopy experiments.[4, 10] The other anion frequencies were estimated by scaling the calculated B3LYP/6-311++G(2*df*,2*p*) harmonic values by the ratio of the experimental fundamental to the calculated harmonic frequency of the neutral for the similar normal mode. These frequencies are given in Table 4.1.

Both neutral and anionic CH_3NO_2 possess C_s symmetry with nine totally symmetric vibrational modes, which have nonzero normal coordinate displacement between the anion and neutral, and six nontotally symmetric modes. Nontotally symmetric modes undergo no normal coordinate displacement upon electron emission and are considered Franck-Condon "inactive," but can have some activity for $2n \leftarrow 0$ transitions because of the overlap of the even wave functions with different harmonic frequencies. All $n \leftarrow 0$ transitions are possible with

nonharmonic potentials; for example, the torsional mode. The calculated geometry changes between the anion and neutral are given in Table 4.1, presented as the $\vec{K}$" displacement vector in the anion normal coordinate frame.[21, 25] The signs of the Cartesian displacement vectors are arbitrary in the harmonic oscillator approximation, but need to be defined self-consistently for the Duschinsky rotation calculations. In this simulation, the direction of the normal coordinates for each mode was chosen such that the B rotational constant of the molecule decreases (I_{yy} component of the moment of inertia increases) for a positive displacement.

Table 4.1 – Frequencies (cm^{-1}) and geometry displacements.

		$CH_3NO_2^-$		CH_3NO_2		K'' / $(g/mol)^{1/2}$Angstrom[a]	
Mode	Assign.[b]	B3LYP[c]	Scaled[d]	B3LYP[c]	Exp.[b]	B3LYP[c]	fit[e]
1	$w(NO_2)$	411.7	403[f]	616.1	603	0.6802	0.65
2	$\delta_s(CH_3)$	1391.5	1369	1402.9	1380	−0.0428	−0.14
3	$\nu_s(NO_2)$	1201.7	1172	1431.9	1397	0.3255	0.34
4	$r_\perp(CH_3)$	1089.6	1084	1136.7	1131	0.1267	0.03
5	ν(CN)	844.1	836	926.9	918	−0.2745	−0.31
6	$\delta(NO_2)$	583.8	579	662.5	657	0.0854	
7	$\nu_s(CH_3)$	2887.5	2777[g]	3081.6	2974	−0.0345	
8	$\nu_s'(CH_3)$	3054.9	2922[g]	3168.4	3045	−0.0034	
9	$\delta_s'(CH_3)$	1461.2	1416	1479.6	1434	0.0122	
10	torsion	204.2	H.R.[h]	11.6	F.R.[h]	0	
11	$r(NO_2)$	446.2	440	481.5	475	0	
12	$r_{\|\|}(CH_3)$	1058.5	1044	1111.4	1096	0	
13	$\nu_a(NO_2)$	1280.5	1252	1619	1583	0	
14	$\delta_a(CH_3)$	1472.5	1416	1466.6	1410	0	
15	$\nu_a(CH_3)$	3108.1	2965[f]	3200.5	3080	0	

[a]Geometry displacements in terms of anion normal coordinate vectors.

[b]Experimental fundamental frequencies (Ref. 26). Assignment labels in column 2 are taken from Ref. 26.

[c]B3LYP/6-311++G(2*df*,2*p*) harmonic frequencies.

[d]Except as noted, scaled theoretical values as described in the text.

[e]Optimized displacements to fit PE spectrum of Compton *et al.* (Ref. 1).

[f]The experimental value from the present work is (380±56) cm^{-1} as derived from the hot bands (see text).

[g]Experimental fundamental frequencies (Refs. 3 and 5).

[h]H.R. threefold hindered rotor with 953 cm^{-1} barrier from B3LYP/6-311++G(2*df*,2*p*) calculation. F.R., free rotor.

4.2.3.1 Franck-Condon Simulations: Internal Rotor

The internal rotation of the methyl and NO_2 groups about the CN bond is a hindered motion in the anion but is essentially a barrier free motion in neutral CH_3NO_2. The torsional potentials are calculated at the B3LYP/6-311++G(2*df*,2*p*) level by scans of the HCNX dihedral angle, where X is a dummy atom placed 90° to the CN bond and defining the bisector of the NO_2 group, while all other distances and angles are allowed to relax. For the anion, the potential energy is well approximated by a cosine function,

Equation 4.1

$$V(\varphi) = (\frac{V_0}{2})(1 - \cos n\varphi),$$

with $n = 3$ and a barrier of $V_0 = 953$ cm^{-1}. For the neutral, the potential is sixfold symmetric, represented by $n = 6$ with a barrier, determined by a high resolution Fourier-transform infrared study, of $V_0 = 2.11$ cm^{-1}.[26] For the present study, with our resolution, it is appropriate to treat neutral CH_3NO_2 as a free internal rotor.

The free internal rotor of neutral CH_3NO_2 is modeled as a particle-in-a-ring to obtain the energy levels and corresponding wavefunctions. In this treatment, the Hamiltonian is given by,

Equation 4.2

$$\hat{H} = -\frac{\hbar^2}{2I}\frac{\partial^2}{\partial\varphi^2},$$

where I is the reduced moment of inertia. The reduced moments of inertia were obtained as

Equation 4.3

$$I = \frac{I_{CH_3} \cdot I_{NO_2}}{I_{CH_3} + I_{NO_2}}$$

with the CH_3 and NO_2 group moments of inertia obtained from the calculated geometries relative to the CN bond axis; this is the simplest approximation for the rotor moment of inertia as described by East and Radom.[27] The energy eigenvalues for the free internal rotor are

Equation 4.4

$$E_{F.R.} = J^2 \frac{\hbar^2}{2I} = J^2 C_T; \qquad J = 0, \pm 1, \pm 2, \pm 3, \ldots$$

where J is the quantum number of the free internal rotor and C_T is the torsional constant calculated as $C_T = 5.621$ cm^{-1} and the corresponding normalized, free internal rotor wavefunctions are given by,

Equation 4.5

$$\psi = \frac{1}{\sqrt{2\pi}} e^{iJ\varphi}.$$

The Hamiltonian of the hindered internal rotor of $CH_3NO_2^-$ is

Equation 4.6

$$\widehat{H} = -\frac{\hbar^2}{2I}\frac{\partial^2}{\partial\varphi^2} + V(\varphi) = -C_T \frac{\partial^2}{\partial\varphi^2} + V(\varphi),$$

where $V(\varphi)$ is the torsional potential and $C_T = 5.609$ cm^{-1}. A truncated basis set of free rotor wavefunctions is applied to the hindered internal rotor Hamiltonian, as outlined by Ingham and Strickler[28], as well as Spangler and Pratt[29, 30]. The resulting Hamiltonian matrix,

Equation 4.7

$$H_{JK} = \left(J^2 C_T + \frac{V_0}{2}\right)\delta_{J,K} - \frac{V_0}{4}\delta_{J,K\pm 3},$$

may be diagonalized to yield the hindered-rotor wavefunctions and the corresponding energy eigenstates. For the present study, a basis set from $J = -20$ to $J = +20$ was found to converge; the energies of the free and hindered internal rotor states may be found in Table 4.2 below.

The Franck-Condon factors for the torsional vibration were simulated in Mathematica (Wolfram Research Inc.). A program was written to generate the eigenvectors of the anionic and neutral CH_3NO_2, according to the procedure outlined above, and project the wavefunctions of the anion onto the neutral free internal rotor wavefunctions. The Franck-Condon overlap integral is given by

Equation 4.8

$$FCF(J,n) = \left|\mathcal{B}_n \int_0^{2\pi} \psi_J^*(\phi)\psi_n(\phi)d\phi\right|^2; \qquad J = -20,-19,\ldots,19,20$$

where ψ_J is the wavefunction of the J^{th} neutral internal rotor, ψ_n is the n^{th} hindered internal rotor wavefunction of the anion, and $\mathcal{B}_n$ is the Boltzmann weighting of the n^{th} state in the anion for a temperature specified in the program. Since the hindered internal rotor states are simply expansions in the orthogonal free internal rotor wavefunctions this may be simplified to

Equation 4.9

$$\psi_J^*(\varphi)\psi_n(\varphi) = \psi_J^*(\varphi)\sum_{J\prime=-20}^{20} a_{J\prime}\psi_{J\prime}(\varphi) = a_J \cdot \delta_{J,J\prime}.$$

The transition intensities are imported into PESCAL[22] and convolved with a Gaussian to match the experimental resolution. This approach effectively treats the torsional mode as an independent harmonic oscillator with no Duschinsky mixing with other modes.

Table 4.2 – Lowest Free and Hindered Internal Rotor States

Quantum Number	Free Internal Rotor Energy [cm^{-1}]	Hindered Rotor Energy [cm^{-1}]
0	0.0	106.4
1	5.6	106.4
2	22.5	106.4
3	50.6	312.3
4	89.9	312.3
5	140.5	312.3
6	202.4	503.1
7	275.4	503.2
8	359.7	503.2
9	455.3	676.3
10	562.1	676.3
11	680.1	677.6
12	809.4	821.0
13	949.9	831.2
14	1101.7	831.2
15	1264.7	936.9
16	1439.0	936.9
17	1624.5	984.5
18	1821.2	1019.5
19	2029.2	1093.8
20	2248.4	1093.8

4.3 Results and Analysis

4.3.1 Interpretation of the photoelectron spectrum: the adiabatic electron affinity and the dipole-bound state

The uncertainty in the AEA determination of Compton *et al.*[1] was due to the shape of the PE spectrum, which is dominated by an extended vibrational progression, peaking at a vertical detachment energy of 0.9 eV. The AEA determination was done by using the last discernible peaks at the low binding energy of the spectrum.

Figure 4.2 shows the PE spectra of $CH_3NO_2^-$ at 397 meV (3200 cm^{-1}) and 322 meV (2600 cm^{-1}) photon energy, and a sample PE image is presented in Figure 4.3. This corresponds to the low binding energy side of Compton's *et al.* spectrum (see Figure 4.2). The spectrum is dominated by a progression of intense peaks with spaced by (76 ± 7) meV or (613 ± 56) cm^{-1}. The lower binding energy range shows a series of smaller features with less regular spacing. It should be noted that all photon energies in this study were chosen carefully to avoid the influence of known vibrational autodetachment resonances of the $CH_3NO_2^-$ anion.[4, 10]

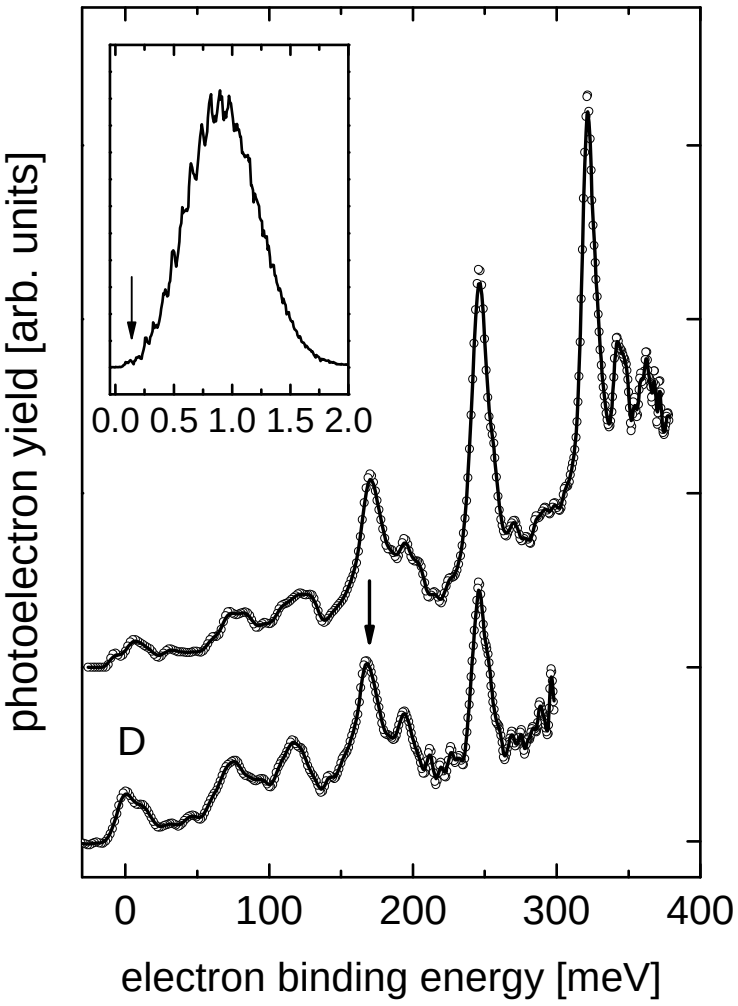

Figure 4.2 – PE spectra of $CH_3NO_2^-$ at 322 meV (2600 cm^{-1}, lower trace), 397 meV (3200 cm^{-1}) and from Ref. 1 (inset, abscissa is in units of eV); the circles are data points, the full lines are five point adjacent averages to guide the eye; the arrow denotes the peak corresponding to the vibrational ground state of the neutral molecule AEA=(168 ± 6) meV; D is the signature of the dipole-bound state.

At this point, three intense features may be assigned to the main vibrational progression, with the vibrational 0-0 origin transition at the nominal peak position of $E_B = (170 \pm 5)$ meV and the features toward lower binding energies are assigned as hot bands. The energy spacing of (613 ± 56) cm^{-1} is in agreement with the value of (645 ± 70) meV or (80 ± 9) meV reported

by Compton *et al.*[1] and corresponds to the 603 cm^{-1} frequency for the NO_2 wag mode of gas-phase CH_3NO_2 reported by Gorse *et al.*[26] The comparison of the spectrum of bare $CH_3NO_2^-$ and that of $CH_3NO_2^- \cdot Ar$ (see Figure 4.4) corroborates this assignment. The series of intense peaks spaced by 76 meV is shifted by (63 ± 7) meV toward higher binding energies upon Ar solvation. The hot bands at lower binding energies are suppressed for $CH_3NO_2^- \cdot Ar$ because of the much lower internal energy of the argon complex. The PE spectrum of $CH_3NO_2^- \cdot Ar_2$ (not shown) is shifted by an additional (61 ± 7) meV relative to that of $CH_3NO_2^- \cdot Ar$. This very regular behavior in the Ar-induced shifts confirms our identification of the hot bands in the spectrum of bare $CH_3NO_2^-$. Therefore, we determine the AEA of CH_3NO_2 to be (168 ± 6) meV (after corrections for torsional and rotational contour shifts discussed below).

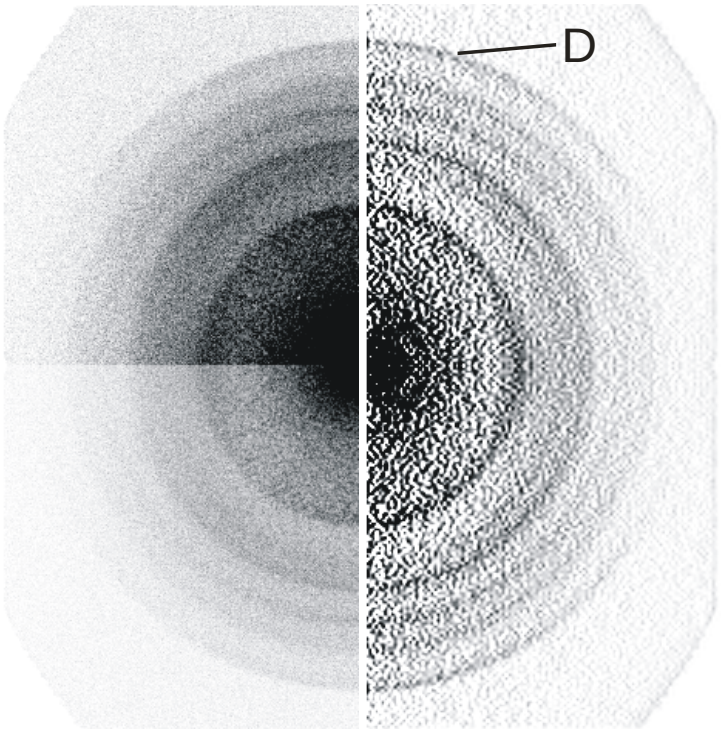

Figure 4.3 – PE image of $CH_3NO_2^-$ at 322 meV (2600 cm^{-1}) photon energy, based on one quadrant of the raw PE image. The left half of the figure contains the raw PE image with the intensity in the upper portion doubled to better show the dynamic range of the image without saturating the gray scale. The right half of the figure shows the BASEX transformed image with the "center-line artifact" from the BASEX transformed image removed. The signature belonging to the dipole-bound state has been labeled "D."

Comparing the geometries of anionic and neutral CH_3NO_2, the most prominent geometry difference between the two charge states is the position of the NO_2 group relative to the CN bond; this difference will likely lead to significant activity in this mode and result in an extended vibrational progression in the PE spectrum. Based on this assumption, we can tentatively assign the most intense peaks in the experimental PE spectrum of $CH_3NO_2^-$ at 397 meV (3200 cm^{-1}) photon energy as the first three members of a progression of the neutral NO_2 wagging mode $\nu_1^{(0)}$ (see Table 4.1 above for the labeling of the modes) with quantum numbers $n_1^{(0)} = 0, 1, \text{and } 2$. In addition, we can identify a peak at (122 ± 5) meV binding energy as a hot band of the anionic NO_2 wagging mode $\nu_1^{(-)}$, i.e., corresponding to the transition $(n_1^{(0)} = 0) \leftarrow (n_1^{(-)} = 1)$, and a peak at (77 ± 5) as a hot band in the same mode but corresponding to the $(n_1^{(0)} = 0) \leftarrow (n_1^{(-)} = 2)$ transition. We therefore arrive at an experimental frequency for the anionic NO_2 wagging mode of (380 ± 56) cm^{-1}. A band at (195 ± 5) meV binding energy is the signature of the transition $(n_1^{(0)} = 1) \leftarrow (n_1^{(-)} = 1)$. The higher order members, i.e., $(n_1^{(0)} > 1)$, of this progression are very weak but observable as shoulders on the higher energy sides of the intense neutral progression. We note that other low-frequency modes may contribute to the observed hot bands. A more thorough discussion on the assignment of the observed vibrational features based on the Franck-Condon simulations will be presented below (see Section 4.3.3).

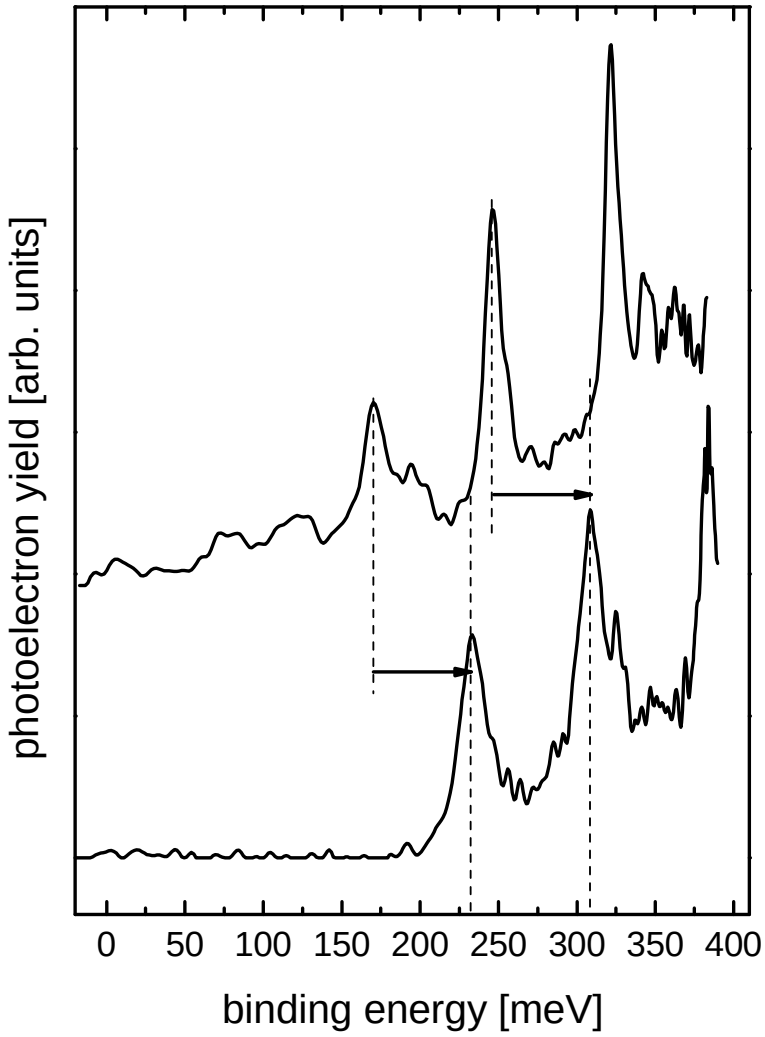

Figure 4.4 – PE spectra of $CH_3NO_2^-$ (upper trace) and $CH_3NO_2^-$·Ar (lower trace) at 397 meV (3200 cm^{-1}) photon energy. The dashed lines and arrows show how the vibrational progression of the neutral molecule shifts by 63 meV toward higher binding energies upon solvation by one Ar atom.

The PE spectra of bare $CH_3NO_2^-$ show a weak feature at a binding energy of (8 ± 8) meV. This feature does not correspond to any of the possible anion vibrational modes with any appreciable Franck-Condon intensity (see below), which makes it highly unlikely to be a hot band. Compton *et al.*[1] determined the binding energy of the dipole-bound state of $CH_3NO_2^-$

populated in Rydberg electron transfer experiments to be (12 ± 3) meV, in agreement with the feature at low binding energies to the dipole-bound state of $CH_3NO_2^-$, which has not been observed previously by PE spectroscopy. The signature of the dipole-bound state is absent in the PE spectrum of $CH_3NO_2^- \cdot Ar$ (as can be seen in Figure 4.4). This behavior is in agreement with previous observations that have determined that the presence of an argon atom will only lead to the formation of the valence-bound state, as solvation should lead to a greater stabilization of the valence state relative to the dipole-bound state.[2] The existence of the dipole-bound state at relatively long lifetimes (i.e., ~ 25 μs) provides evidence that the dipole bound state is metastable.[2] As will be discussed below, the anisotropy of the photodetached electrons from this feature (taken at several photon energies) does not follow the same trend as those from clearly valence-bound hot bands, hinting at the involvement of a different electronic state.

4.3.2 Photoelectron Angular Distributions

Anisotropy parameters were determined as a function of electron kinetic energy for several photon energies: 285 meV (2300 cm^{-1}), 310 meV (2500 cm^{-1}), 322 meV (2600 cm^{-1}), 397 meV (3200 cm^{-1}). The anisotropy parameters were fitted at known vibrational features, including hot bands, in the PE spectrum; additionally, the anisotropy parameter was determined for the feature at (8 ± 8) meV, tentatively assigned as the dipole-bound state, for each wavelength.

At the low kinetic energies, accessed by the photon energies used in this study, Wigner's threshold law[31] governs the relative weighting of the allowed partial waves. This stipulates that the relative cross section σ_ℓ of a partial wave with given orbital angular momentum ℓ behaves as

Equation 4.10

$$\sigma_\ell \propto E_K^{\ell+1/2}$$

As s waves (i.e., $\ell = 0$) are isotropic ($\beta = 0$), and dominate at low kinetic energies over the contributions of partial waves with higher orbital angular momentum, we expect the anisotropy parameter to progressively deviate from $\beta = 0$ as E_K increases. For a given electronic final state, the variation of β with energy is expected to be monotonic and smooth. Inspecting the experimental results for $CH_3NO_2^-$ (see Figure 4.5) we observe that the values of the anisotropy parameter for the valence states (including hot bands) follow a consistent trend, increasing from $\beta \approx 0$ (outgoing s-wave) at low E_K to $\beta \approx 1.25$ for $E_K \approx 325$ meV. This is consistent with the contribution from the s partial wave dominating at low kinetic energies, while higher angular momenta play an increasing role as E_K increases. We caution that Wigner's threshold law strictly only holds for electron-molecule interaction potentials that fall off faster than $1/r^2$. Interactions with polar molecules, especially those with a dipole moment sufficiently large to support a bound state, can behave stepwise and oscillatory.[32]

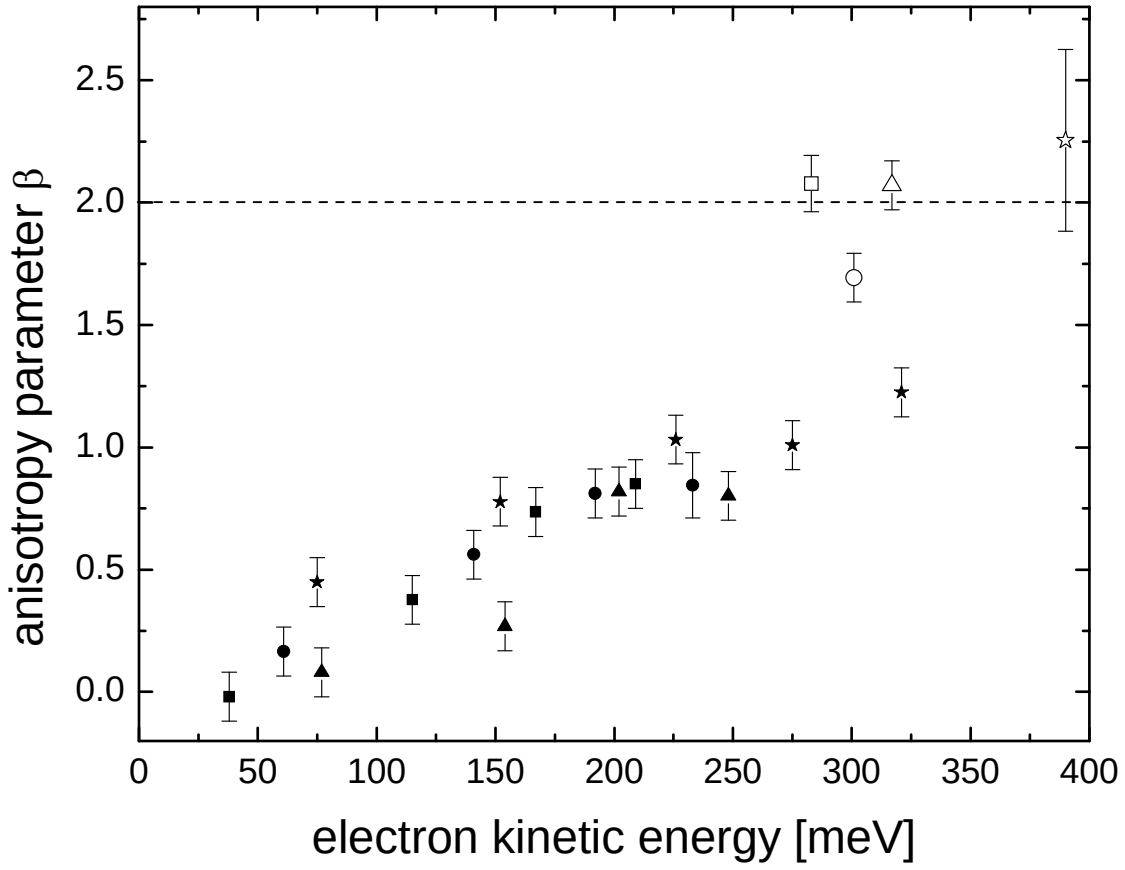

Figure 4.5 – Anisotropy parameters are presented as a function of electron kinetic energy for different photon energies. Squares, circles, triangles, and stars correspond to data taken at 285 meV (2300 cm^{-1}), 310 meV (2500 cm^{-1}), 322 meV (2600 cm^{-1}), and 397 meV (3200 cm^{-1}), respectively. Filled symbols correspond to the valence electronic state, while the open symbols belong to the dipole-bound state. The data points marked with larger circles belong to the hot bands at binding energies of 77 and 122 meV. Error bars have been conservatively estimated to be ±0.1, except in cases where fits of the angular distributions resulted in larger error bars because of poorer signal-to-noise ratios. The dashed line shows the theoretical maximum value for the anisotropy parameter (β = 2).

In contrast to the valence state (including the hot bands), photodetachment from the dipole-bound state results in $\beta \approx 2$ for all data points corresponding to this state for all photon energies (see Figure 4.5). This dramatic difference confirms that the electrons in this feature originate from a different electronic ground state of the anion. Moreover, the large β value is consistent with a nearly pure p character for the outgoing wave, similar to photodetachment from

H^- ions,[33, 34] resulting from photodetachment of an *s*-like orbital. The dipole-bound state is expected to be spatially extended and *s*-like in shape. This is consistent with our observations along the lines of this simple argument. We note, however, that an outgoing *p*-wave is not the only possibility to generate a $\beta \approx 2$ anisotropy parameter.[35, 36]

4.3.3 Franck-Condon Simulation

In the photodetachment transition from $CH_3NO_2^-$ to CH_3NO_2, the largest geometry displacement is along the NO_2 wagging normal coordinate with the known frequency[26] of 603 cm^{-1} in the neutral. As discussed above, this mode accounts for the major Franck-Condon active progression in the PE spectrum according to the simulation based on the DFT calculations. Four other modes, listed as modes 2-5 in Table 4.1 above, also show substantial Franck-Condon activity, primarily for their 1←0 and 2←0 transitions. Together these five modes account for over 90% of the Franck-Condon profile intensities. Combination bands involving modes 3-5 with frequencies of 1100-1300 cm^{-1} tend to overlap with the transitions from the NO_2 wagging mode at moderate resolution, causing shifts in the observed peaks; this near degeneracy accounts for the observed spacing of 645 cm^{-1} reported by Compton *et al.*[1]

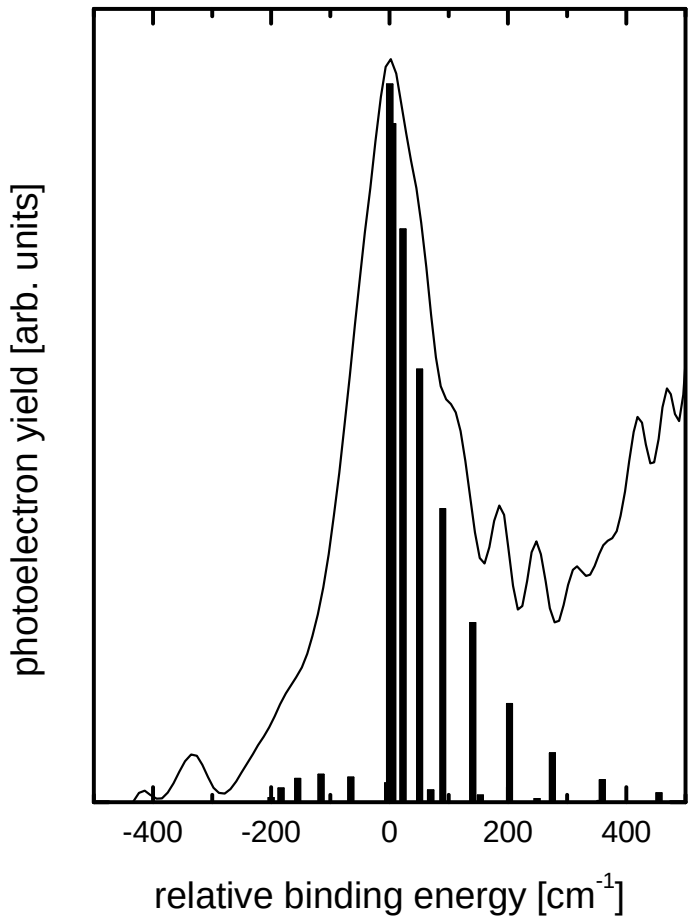

Figure 4.6 – Comparison of the torsional Franck-Condon simulation (vertical sticks) at 100 K temperature and the experimental results for $CH_3NO_2^-$·Ar, shifted by the EA of the Ar complex (full line).

As a consequence of the differences in geometry between anionic and neutral CH_3NO_2, the character of the internal rotation of the methyl group changes completely upon electron detachment. In the anion, the methyl rotor is strongly hindered, while it is essentially a free rotor in the neutral. This leads to each vibrational band being accompanied by combination bands involving the hindered-to-free internal rotor transitions. Figure 4.6 shows that the simulated spectrum for $CH_3NO_2^-$ at 100 K in comparison with the experimental PE spectrum will be virtually free of hot bands, as the presence of the weakly bound argon demands. While the

individual transitions are not resolved in the experimental spectrum, the shape of the 0←0 band is clearly asymmetric with a steeper low binding energy slope. On the basis of our Franck-Condon calculations, we argue that this asymmetry is mainly due to the hindered-to-free methyl rotor transitions. A stick spectrum of the Franck-Condon transitions for the torsional modes is shown in Figure 4.6. Because the upper state is nearly a free rotor and the lower state hindered-rotor ground-state wavefunction includes components of a series of free-rotor basis set functions that overlap with the free-rotor wave functions, the simulated spectrum is qualitatively reminiscent of rotational structure. In the independent oscillator approximation, this structure is repeated for every vibrational transition in the nitromethane spectrum. At the available experimental resolution, the individual torsional transitions are not resolved but they contribute to the broadening of the observed transitions.

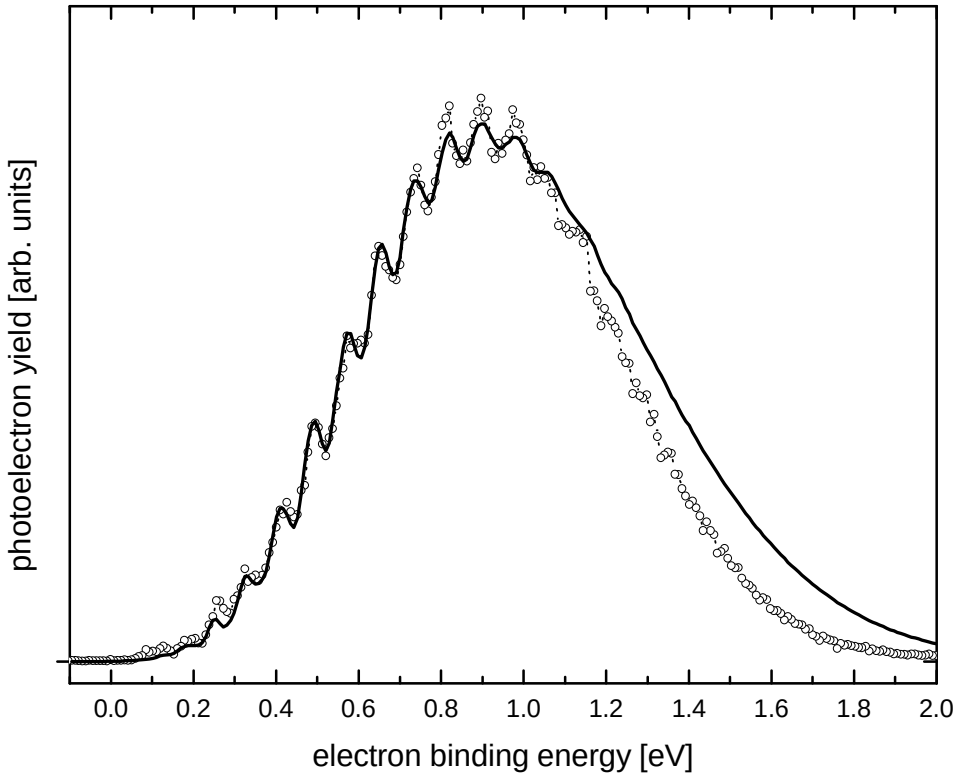

Figure 4.7 – Comparison of the experimental PE spectrum by Compton et al. (Ref 1) with a fitted Franck-Condon simulation (see text).

Rotational contours were calculated as described previously[37, 38] using DFT geometries and treating the anion and neutral as asymmetric tops. At the experimental resolution, the rotational contours are only slight asymmetric and the peak shift is -1.2 meV at 250 K. The contour due to the internal torsional transitions shifts the peaks an additional -1.0 meV. Inclusion of the shifts, at a temperature of 250 K, gives a net shift of (-2.2 ± 1) meV. This shift has been accounted for in the electron affinity values reported above.

Because the low-energy imaging PE spectra exhibit only the first few transitions of the Franck-Condon envelope, Franck-Condon fits where the geometry displacements are optimized

are not well constrained by the present experiments. In addition, variations in the photodetachment cross sections are expected owing to threshold effects for imaging spectra taken at low photon energies. Therefore, we first compare the Franck-Condon simulations to the CH_3NO_2 PE spectrum of Compton *et al.*,[1] which was taken at a photon energy of 2.54 eV and exhibits the entire Franck-Condon band profile. Figure 4.7 compares the PE spectrum with Franck-Condon simulations using normal coordinates from the DFT calculations, frequencies given in Table 4.1, and the origin assignment as obtained from our imaging experiments. The peaks are convolved by a Gaussian function with a FWHM of 30 meV as reported for the instrumental resolution.[1] An anion vibrational temperature of 300 K is assumed. The raw calculated displacements already gave a very good match with the experimental spectrum, but the displacements for the first five modes, the electron affinity, and a scaling factor were optimized to provide a least-squares fit to the experiment over the electron binding energy range of $0 - 1.3$ eV. The optimized displacements are given in Table 4.1. The changes from the calculated displacements are minor and should be considered as qualitative values because individual transitions for the five optimized modes are not resolved in the experiment. The optimized electron affinity is 168 meV, in excellent agreement with the imaging result of (168 ± 6) meV. As shown in Figure 4.7, the simulation provides an excellent fit to the experimental PE spectrum, especially considering that anharmonicity effects are not included, even though the progression of the NO_2 wagging mode extends to fairly high vibrational levels. This agreement confirms that the PE spectrum of Compton *et al.*[1] is consistent with our origin assignment from low-energy PE imaging. As indicated by Compton *et al.*, however, their spectrum alone is insufficient for a definitive assignment of the origin. Indeed, we could also produce reasonable Franck-Condon fits with assignments of $\mathrm{EA} \approx 20, 95, \text{or } 245$ meV.

Therefore, the higher resolution and lower temperature imaging experiments are essential for determining a precise electron affinity.

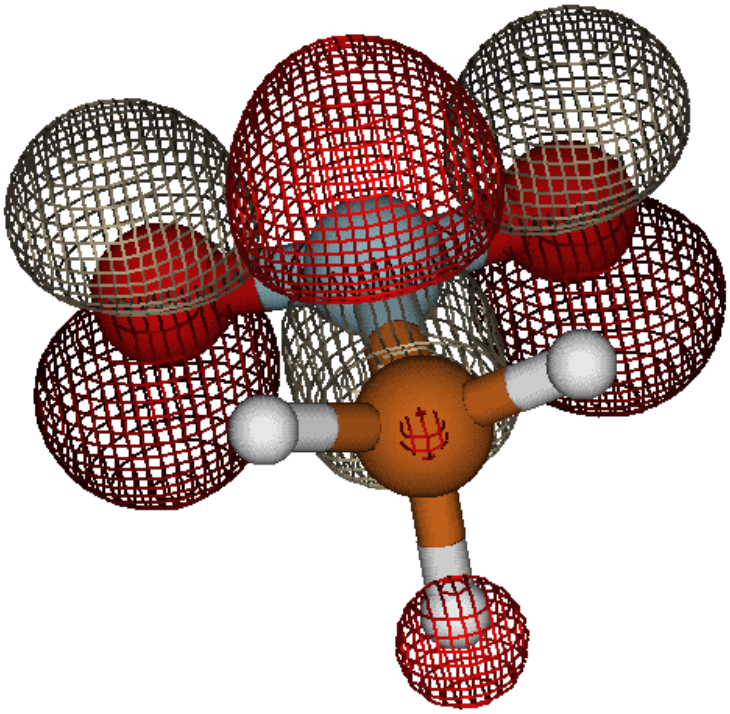

Figure 4.8 – HOMO of $CH_3NO_2^-$. The HOMO is mainly localized on the nitro group, but small parts also penetrate into the rest of the molecule, notably the σ^* antibonding orbital of the CH group *syn* to the nitro group.

For the present purposes, we now have a validated set of Franck-Condon intensity parameters constrained to match the full experimental PE spectrum.[1] These may be used to compare Franck-Condon simulations with the present experiments. However, because the imaging spectra are taken at near-threshold photon energies, it is also necessary to consider the dependence of the photodetachment cross section on PE velocity, which can modify the Franck-Condon intensities. As discussed earlier (see Chapter 1), there is no simple or general functional form for the velocity dependence for molecular anion photodetachment intensities, as it depends on the details of the interference of outgoing electron waves from molecular orbitals arising from

a mixture of atomic orbitals on different centers. Nevertheless, some general considerations apply (neglecting the influence of the dipole moment of the neutral molecule): (1) First, the leading term for the velocity dependence is proportional to $E_K^{1/2}$. This electron velocity factor appears in the coefficient of the expressions for atomic negative ion photodetachment cross sections given by Massey,[39] for molecular photodetachment by Reed *et al.*,[40] and was cited by Ervin and co-workers[37, 38] as appropriate for scaling Franck-Condon factors in PE spectroscopy simulations. Because $E_K^{1/2}$ gives a relatively slow variation at moderate electron kinetic energies, E_K, this factor usually has a very minor effect on the Franck-Condon simulation for conventional negative ion PE spectroscopy, i.e., for photon energies in the 2-4 eV range and electron kinetic energies greater than 0.3 eV over the energy range of typical vibronic transitions. The $E_K^{1/2}$ scaling factor is exact for pure s-wave detachment and will predominate over higher-order terms very near threshold. However, scaling proportional to $E_K^{1/2}$ is incorrect in general when detachment involves higher-order electron waves with possible interference effects. Pure p-wave detachment (or higher-order spherical harmonics) with $E_K^{3/2}$ dependence (or higher powers) can become relevant at slightly higher kinetic energies, until the detachment behavior is no longer governed by Wigner's law. Detailed evaluation of the photodetachment matrix elements as a function of photon energy and averaging over molecular orientations is required for complete treatment.[40-42] (2) Second, using the approach outlined by Reed *et al.*,[40] which is discussed in more detail in Chapter 2, a comparison of the overall group symmetry of the highest occupied molecular orbital (HOMO) from which the electron is detached to atomic orbital symmetry can be used to predict the dominant near-threshold electron detachment symmetry. For the present case, the HOMO of $CH_3NO_2^-$ is an A' orbital centered on the NO_2 group composed predominantly of p-orbitals pointing out of the ONO plane with the same phase on the

O atom and the opposite phase on the N atom. This orbital is illustrated in Figure 4.8; in the pseudoatomic limit the HOMO exhibits d-like symmetry with two angular nodes (one in the ONO plane and one passing between the N atom and the two O atoms). That would imply that the detachment would result in a p-wave as a first-order approximation. However, the HOMO also includes other atomic orbital components with smaller coefficients, which will complicate this picture. (3) Third, the angular distribution of the photodetachment relative to the electric field vector of the laser provides complementary information regarding the symmetry of the photodetached electron wave. In the present case, the detachment at the lowest electron velocities exhibits isotropic s-wave behavior ($\beta \approx 0$) as shown in Figure 4.5, which implies $\ell = 0$, but increases with increasing photoelectron velocities suggesting that higher-order terms become important.

Experimental evidence shows that near-threshold low-electron-velocity detachment transitions in imaging experiments are indeed suppressed compared to Franck-Condon intensities. For example, Surber and Sanov[43] noted the diminution of near-threshold transitions compared to Franck-Condon intensities in the CS_2^- imaging PE spectrum. This effect is also evident in the present experiments as may be seen by comparing the relative intensities of the 0←0 and 1←0 NO_2 wagging transitions in the spectra in Figure 4.2 taken at several different photon energies. The 1←0 transition has a lower relative intensity in the spectrum taken at lower photon energy where it is closer to threshold.

The imaging spectrum at 397 meV (3200 cm^{-1}) photon energy is compared to Franck-Condon simulations in Figure 4.9. Three simulations are shown: one without electron velocity scaling (simple Franck-Condon approximation), one scaled by $E_K^{1/2}$ (pure s-wave

detachment), and one scaled by $E_K^{3/2}$ (pure p-wave detachment). Comparing the simulation without velocity scaling, it is obvious that transitions at low electron velocity (high electron binding energy) are strongly suppressed. The simulations that are scaled by $E_K^{1/2}$ or $E_K^{3/2}$ better match the relative intensities of the observed spectrum, but neither is an exact fit over the whole energy range. That behavior suggests that a more sophisticated calculation of the photodetachment cross sections as function of photoelectron velocity, including multiple terms, would be required to match the experimental intensities. Nevertheless, the overall match between the experimental spectrum and the simulations is sufficient to verify the assignments of the transitions discussed above.

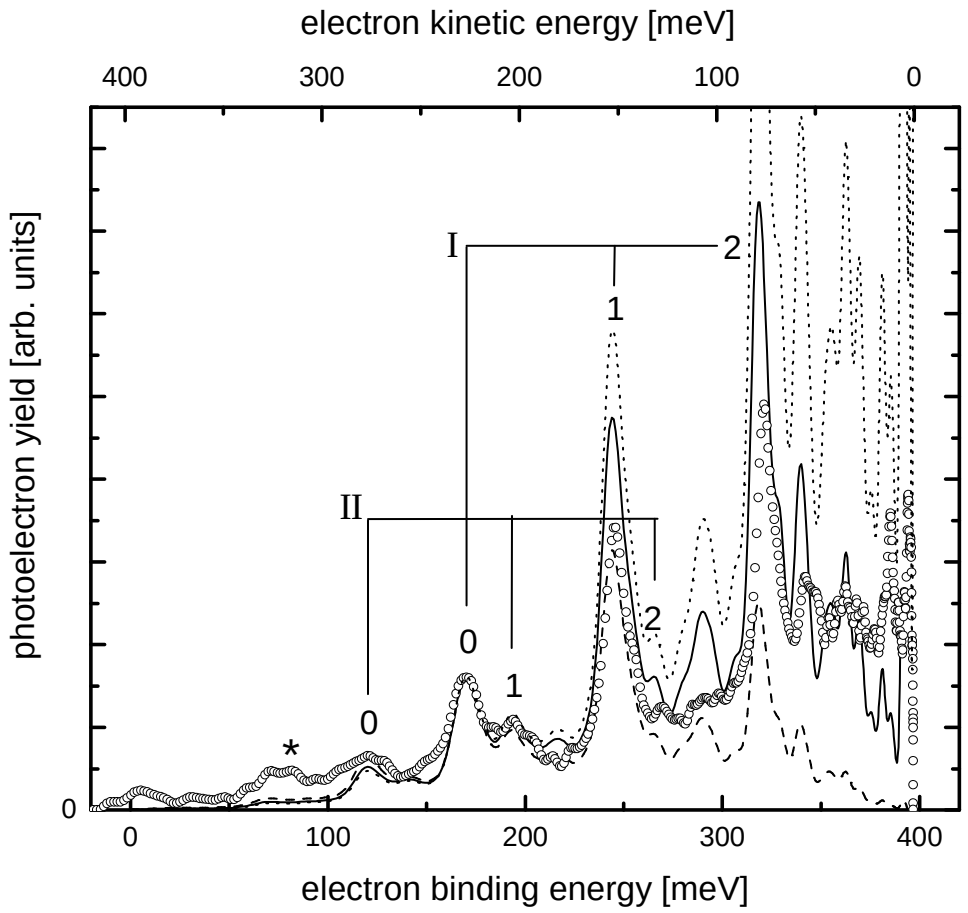

Figure 4.9 – Franck-Condon fits to the experimental PE spectrum of $CH_3NO_2^-$ (open circles) at 397 meV (3200 cm^{-1}) with no velocity scaling (dotted line), scaled with $E_K^{1/2}$ (pure *s*-wave, full line), and scaled with $E_K^{3/2}$ (pure *p*-wave, dashed line); see text for details. The sequences marked in the spectrum are based on the NO_2 wagging mode ν_1 with transitions *n*←0 (series I) and *n*←1 (series II). The asterisk marks the 0←2 hot band of the NO_2 wagging mode. Note that the top scale shows the electron kinetic energy while the bottom scale gives the electron binding energy.

The intensity of the hot band assigned in Figure 4.9 as the $0 \leftarrow 2$ ($E_B \approx 77$ meV) transition to the NO_2 wagging mode is about a factor of four higher than predicted by the Franck-Condon simulations. The simulations in Figure 4.9 use an anion temperature of 250 K, which roughly reproduces the relative intensities of the $0 \leftarrow 0$ origin and nearby $1 \leftarrow 1$ sequence band of the wagging mode. At this temperature, the observed intensity of the $0 \leftarrow 2$ band is too high

relative to the $0 \leftarrow 1$ and $0 \leftarrow 0$ transitions to be explained by a Boltzmann distribution. However, if the anion vibrational temperature is increased to 400 K to match the $0 \leftarrow 2$ hot band intensity, then the intensities of the $n \leftarrow 2$ transitions for $n = 1, 2, \text{and } 3$ are too strong compared to the experiment. The source of this discrepancy is uncertain; however, it is possible that when sufficient energy is pooled into the low-lying modes of nitromethane, i.e., the wagging mode, the internal rotor, etc. the vibrational modes are not sufficiently modeled as independent harmonic oscillators resulting in a poor recovery of the spectrum within the limitations of our simulations. The disappearance of the peak in the cold $CH_3NO_2^- \bullet$ Ar spectrum (Figure 4.4) and the fact that its anisotropy follows the same trend as the main progression (Figure 4.5) imply that this feature is indeed due to hot bands and is unrelated to the dipole-bound state (peak D in Figure 4.2). Finally, we note that the two vibrational hot bands predicted to be nearest the dipole-bound detachment peak at $E_B = (8 \pm 8)$ meV are $0 \leftarrow 3$ NO_2 wag transition at $E_B = 19.1$ meV and a combination of $0 \leftarrow 1$ in the NO_2 wag and $0 \leftarrow 1$ in the CN stretch at $E_B = 15.4$ meV. Even allowing for frequency shifts (and ignoring the distinctive anisotropy of peak D), the calculated Franck-Condon intensities of these hot bands are each less than 0.3% of the $0 \leftarrow 0$ origin peak, much too small to account for the observed feature.

4.3.4 CN bond energy

As was outlined by Sanov *et al.*,[44] the AEA may be used to establish the bond dissociation energy of the C-N bond in $CH_3NO_2^-$: $BDE_{C\text{-}N} = 0.477$ eV, using the following thermodynamic quantities in the thermochemical cycle illustrated in Figure 4.10. The presence

of the excess electron serves to destabilize the CN bond in nitromethane making the bond almost five times weaker than in neutral CH_3NO_2.

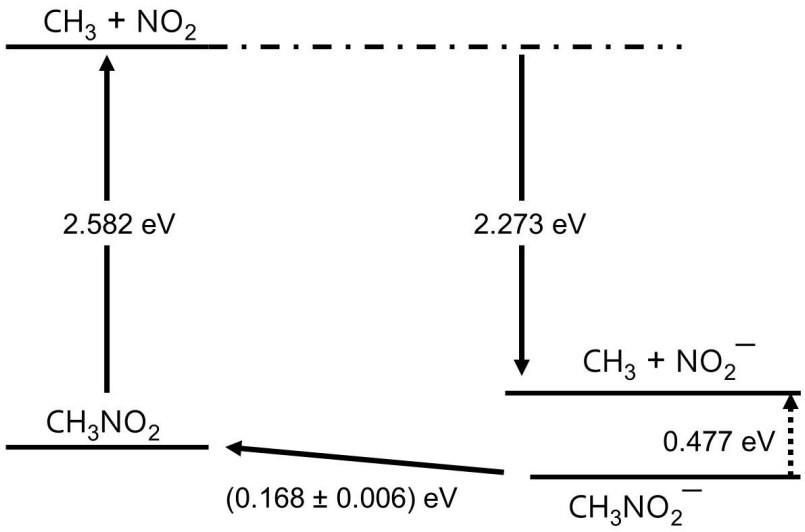

Figure 4.10 – Thermochemical cycle for the determination of the BDE_{CN} in nitromethane anion.

4.4 Summary and Conclusions

We have studied the photoelectron energy spectra and angular distributions for low-energy photodetachment of nitromethane anions. We have determined a more accurate and precise value of the AEA of nitromethane (168 ± 6) meV, and we were able to unambiguously assign many of the vibrational features in the PE spectrum. The most intense peaks observed in the PE spectrum are due to progressions of the neutral NO_2 wagging mode. We observe a long-lived ($> 25\ \mu s$) dipole-bound state of the nitromethane anion, clearly identifiable through its anisotropy, which is very different from the valence-state based vibrational features. We postulate the existence of bound-to-free internal rotor transitions of the internal methyl rotor, which are unresolved in the present PE spectra, but are the cause for an asymmetry in the

prominent vibrational features and contribute strongly to the spectral congestion of the PE spectra. Future high-resolution PE spectroscopy experiments at even lower photon energies may be able to resolve these features.

4.5 References for Chapter 3

1. R. N. Compton, H. S. Carman, C. Desfrancois, H. Abdoul-Carmine, J. P. Schermann, J. H. Hendricks, S. A. Lyapustina and K. H. Bowen,"On the binding of electrons to nitromethane: Dipole and valence bound anions." *Journal of Chemical Physics* **105** (9), 3472-3478 (1996).

2. F. Lecomte, S. Carles, C. Desfrancois and M. A. Johnson,"Dipole bound and valence state coupling in argon-solvated nitromethane anions." *Journal of Chemical Physics* **113** (24), 10973-10977 (2000).

3. L. Suess, R. Parthasarathy and F. B. Dunning,"Rydberg electron transfer to CH_3NO_2: Lifetimes and characteristics of the product $CH_3NO_2^-$ ions." *Journal of Chemical Physics* **119** (18), 9532-9537 (2003).

4. J. M. Weber, W. H. Robertson and M. A. Johnson,"Argon predissociation and electron autodetachment spectroscopy of size-selected $CH_3NO_2^-\cdot Ar_n$ clusters." *Journal of Chemical Physics* **115** (23), 10718-10723 (2001).

5. A. Modelli and M. Venuti,"Empty level structure and dissociative electron attachment in gas-phase nitro derivatives." *International Journal of Mass Spectrometry* **205** (1-3), 7-16 (2001).

6. I. C. Walker and M. A. D. Fluendy,"Spectroscopy and dynamics of nitromethane (CH3NO2) and its anionic states." *International Journal of Mass Spectrometry* **205** (1-3), 171-182 (2001).

7. W. Sailer, A. Pelc, S. Matejcik, E. Illenberger, P. Scheier and T. D. Mark,"Dissociative electron attachment study to nitromethane." *Journal of Chemical Physics* **117** (17), 7989-7994 (2002).

8. C. Q. Jiao, C. A. DeJoseph and A. Garscadden,"Formation of positive and negative ions in CH3NO2." *Journal of Physical Chemistry A* **107** (42), 9040-9044 (2003).

9. E. Alizadeh, F. F. da Silva, F. Zappa, A. Mauracher, A. Probst, S. Denifl, A. Bacher, T. D. Mark, P. Limao-Vieira and P. Scheier,"Dissociative electron attachment to nitromethane." *International Journal of Mass Spectrometry* **271** (1-3), 15-21 (2008).

10. H. Schneider, K. M. Vogelhuber, F. Schinle, J. F. Stanton and J. M. Weber,"Vibrational spectroscopy of nitroalkane chains using electron autodetachment and Ar predissociation." *Journal of Physical Chemistry A* **112** (33), 7498-7506 (2008).

11. G. L. Gutsev and R. J. Bartlett,"A theoretical study of the valence- and dipole-bound states of the nitromethane anion." *Journal of Chemical Physics* **105** (19), 8785-8792 (1996).

12. T. Sommerfeld,"Coupling between dipole-bound and valence states: the nitromethane anion." *Physical Chemistry Chemical Physics* **4** (12), 2511-2516 (2002).

13. G. L. Gutsev, P. Jena and R. J. Bartlett,"Thermodynamical stability of CH_3ONO and CH_3ONO^-: A coupled-cluster and Hartree-Fock-density-functional-theory study." *Journal of Chemical Physics* **110** (1), 403-411 (1999).

14. M. J. Frisch, G. W. Trucks, H. B. Schlegel, G. E. Scuseria, M. A. Robb, J. R. Cheeseman, J. A. Montgomery, J. Vreven, T. , K. N. Kudin, J. C. Burant, J. M. Millam, S. S. Iyengar, J. Tomasi, V. Barone, B. Mennucci, M. Cossi, G. Scalmani, N. Rega, G. A. Petersson, H. Nakatsuji, M. Hada, M. Ehara, K. Toyota, R. Fukuda, J. Hasegawa, M. Ishida, T. Nakajima, Y. Honda, O. Kitao, H. Nakai, M. Klene, X. Li, J. E. Knox, H. P. Hratchian, J. B. Cross, V. Bakken, C. Adamo, J. Jaramillo, R. Gomperts, R. E. Stratmann, O. Yazyev, A. J. Austin, R. Cammi, C. Pomelli, J. W. Ochterski, P. Y. Ayala, K. Morokuma, G. A. Voth, P. Salvador, J. J. Dannenberg, V. G. Zakrzewski, S. Dapprich, A. D. Daniels, M. C. Strain, O. Farkas, D. K. Malick, A. D. Rabuck, K. Raghavachari, J. B. Foresman, J. V. Ortiz, Q. Cui, A. G. Baboul, S. Clifford, J. Cioslowski, B. B. Stefanov, G. Liu, A. Liashenko, P. Piskorz, I. Komaromi, R. L. Martin, D. J. Fox, T. Keith, M. A. Al-Laham, C. Y. Peng, A. Nanayakkara, M. Challacombe, P. M. W. Gill, B. Johnson, W. Chen, M. W. Wong, C. Gonzalez and J. A. Pople, Gaussian 03, Wallingford CT, 2004.

15. A. D. Becke,"Density-Functional Thermochemistry .3. The Role of Exact Exchange." *Journal of Chemical Physics* **98** (7), 5648-5652 (1993).

16. C. T. Lee, W. T. Yang and R. G. Parr,"Development of the Colle-Salvetti Correlation-Energy Formula into a Functional of the Electron-Density." *Physical Review B* **37** (2), 785-789 (1988).

17. A. D. McLean and G. S. Chandler,"Contracted Gaussian-Basis Sets for Molecular Calculations .1. 2nd Row Atoms, Z=11-18." *Journal of Chemical Physics* **72** (10), 5639-5648 (1980).

18. R. Krishnan, J. S. Binkley, R. Seeger and J. A. Pople,"Self-Consistent Molecular-Orbital Methods .20. Basis Set for Correlated Wave-Functions." *Journal of Chemical Physics* **72** (1), 650-654 (1980).

19. J. A. Pople, M. Head-Gordon and K. Raghavachari,"Quadratic Configuration-Interaction - a General Technique for Determining Electron Correlation Energies." *Journal of Chemical Physics* **87** (10), 5968-5975 (1987).

20. J. T. H. Dunning,"Gaussian basis sets for use in correlated molecular calculations. I. The atoms boron through neon and hydrogen." *The Journal of Chemical Physics* **90** (2), 1007-1023 (1989).

21. K. M. Ervin, T. M. Ramond, G. E. Davico, R. L. Schwartz, S. M. Casey and W. C. Lineberger,"Naphthyl radical: Negative ion photoelectron spectroscopy, Franck-Condon simulation, and thermochemistry." *Journal of Physical Chemistry A* **105** (48), 10822-10831 (2001).

22. K. M. Ervin, PESCAL, University of Nevada, Reno, 2008.

23. F. Duschinsky,"The importance of the electron spectrum in multi atomic molecules. concerning the Franck-Condon principle." *Acta Physicochimica URSS* **7** (4), 551-566 (1937).

24. T. E. Sharp and H. M. Rosenstock,"Franck-Condon Factors for Polyatomic Molecules." *Journal of Chemical Physics* **41** (11), 3453-& (1964).

25. P. Chen, in *Unimolecular and Bimolecular Reaction Dynamics*, edited by C.-Y. Ng, T. Baer and I. Powis (John Wiley & Sons, Chichester, 1994), pp. 371.

26. D. Gorse, D. Cavagnat, M. Pesquer and C. Lapouge,"Theoretical and Spectroscopic Study of Asymmetric Methyl Rotor Dynamics in Gaseous Partially Deuterated Nitromethanes." *Journal of Physical Chemistry* **97** (17), 4262-4269 (1993).

27. A. L. L. East and L. Radom,"Ab initio statistical thermodynamical models for the computation of third-law entropies." *Journal of Chemical Physics* **106** (16), 6655-6674 (1997).

28. K. C. Ingham and Strickle.Sj,"Hindered Rotation in Ground and Excited Electronic States of Ortho-Xylene." *Journal of Chemical Physics* **53** (11), 4313-& (1970).

29. L. H. Spangler and D. W. Pratt,"Laser-Induced Phosphorescence Spectroscopy in Supersonic Jets - the Lowest Triplet-States of Glyoxal, Methylglyoxal, and Biacetyl." *Journal of Chemical Physics* **84** (9), 4789-4796 (1986).

30. L. H. Spangler,"Structural information from methyl internal rotation spectroscopy." *Annual Review of Physical Chemistry* **48**, 481-510 (1997).

31. E. P. Wigner,"On the Behavior of Cross Sections near Thresholds." *Physical Review* **73** (9), 1002-1009 (1948).

32. P. C. Engelking,"Strong Electron-Dipole Coupling in Photodetachment of Molecular Negative-Ions - Anomalous Rotational Thresholds." *Physical Review A* **26** (2), 740-745 (1982).

33. J. Cooper and R. N. Zare,"Angular Distribution of Photoelectrons." *Journal of Chemical Physics* **48** (2), 942-943 (1968).

34. J. L. Hall and M. W. Siegel,"Angular Dependence of the Laser Photodetachment of the Negative Ions of Carbon, Ozygen, and Hydrogen." *Journal of Chemical Physics* **48** (2), 943 (1968).

35. C. H. Greene,"Manifestation of Dynamically Unfavored Transitions in the Angular-Distribution of Photofragments." *Physical Review Letters* **44** (13), 869-871 (1980).

36. C. Pan, A. F. Starace and C. H. Greene,"Parallels between High Doubly-Excited State Spectra in H^- and Li^- Photodetachment." *Journal of Physics B-Atomic Molecular and Optical Physics* **27** (8), L137-L142 (1994).

37. K. M. Ervin, J. Ho and W. C. Lineberger,"Ultraviolet Photoelectron Spectrum of NO_2." *Journal of Physical Chemistry* **92** (19), 5405-5412 (1988).

38. C. T. Wickham-Jones, K. M. Ervin, G. B. Ellison and W. C. Lineberger,"NH_2 Electron-Affinity." *Journal of Chemical Physics* **91** (4), 2762-2763 (1989).

39. H. W. W. Massey, *Negative Ions*. (Cambridge Press, Cambridge, 1976).

40. K. J. Reed, A. H. Zimmerman, H. C. Andersen and J. I. Brauman,"Cross-Sections for Photodetachment of Electrons from Negative-Ions near Threshold." *Journal of Chemical Physics* **64** (4), 1368-1375 (1976).

41. W. B. Clodius, R. M. Stehman and S. B. Woo,"Zero-Core-Contribution Calculation of a Polyatomic Photodetachment Cross-Section - NO_2." *Physical Review A* **28** (2), 760-765 (1983).

42. R. M. Stehman and S. B. Woo,"Zero-Core-Contribution Calculation of Photodetachment Cross-Sections of O_2^- and S_2." *Physical Review A* **23** (6), 2866-2876 (1981).

43. E. Surber and A. Sanov,"Photoelectron imaging spectroscopy of molecular and cluster anions: CS_2^- and $OCS^-(H_2O)_{1,2}$." *Journal of Chemical Physics* **116** (14), 5921-5924 (2002).

44. D. J. Goebbert, D. Khuseynov and A. Sanov,"Photodissociation of nitromethane cluster anions." *Journal of Chemical Physics* **133** (8) (2010).

5 The Photoelectron Spectroscopy of Nitroethane Anions

This chapter has been reproduced in part with permission from Adams, C.L., and Weber, J.M., "Photoelectron imaging spectroscopy of nitroethane anions." *Journal of Chemical Physics*, 2011. **134**: 244301.

5.1 Introduction

Weakly bound states of excess electrons in molecular systems have received much attention because they can be supported by a number of different mechanisms, with diffuse dipole-bound states[1-7] and more localized but still weakly bound valence anions being the two main motifs. Some molecules can support both of these types of anion states.[2, 6] In a joint study using photoelectron (PE) spectroscopy experiments by the Bowen group in concert with Rydberg electron transfer experiments by the Schermann and Compton groups[4] it was shown that nitromethane is capable of forming both a dipole-bound state and a valence anion state. It was argued that formation of the valence anion in attachment of free electrons is facilitated by capture into the dipole-bound state and subsequent relaxation into the valence state.[1, 2, 4] A recent combined experimental and theoretical study by the groups of Bowen, Compton and Sommerfeld showed that the same processes are at play in nitroethane.[4]

These two small nitroalkanes are very similar in several respects, for example in terms of their dipole moments and of their adiabatic and vertical electron binding energies (see Table 5.1). In particular, the adiabatic electron binding energies in both systems have been shown to be lower than many of the fundamental vibrations of the anion, making these molecule model systems for studying the interaction of vibrational excitation and electron emission.[8, 9]

Table 5.1 – Dipole Moments and AEA's of Nitromethane and Nitroethane

	Dipole Moments (Debye)	AEA [meV]		VDE [eV]
		this work	refs. 4 and 5	
CH_3NO_2	3.46[10]	168 ± 6	300 ± 200	0.9 ± 0.1
$CH_3CH_2NO_2$	3.4[a]	191 ± 6	260 ± 80	0.9 ± 0.1

[a]see refs 11 and 12 for discussion on the dipole moment of nitroethane

One important cornerstone in the descriptions of such systems is an accurate determination of the adiabatic electron affinity. A PE spectrum of nitroethane anion was recorded by Bowen and coworkers several years ago.[4] The spectrum revealed an extended, unresolved vibrational progression, affording a determination of the vertical detachment energy of $0.92 \pm 0.1)$ eV and an estimate for the AEA at (0.3 ± 0.2) eV. The relatively large uncertainty in the latter value is a caused by the combination of a substantial geometry difference between the molecular geometries in the anionic and neutral charge states and a large spectral congestion due to a large number of Franck-Condon active modes, making the transition between the vibrational ground states of the anion and the neutral molecule ($0 \leftarrow 0$ transition) difficult to pinpoint. In the structurally related nitromethane anion,[9, 13] the largest geometry difference between the anion and the neutral is the angel between the NO_2 plane and the CN bond, where the accommodation of the excess electron (in an orbital of mainly π^* character) changes the geometry of the nitro group towards a trigonal pyramidal configuration. The vibrational mode connecting these two geometry motifs is the nitro wagging mode, which leads to a similarly strong progression in the PE spectrum of nitromethane.[9]

In this chapter, PE spectra of bare and Ar-solvated nitroethane anions are presented. Using argon solvation and Franck-Condon simulations, the AEA of nitroethane is determined to be (191 ± 6) meV. This is used to determine the C-NO_2 bond dissociation energy in nitroethane. Finally, several of the active modes in the PE spectrum are assigned with the aid of the Franck-Condon simulations and the dipole-bound state is tentatively assigned to a weak feature at (27 ± 5) meV.

5.2 Computational Details

5.2.1 *Ab Initio* Calculations

In order to understand the PE spectrum of nitroethane, information on the molecular structures and the vibrational frequencies of the anion and the neutral molecule is needed. In this study, we performed calculations using the GAUSSIAN 03 program suite.[14] We used density functional theory with the Becke-3-Lee-Yang-Parr (B3LYP) hybrid functional[15, 16] and the 6-311++G(2*df*,2*p*) basis set to obtain geometries and vibrational frequencies for $CH_3CH_2NO_2^-$ and $CH_3CH_2NO_2$ (calculated frequencies are listed in Table 5.2 below). This method was chosen since it has been shown in our previous study on nitromethane[9] to be computationally efficient and provide reliable frequencies. The calculated electron affinity and vertical detachment energy (VDE) of nitroethane, after accounting for vibrational zero-point energy corrections, are $EA_{Calc} = 0.45$ eV and $VDE_{Cal} = 1.20$ eV. It should be mentioned that recent calculations on the nitromethane anion (which is very similar in its electronic structure, owing to the localization of the excess electron on the NO_2 group), indicated that at this level of theory one would expect

an overestimate of the adiabatic electron affinity and that multiconfigurational wavefunctions are necessary to achieve sufficient convergence with experimental results.[13]

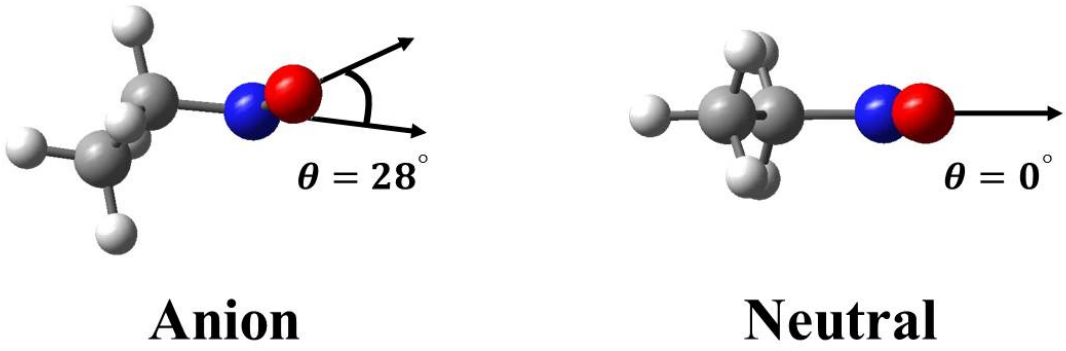

Figure 5.1 - Geometries of $CH_3CH_2NO_2^-$ and $CH_3CH_2NO_2$; θ denotes the angle between the ONO plane and the CN bond axis, which is the most salient geometry change upon electron loss.

Two conformers of the nitroethane anion were found, in agreement with an earlier study by Schneider *et al.*[8] The conformations were calculated to be separated by 660 cm^{-1} after zero-point vibrational energy corrections were taken into account. In the lower energy conformer, the NO_2 is *syn* to one of the CH bonds in the CH_2 group, while the NO_2 is *syn* to the CC bond in the higher energy conformer. A careful and detailed analysis of the infrared spectra of nitroethane by Schneider *et al.*,[8] performed using the same source and similar source conditions, indicated that only the lower energy conformer was significantly populated in the anion beam. Additionally, exploratory Franck-Condon simulations performed on the higher energy conformer indicated the higher energy conformer was not compatible with the PE spectra. Therefore, the focus of the study will be on the lower energy conformer.

5.2.2 Franck-Condon Analysis

The Franck-Condon profiles were simulated using the PESCAL program developed by Ervin and coworkers.[17] With the exception of the torsional vibration about the CN bond (discussed separately), the vibrational normal modes from the calculations were used to generate the Franck-Condon factors within the independent harmonic oscillator approximation with the full treatment of Duschinsky rotation using the Sharp-Rosenstock-Chen recursion method.[18, 19]

The calculated vibrational frequencies of neutral $CH_3CH_2NO_2$, excluding the torsion, were replaced with experimentally determined vibrational frequencies from a gas-phase IR study[20] of $CH_3CH_2NO_2$. Of the twenty-four vibrational modes of $CH_3CH_2NO_2^-$, five have been experimentally determined;[8] the remaining frequencies were determined by scaling the calculated frequencies by the ratio of the experimental fundamental to the calculated harmonic frequency of the neutral for the similar mode. The frequencies may be found in Table 5.2 below.

Symmetry considerations often play an important role in the simplification of the interpretation of a PE spectrum. Wherein, if a normal coordinate of a harmonic mode is antisymmetric to some symmetry element within the common point group of the anion and neutral, that mode will have a zero normal coordinate displacement and be considered Franck-Condon "inactive", contributing very little to the PE spectrum. Unfortunately, the nitroethane anion and neutral share C_1 symmetry and all modes must be considered active (nonzero normal coordinate displacement). The geometry displacements, $\vec{K}$", were defined along the anion normal coordinate frame and calculated within the FCFGAUS program[21] developed by Ervin and coworkers, they are displayed in Table 5.2 below.

Table 5.2 - Frequencies (cm^{-1}) and geometry displacements.

	$CH_3CH_2NO_2^-$		$CH_3CH_2NO_2$		$K''/(g/mol)^{1/2}$ Å[c]
Mode[a]	B3LYP	Scaled	B3LYP	Expt.[b]	B3LYP
24	H.I.R.[e]		F.I.R.[e]		N/A[e]
23	210.6	205.6	220.8	221	0[f]
22	408.4	400.3	594.8	583	-0.8211
21	802.6	793	814.7	805	-0.1564
20	1111.9	1096.1	1152.4	1136	-0.0685
19	1294.5	1258.1	1300.6	1264	0.0365
18	1474.6	1455.5	1490.3	1471	-0.0059
17	3055.9	2940[d]	3117.8	2972	-0.0953
16	3075.4	2913[d]	3119	3001	0.1666
15	276.2	272.9	288.4	285	-0.0156
14	481.5	478	507.7	504	0.1193
13	594.3	625.5	636.6	670	0.0349
12	783.1	776.7	883.2	876	-0.3418
11	992.1	984.7	1003.5	996	0.1051
10	1088.7	1070.5	1120.8	1102	-0.3861
9	1356	1327.8	1356.1	1328	0.0026
8	1211.9	1178.4	1405.9	1367	-0.2372
7	1387.4	1350.7	1434	1396	-0.0719
6	1470	1439.6	1478.6	1448	0.0369
5	1507.3	1472.8	1505.5	1471	0.0393
4	1234.5	1204.1	1615.9	1576	0.0407
3	3004.6	2846[d]	3054	2926	-0.1831
2	2870.7	2769[d]	3082.5	2957	-0.1958
1	3109.2	2979[d]	3141.9	3019	0.0568

[a] Modes are labeled in agreement with Groner et al.[20]

[b] Experimental fundamental frequencies.[20]

[c] Geometry displacements are defined in terms of the anion normal coordinate vectors.

[d] Experimental fundamental frequencies.[8]

[e] The character of this mode changes from a hindered internal rotor (H.I.R.) in the anion to a free internal rotor (F.I.R.) in the neutral. The calculated K" value for this mode is -2.1095, but the CN torsion has been treated separately (see text).

[f] The calculated *K"* value for this mode is -0.2337, but it has not been used in the simulations (see text).

5.2.2.1 Treatment of Internal Rotors

The GAUSSIAN 03[14] output gives harmonic modes for all twenty-four vibrational degrees of freedom. While this is a fair approximation for the twenty-two modes that do not correspond to internal rotations the potential energy curve for the CC and CN internal rotors must be modeled with a periodic potential. Since, at the present time, PESCAL[17] cannot treat internal rotors it was necessary to treat these modes independently.

The torsional vibrational about the CN bond is a hindered internal rotor in $CH_3CH_2NO_2^-$ but is nearly a free rotor in $CH_3CH_2NO_2$. This leads to substantial activity in the PES due to the hindered-to-free rotor transitions, as has been seen in a previous study of PE study of nitromethane anion. On the other hand, the potential energy curve of the CC rotor undergoes very little change upon electron emission which should lead to very little activity in this mode in the PE spectrum; based on this, we exclude this mode in the Franck-Condon simulations.

The torsional potentials were generated at the B3LYP/6-311++G(2*d*,*p*) level by scanning the dihedral angle, HCNX, where X is a vector perpendicular to the plane of the NO_2 group and H is one of the H atoms in the methylene group. This was done for the anion, as well as the neutral. In the neutral molecule, all other bond angles and distances were allowed to relax during the scan. This yielded a two-fold symmetric potential with a barrier of 35 cm^{-1}. For the anion, as mentioned earlier, rotation about this bond will lead to a higher energy conformer, where the NO_2 group is *syn* to the CC bond. The part of the anion potential energy curve around the low-energy isomer was calculated by scanning the HCNX dihedral angle and allowing the remaining bond lengths and angles to relax at each HCNX dihedral angle. The barrier to isomerisation and the potential energy curve in the region of the higher energy conformer was generated by scanning the HCNX dihedral angle while the rest of the geometry was restricted to that of the

lower-energy conformer. This procedure was necessary to prevent the molecular geometry from reverting to the lower energy conformer during geometry optimization. The potential energy curves along with the geometries at selected positions are illustrated in Figure 5.3.

Each curve was fitted with the following expansion in cosine terms,

Equation 5.1

$$V(\varphi) = A + \sum_{l=1}^{m} \mathrm{V}_l \cdot \mathrm{Cos}[l \cdot \varphi]\,,$$

where $m = 6$ for the neutral and $m = 10$ for the anion. The fits to the potential energy curve are represented in Figure 5.3. The reduced moments of inertia for torsion are defined as

Equation 5.2

$$I_{C-N} = \frac{I_{\mathrm{CH_3CH_2}} \cdot I_{\mathrm{NO_2}}}{I_{\mathrm{CH_3CH_2}} + I_{\mathrm{NO_2}}},$$

where the geometries of the ethyl and nitro groups were obtained from their lowest energy structures. Additionally, I_{C-N} was tabulated for all values of φ to ensure that the variation of the reduced moment of inertia was negligible; the results indicated a deviation of less than five percent which is acceptable within the goals of this study. The calculated values for the reduced moment of inertia (lowest energy structures) for the nitroethane anion and neutral are $I_{C-N}(\mathrm{anion}) = 3.32 \cdot 10^{-46}$ kg·m^2 and $I_{C-N}(\mathrm{neutral}) = 3.16 \cdot 10^{-46}$ kg·m^2.

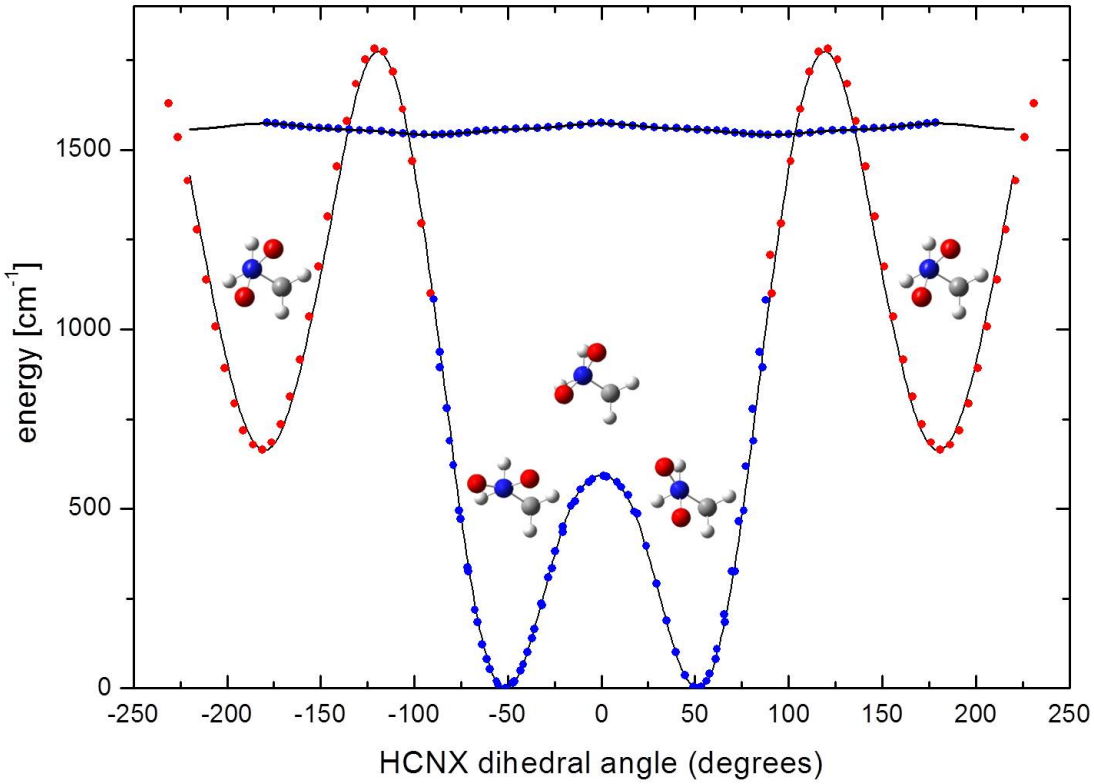

Figure 5.2 - Calculated potential energy curves (circles) generated by rotation about the CN bond in the nitroethane anion (lower curve) and neutral (upper curve). The black line illustrates the fit to each calculated potential (see text). The filled blue circles represent points calculated using a relaxed-geometry scan while the filled red circles are points generated by a fixed-geometry scan (see text). The different nitroethane anion conformers are illustrated above their respective positions along the potential energy curve. The anion has two isoenergetic conformers separated by a 660 cm^{-1} barrier and flanked by a higher energy conformer with a large barrier to isomerization. The neutral has a relatively flat potential nearly coinciding with that of a free internal rotor.

As was described in detail earlier in Chapter 4 (and according to the approach outline by Spangler)[22] , the Hamiltonian for the hindered internal rotor is

Equation 5.3

$$\widehat{H} = -\frac{\hbar^2}{2I}\frac{\partial^2}{\partial\varphi^2} + V(\varphi) = -C_T\frac{\partial^2}{\partial\varphi^2} + V(\varphi),$$

where $V(\varphi)$is the torsional potential (Equation 5.1) and $C_T(\text{anion}) = 0.844\ \text{cm}^{-1}$ for $CH_3CH_2NO_2^-$ and $C_T(\text{neutral}) = 0.901\ \text{cm}^{-1}$ for $CH_3CH_2NO_2$. As before, a truncated basis set of free rotor wavefunctions,

Equation 5.4

$$\psi = \frac{1}{\sqrt{2\pi}}e^{iJ\varphi},$$

is applied to the hindered internal rotor Hamiltionian resulting in the following matrix elements in the Hamiltionian matrix,

Equation 5.5

$$H_{JK} = (J^2C_T + A)\delta_{J,K} + \sum_{l=1}^{m}\frac{\mathrm{V}_l}{2}\cdot\delta_{J,K\pm l}.$$

The matrix is diagonalized to yield the hindered-rotor wavefunctions and corresponding energy eigenstates. A basis set from $J = -20$ to $J = 20$ was found to converge; the energies for the anion and neutral hindered rotors are listed in Table 5.3.

The Franck-Condon factors for the torsional vibration were simulated in Mathematica (Wolfram Research Inc.) using a newly written program that was capable of simulating hindered-to-hindered rotor transitions. The Franck-Condon overlap integral is given by,

Equation 5.6

$$FCF(m,n) = \left[\mathcal{B}_n \int_0^{2\pi} \psi_m^*(\varphi)\psi_n(\varphi)d\varphi\right]^2; \qquad m = 0, 1, \ldots, 40$$

where ψ_m is the wavefunction of the m^{th} neutral hindered rotor, ψ_n is the n^{th} hindered internal rotor wavefunction of the anion, and $\mathcal{B}_n$ is the Boltzmann weighting of the n^{th} state in the anion for a temperature specified in the program. Given the anion and neutral hindered internal wavefunctions are composed of orthogonal wavefunctions this may be simplified to

Equation 5.7

$$\psi_m^*(\varphi)\psi_n(\varphi) = \sum_{J\prime=-20}^{20} a_{J\prime}\,\psi_{J\prime}^*(\varphi) \sum_{J''=-20}^{20} b_{J''}\,\psi_{J''}(\varphi) = a_J \cdot b_{J''} \cdot \delta_{J,J''}$$

where $\psi_{J\prime}(\varphi)$ and $\psi_{J''}(\varphi)$ are free internal rotor basis wavefunctions. The resulting transition intensities were imported into PESCAL and convolved with a Gaussian to match the experimental resolution.

Table 5.3 – Lowest Hindered Internal Rotor States

Quantum Number	Neutral Hindered Rotor Energy [cm^{-1}]	Anion Hindered Rotor Energy [cm-1]
0	7.2	47.1
1	7.2	47.2
2	17.4	140.9
3	17.5	141.5
4	23.3	233.8
5	24.0	236.1
6	28.5	329.0
7	30.9	332.4
8	34.1	426.9
9	39.5	429.9
10	40.8	514.1
11	49.5	529.1
12	49.8	586.5
13	61.1	607.1
14	61.2	635.4
15	74.5	702.8
16	74.5	705.6
17	89.7	744.9
18	89.7	781.8
19	106.8	791.5
20	106.8	873.4
21	125.7	896.3
22	125.7	959.9
23	146.3	1043.4
24	146.3	1052.1

5.4 Results and Discussion

5.4.1 Experimental Results

The spectrum by Bowen and coworkers[4] was taken at a photon energy of 2.540 eV. The long progression is identified as the excitation into the ground electronic state of $CH_3CH_2NO_2$ and extends from about $0 - 2$ eV in binding energy, with a vertical detachment energy of 0.92 eV. Without vibrationally resolved features, it was necessary to estimate the adiabatic electron affinity based on the location of a discernible threshold, necessitating generous error bars.

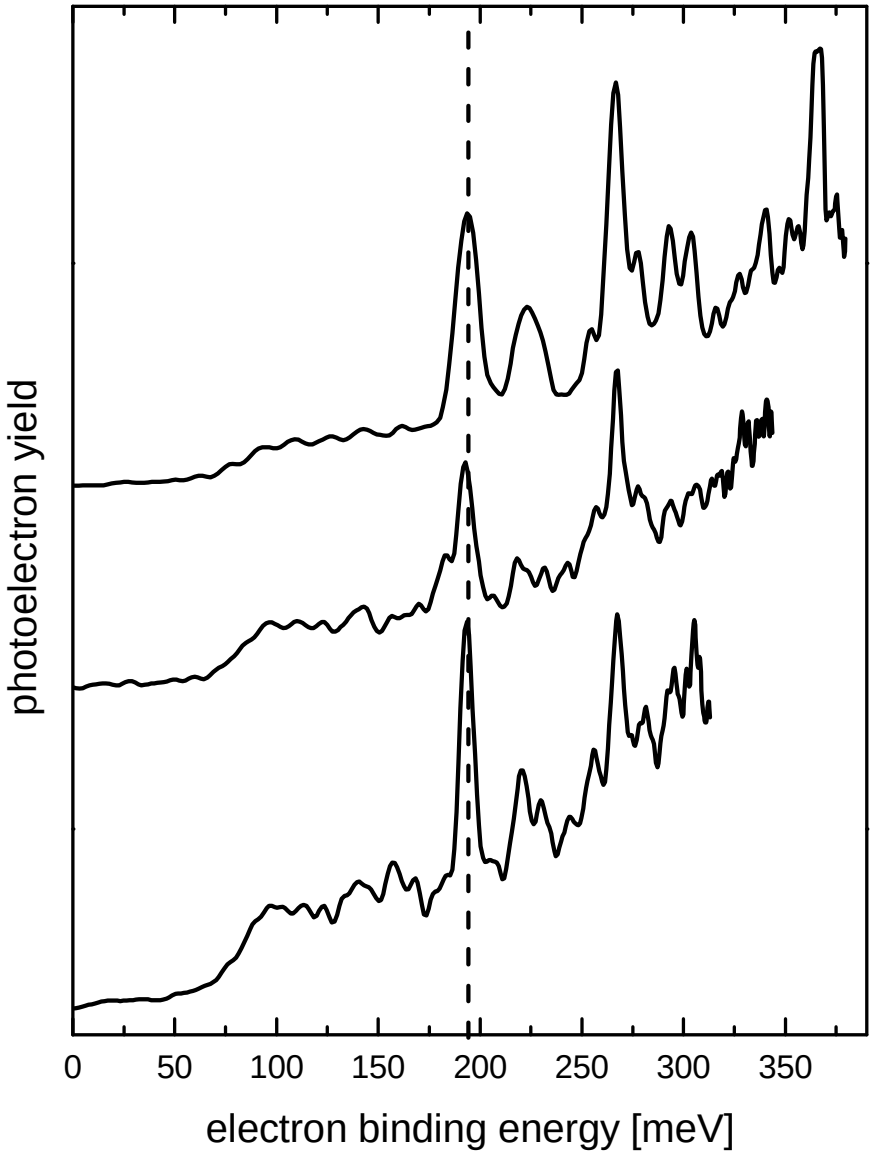

Figure 5.3 - PE spectra of $CH_3CH_2NO_2^-$ at 389 meV (upper trace), 347 meV (center trace), and 322 meV (lower trace) photon energy. The dashed line denotes the (0←0) transition corresponding to an AEA of (191 ± 6) meV.

The PE spectra of $CH_3CH_2NO_2^-$ shown in Figure 5.3 above were obtained using photon energies of 380 meV (3140 cm^{-1}), 347 meV (2800 cm^{-1}), and 322 meV (2600 cm^{-1}). The PE image obtained at 380 meV (3140 cm^{-1}) is shown in Figure 5.4. Care was taken to ensure that

none of the photon energies used were in the vicinity of any vibrational autodetachment resonances of $CH_3CH_2NO_2^-$.[8] The spectrum at the highest photon energy reveals three prominent bands, with the first at (193 ± 5) meV binding energy. Interspersed between the bands are many weaker transitions without immediately recognizable patterns. The low-binding energy side of the spectrum reveals a broad, spectrally congested tail that extends to a binding energy of about 75 meV.

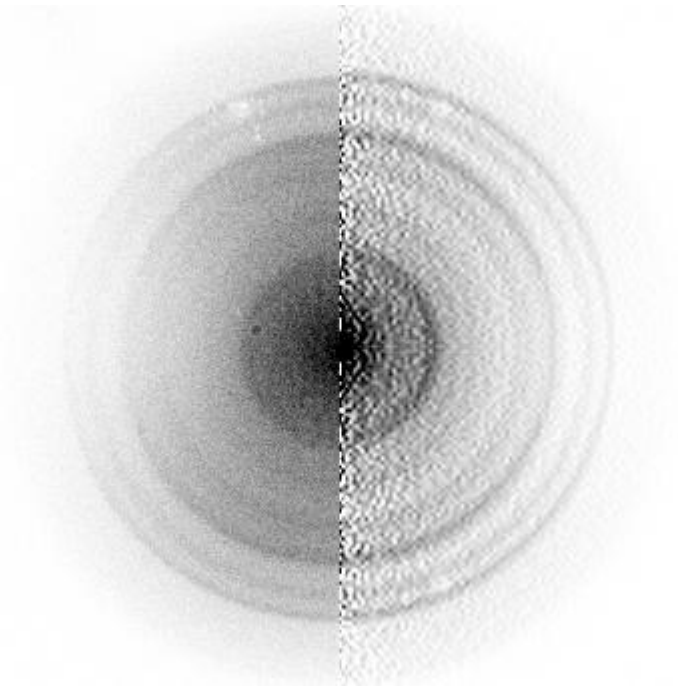

Figure 5.4 – PE image obtained at a photon energy of 389 meV (3140 cm^{-1}). The left half of the image is the raw PE image. The right half is the BASEX reconstructed image.

The spectrum of $CH_3CH_2NO_2^- \cdot Ar$ contains two prominent bands, shown in Figure 5.5 below. The features on the low-energy side of the first peak and many of the interspersed features seen in the spectrum of bare $CH_3CH_2NO_2^-$ have been strongly suppressed or eliminated. Their absence from the spectrum indicates that many of these features are contributions from hot bands which are suppressed in the spectrum of $CH_3CH_2NO_2^- \cdot Ar$ as a result of the much lower

internal energy in this anion. The first two prominent peaks in the spectra of both Ar-solvated and bare nitroethane anion are spaced by (73 ± 7) meV or (595 ± 56) cm^{-1}. This spacing is in very good agreement with the experimentally determined energy of the nitro wagging mode (υ_{22} in Table 5.2 above) in neutral nitromethane of 583 cm^{-1}.[20] The prominent features are shifted to higher binding energies by (61 ± 7) meV which is in good agreement with the shift observed in nitromethane (63 ± 7) meV,[9] and we attribute this shift to the solvation energy of the $CH_3CH_2NO_2^- \cdot Ar$ complex. A PE spectrum of $CH_3CH_2NO_2^- \cdot Ar_2$ exhibited an additional shift of (55 ± 7) meV compared to the $CH_3CH_2NO_2^- \cdot Ar$ spectrum. The Ar-induced shift in the PE spectra allows us to identify the contributions from hot bands and assign the band at (193 ± 5) meV binding energy to the transition between the ground states of the anion and neutral molecule (0←0 transition). As a consequence, we determine the adiabatic electron affintiy of nitroethane to be (191 ± 6) meV after correcting for torsional band contour shifts, as discussed below. Better assignments of the vibrational features require the aid of the Franck-Condon simulations which is discussed below.

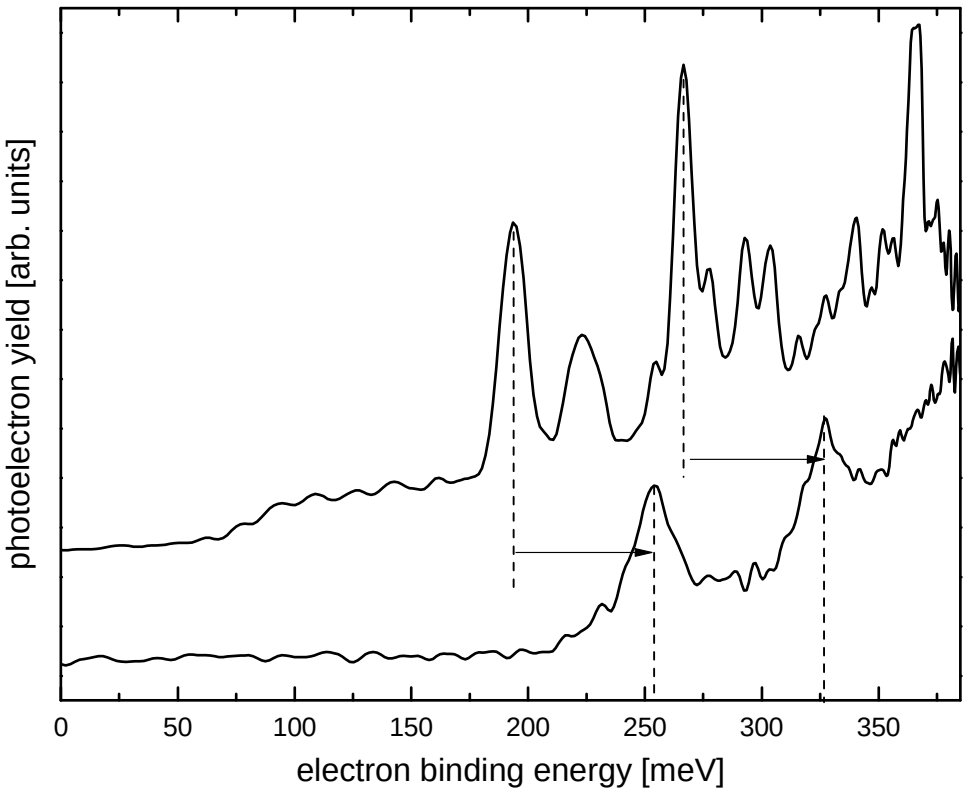

Figure 5.5 - PE spectra of $CH_3CH_2NO_2^-$ (upper curve) and $CH_3CH_2NO_2^-$·Ar (lower curve) taken at 389 meV photon energy. The arrows and drop lines illustrate the shift of the spectrum upon Ar solvation by (61 ±7) meV.

The PE spectrum of nitroethane shows a very weak feature at (27 ± 5) meV binding energy. The intensity of this feature depends on source conditions, and it can be seen best in photoelectron velocity distributions (see Figure 5.6 below), where it is remarkably sharp and well separated from the broad background of hot bands at higher binding energies (i.e., lower velocities). The broad, spectrally congested tail observed at higher binding energies in the photoelectron velocity distribution is due to a multitude of overlapping hot-band transitions. At a binding energy of 27 meV, there are no hot bands with appreciable intensity, making it unlikely that this feature is due to a hot band. Bowen and coworkers determined the binding energy of

the dipole bound state of nitroethane to be ~ 25 meV.[4] In agreement with their experimental binding energy value, we assign the feature observed at (27 ± 5) meV in our PE spectra to be the signature of the dipole-bound anion state of nitroethane. This is the first observation of dipole-bound state of nitroethane using PE spectroscopy.

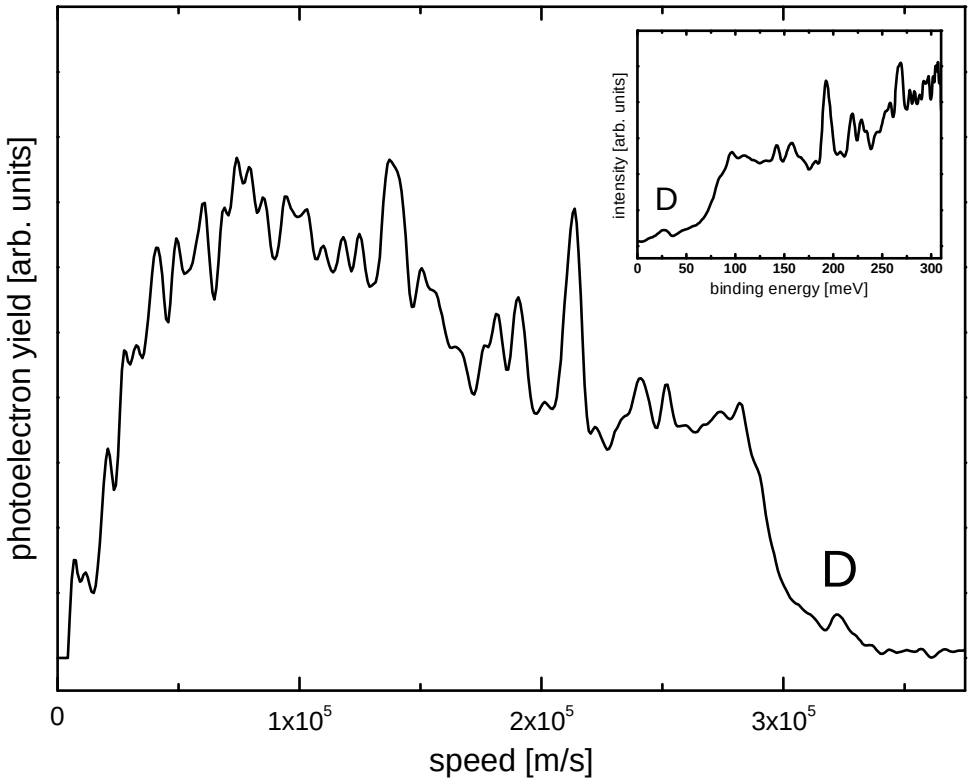

Figure 5.6 - PE spectrum of $CH_3CH_2NO_2^-$ taken at a photon energy of 322 meV. The spectrum is plotted as a function of electron speed to best illustrate the dipole-bound state; the inset shows the PE spectrum as a function of binding energy. In each spectrum the dipole-bound state is labeled "D".

Based on our measurement of the adiabatic electron affinity, the adiabatic C-NO_2 bond dissociation energy, $\mathrm{BDE}_{\mathrm{C-NO_2}} = (0.539 \pm 0.012)$ eV can be determined from other thermodynamic quantities[23, 24] in the thermochemical cycle shown in Figure 5.7 below. The

effect of the excess electron in the antibonding orbital of the nitroethane molecule serves to destabilize the CN by ~ 2 eV. The strong similarities in the electronic structure of nitromethane and nitroethane anions, in which the electron is largely localized on the NO_2 group, result in almost identical C-NO_2 bond energies with the C-NO_2 bond in nitromethane anion, as recently calculated by Sanov *et al.*[25]

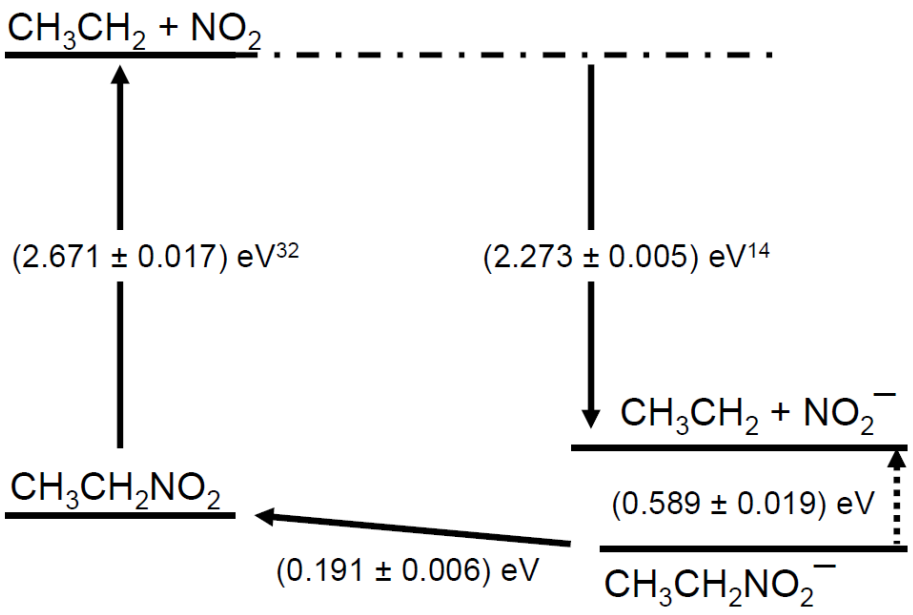

Figure 5.7 - Thermochemical cycle for the determination of the C-NO_2 bond dissociation energy, $BDE_{C\text{-}NO_2}$, in nitroethane anion.

5.4.2 Threshold Effects and Angular Distributions

As outlined in Chapter 2, the approach by Reed *et al.*[26] utilizes symmetry arguments to extend Wigner's Threshold laws[27] to near-threshold photodetachment of molecular anions, offering insight into the dominant symmetry-allowed partial waves. However, two issues arise in applying this to nitroethane: the anion and neutral share no common symmetry and the dipole

moment of $CH_3CH_2NO_2$ is supercritical (i.e., capable of supporting a dipole-bound state; the dipole moment is (3.4 ± 0.2) D). Wigner's threshold law for photodetachment is founded on the idea that the longest range potential will dictate the behavior of the cross-section at threshold.[28] In photodetachment, in the absence of a dipole moment, the longest range potential that exists is that of the centrifugal barrier and will therefore dictate the threshold behavior. However, if a dipole is present the long-range term that dictates the cross-section will be the sum of the two potentials. In past experiments on OH^- it has been shown that the dipole moment was important in determining the threshold behavior and led to a modification in the leading term in the threshold law.[28] Characterizing the contribution of the dipole is impractical for such a large molecule as nitroethane anion and is well beyond the scope of this study. However, inspection of the angular distributions should yield some insight into the partial waves contributing above threshold, giving us a sense of the leading term contributing to the cross-section.

Analysis of the angular distributions in photodetachment from $CH_3CH_2NO_2^-$ at different kinetic energies (see Figure 5.8 below) reveals an isotropic distribution ($\beta = 0$) at low kinetic energies and an increasing anisotropy parameter as the kinetic energy increases. This behavior indicates that s-wave detachment dominates at low kinetic energies but contributions from higher-order partial waves become significant at larger kinetic energies.

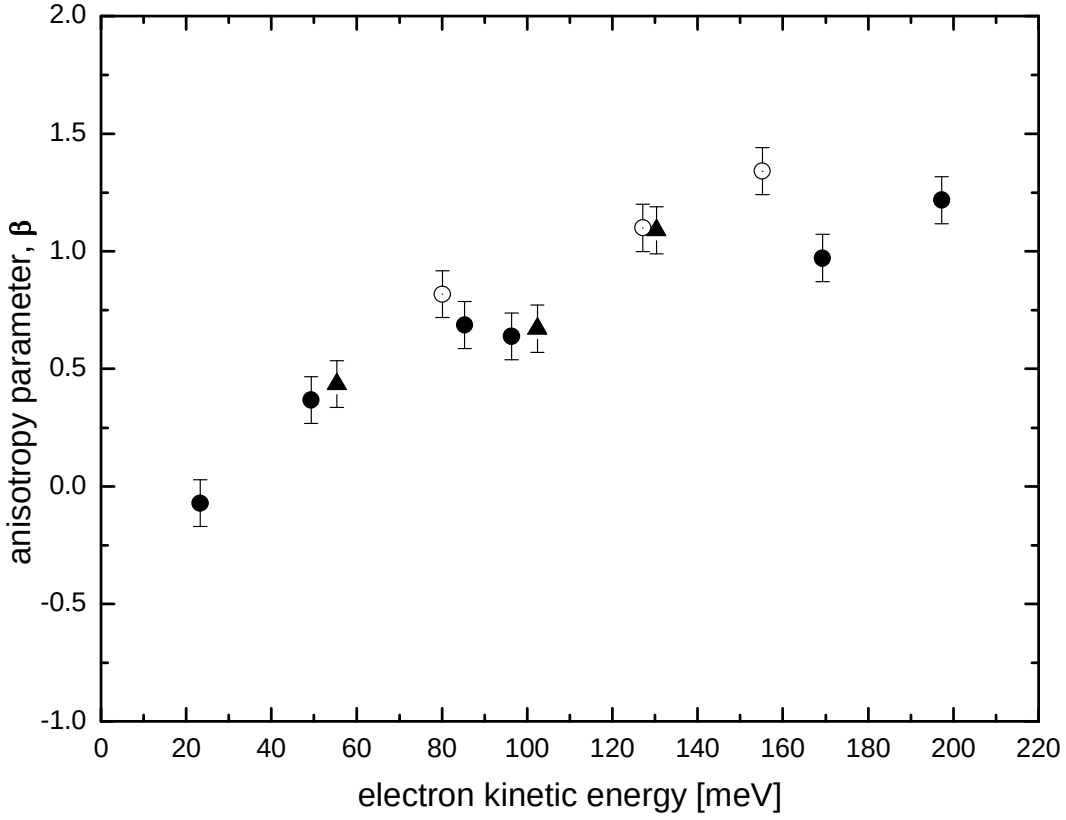

Figure 5.8 - Anisotropy parameters as a function of electron kinetic energy obtained at different photon energies where solid circles, hollow circles, and triangles represent parameters from images taken at photon energies of 389 meV, 347 meV, and 322 meV, respectively. The error bars are conservatively estimated to be ± 0.1.

The dominance of the *s*-wave contribution at low kinetic energy implies that the leading term in the threshold law is proportional to $E_{KE}^{1/2}$. However, the increase of β at higher kinetic energies indicates that higher angular momenta also play a role. As a direct result of threshold effects, the relative intensity of hot bands increases at lower photon energies. This has been observed in several other studies[29, 30] including a previous study on nitromethane anion. The inclusion of threshold effects will be necessary to accurately model the PE spectrum in the Franck-Condon simulation.

We note that the signature of the dipole-bound state can have a significantly different anisotropy parameter than signatures of valence anion states with comparable kinetic energies.[9] However, the signal-to-noise ratio in our PE images is insufficient to obtain a reliable anisotropy parameter for this feature.

5.4.3 Franck-Condon Simulations

The PE spectra revealed three prominent peaks with weaker transitions interspersed between them, superimposed on a congested, broad background of unresolved transitions. In order to assign the most important contributions to the PE spectrum, Franck-Condon simulations were performed and compared to the PE spectrum recorded at 389 meV photon energy since this spectrum captures the most transitions in the present study. The simulations revealed 136 transitions within at least 1% of the intensity of the $0 \leftarrow 0$ transition in this small spectral window, in addition to more numerous, even weaker transitions, explaining the spectral congestion.

Our tentative assignment of two transitions at (193 ± 5) meV and (267 ± 5) meV belonging to the $(0 \leftarrow 0)$ and $(1 \leftarrow 0)$ transitions of the nitro wagging mode υ_{22} (see above) are confirmed by the Franck-Condon simulations. The prominent peak at (366 ± 5) meV can be assigned to overlapping features of the $(1 \leftarrow 0)$ transition of the symmetric NO_2 stretching mode, υ_8, and the combination band arising from the $(1 \leftarrow 0)$ transition of υ_{21} and the $(1 \leftarrow 0)$ transition of υ_{22}.

Many of the weaker features observed in the spectrum are identified as originating from hot bands, consistent with their suppression upon argon solvation. The main contributions from

hot bands are based on the $(0 \leftarrow 1)$ transition of the CCN bending mode υ_{15} and on the $(0 \leftarrow 1)$ transition of the nitro wagging mode υ_{22}.

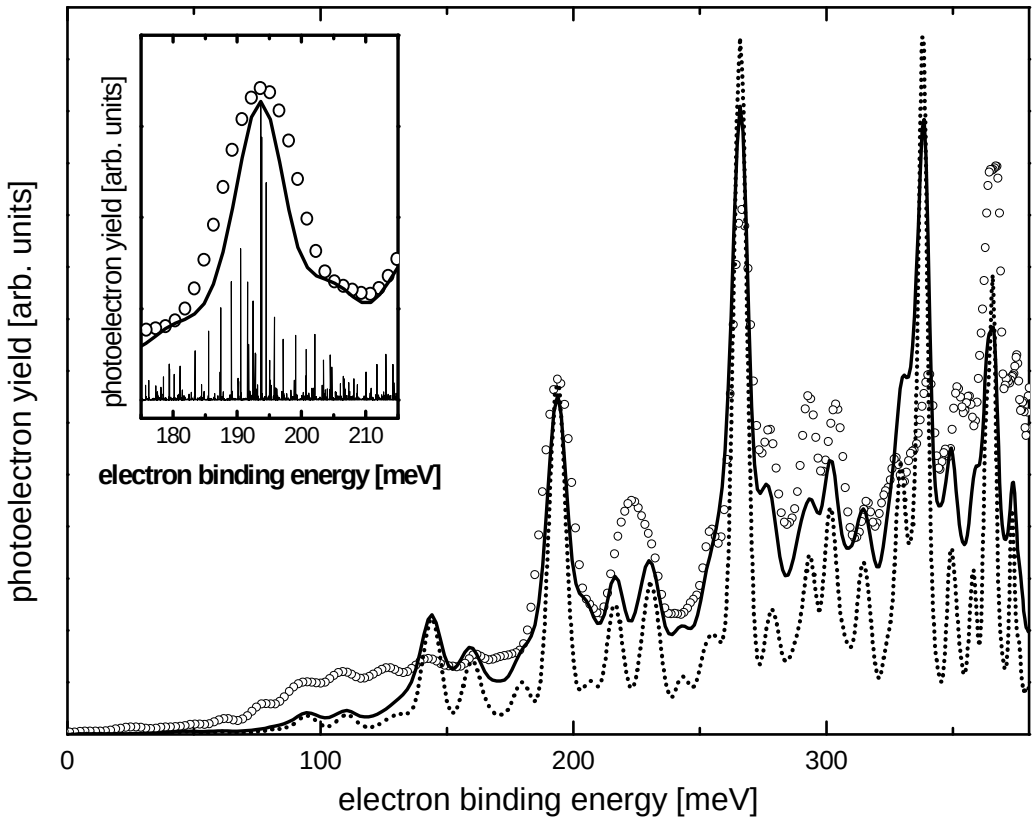

Figure 5.9 - Experimental PE spectrum taken at a photon energy of 389 meV (open circles) along with Franck-Condon simulations performed with the inclusion of the hindered-to-free internal rotor transitions (solid line) and in their absence (dotted line). The inset is centered about the (0←0) transition and includes a stick spectrum of the individual calculated transitions to emphasize the contribution of the hindered-to-free CN rotor transitions to the peak profile.

In principle, Franck-Condon simulations can be performed without including the CN torsion. However, as a result of its exclusion the simulations underestimate the width of many of the prominent features and fail to recover the broad background of unresolved transitions. Broadening the simulated spectral resolution instead of accounting for CN torsion does not lead to a better description of the spectrum. In order to accurately simulate the spectrum it was

necessary to include the transitions involving the changing character of the CN torsion from a hindered to a nearly free internal rotor. Incorporating these transitions leads to combination bands of the CN torsional transitions with each vibrational feature observable in the spectrum. These combination bands are not individually resolved in our PE spectrum, due to the large reduced moment of inertia for the CN torsion. Instead, these hindered-to-free torsion transitions superimpose a profile of each individual vibrational transition. One important consequence is that the peak of the profile of each (non-torsional) transition is shifted by $+(1.9 \pm 1)$ meV towards higher binding energies and broadened asymmetrically (see Figure 5.9 above). This serves to broaden the peak of transition to the observed width while the wings of the torsional profile add to the broad background. As mentioned above, the individual transitions are too closely spaced to be resolved in our experiment; however, the success of the fit upon inclusion of the internal rotation strongly suggests that the torsional transitions are responsible for much of the broadening and congestion in the spectrum. The shift in the profile of each transition must be accounted for in the determination of the adiabatic electron affinity from the experimentally observed $0 \leftarrow 0$ transition and has been included in the adiabatic electron affinity values reported in the present work. It should be noted, given the uncertainty in the barrier height for internal rotation in the neutral, that the simulation was also performed for a hindered-to-free internal rotor transition; the results indicated that the peak profile, at this level of uncertainty, was stable to small changes in the barrier height.

As discussed above, the intensities of the features may be written as

Equation 5.8

$$I_{\nu',\nu''}(E_K) \propto FCF_{\nu',\nu''} \cdot \vartheta(E_K),$$

where $FCF_{v',v''}$ are the Franck-Condon factors for a particular transition and $\vartheta(E_K)$ describes the modification of the photodetachment cross section by threshold effects. Following a pure s-wave threshold law in absence of a dipole moment, $\vartheta(E_K)$ is proportional to $E_K^{1/2}$, while $\vartheta(E_K) \propto E_K^{3/2}$ for pure p-wave detachment. Simulations were performed for these two threshold laws and without taking threshold effects into account. As Figure 5.10 shows, the unscaled simulation overestimates the bands at higher binding energy (i.e., low kinetic energy) while the p-wave simulation underestimates them. The best fit was achieved by using an s-wave threshold law but this fit still slightly misrepresents the intensities of the low kinetic energy bands. Interestingly, at low kinetic energy the best fit would be afforded by a function that rises faster than $E_K^{1/2}$. This behavior mirrors observations by Lineberger *et al.*[28] for OH^- that indicated the presence of a dipole potential modified the leading term of the threshold law such that the cross section rises faster than Wigner's law[27] (in the absence of a dipole moment) would predict.

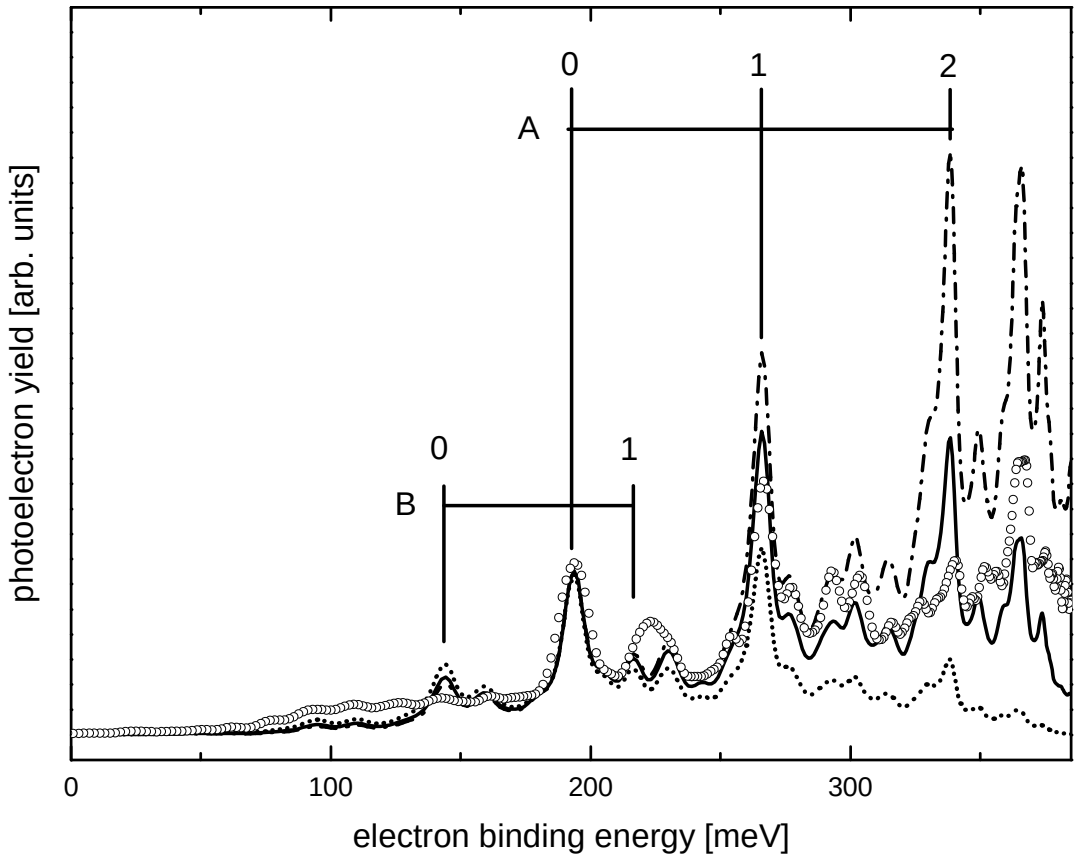

Figure 5.10 - Experimental PE spectra taken at a photon energy of 389 meV (open circles) along with the Franck-Condon simulations performed without threshold scaling (dash-dotted line), scaled by $E^{3/2}$ (dotted line) and scaled by $E^{1/2}$ (solid line). The sequences marked in the spectrum are based on the nitro wagging mode ν_{22} with transitions $n \leftarrow 0$ (series A) and $n \leftarrow 1$ (series B).

The spectrum was found to be well represented at a simulation temperature of 250 K, similar to the previous PE study conducted in our laboratory on nitromethane anion.[9] This temperature recovers the transitions based on the CCN bending (1←0) and the nitro wagging (1←0) hot bands. However, the (2←0) transitions for both of these modes were underestimated by the simulations. Interestingly, a similar effect has been observed in the PE spectra of nitromethane anion. In the present case, these features could be fitted at a temperature of 350 K but the resulting fit is not consistent with the rest of the PE spectrum. Given the similarities of

nitromethane and nitroethane anion (i.e., namely that the excess electron, localized on the NO_2 group, leads to almost identical distortions about the nitrogen) it is likely that when sufficient internal energy is pooled in the rotor and wagging modes of the molecule, the potential energy surface is poorly recovered within the independent harmonic oscillator approximation, thus leading to an inadequate recovery of the spectrum within the approximations used for the Franck-Condon analysis. We should note that the higher simulation temperature cannot account for the feature assigned to the dipole-bound state.

5.5 Summary

Near-threshold PE imaging spectroscopy has been used to obtain the PE spectrum and angular distributions of Ar-solvated and bare nitroethane anions. The adiabatic electron affinity is determined to be (191 ± 6) meV, providing the most precise and accurate value to date. The adiabatic electron affinity was utilized in a thermochemical cycle to establish a C-NO_2 bond dissociation energy, $\mathrm{BDE}_{\mathrm{C-NO_2}} = (0.539 \pm 0.012)$ eV, for the nitroethane anion. We were able to characterize many of the vibrational features observed in the PE spectrum. The most intense features are due to progression of the nitro wagging mode of neutral nitroethane. In close analogy to the case of nitromethane,[9] hindered-to-free internal rotor transitions in the CN torsional coordinate were identified to be the origin of much of the spectral congestion and of torsional broadening of vibrational features. Angular distributions indicate that *s*-wave detachment dominates at low kinetic energies but contributions from higher-order partial waves become significant at higher kinetic energies. We observe the dipole-bound anion state of nitroethane as a very weak feature at (27 ± 5) meV, consistent with earlier Rydberg electron transfer studies.[4]

5.6 References for Chapter 5

1. G. L. Gutsev and R. J. Bartlett,"A theoretical study of the valence- and dipole-bound states of the nitromethane anion." *Journal of Chemical Physics* **105** (19), 8785-8792 (1996).

2. T. Sommerfeld,"Coupling between dipole-bound and valence states: the nitromethane anion." *Physical Chemistry Chemical Physics* **4** (12), 2511-2516 (2002).

3. M. Gutowski, P. Skurski, A. I. Boldyrev, J. Simons and K. D. Jordan,"Contribution of electron correlation to the stability of dipole-bound anionic states." *Physical Review A* **54** (3), 1906 (1996).

4. S. T. Stokes, K. H. Bowen, T. Sommerfeld, S. Ard, N. Mirsaleh-Kohan, J. D. Steill and R. N. Compton,"Negative ions of nitroethane and its clusters." *Journal of Chemical Physics* **129** (6) (2008).

5. R. N. Compton, H. S. Carman, C. Desfrancois, H. Abdoul-Carmine, J. P. Schermann, J. H. Hendricks, S. A. Lyapustina and K. H. Bowen,"On the binding of electrons to nitromethane: Dipole and valence bound anions." *Journal of Chemical Physics* **105** (9), 3472-3478 (1996).

6. F. Lecomte, S. Carles, C. Desfrancois and M. A. Johnson,"Dipole bound and valence state coupling in argon-solvated nitromethane anions." *Journal of Chemical Physics* **113** (24), 10973-10977 (2000).

7. K. Yokoyama, G. W. Leach, J. B. Kim and W. C. Lineberger,"Autodetachment spectroscopy and dynamics of dipole bound states of negative ions: $^2A_1$-$^2B_1$ transitions of H_2CCC^-." *Journal of Chemical Physics* **105** (24), 10696-10705 (1996).

8. H. Schneider, K. M. Vogelhuber, F. Schinle, J. F. Stanton and J. M. Weber,"Vibrational spectroscopy of nitroalkane chains using electron autodetachment and Ar predissociation." *Journal of Physical Chemistry A* **112** (33), 7498-7506 (2008).

9. C. L. Adams, H. Schneider, K. M. Ervin and J. M. Weber,"Low-energy photoelectron imaging spectroscopy of nitromethane anions: Electron affinity, vibrational features, anisotropies and the dipole-bound state." *Journal of Chemical Physics* **130**, 074307-074301 - 074310 (2009).

10. W. M. Haynes, *CRC Handbook of Chemistry and Physics*, 91 ed. (CRC Press, Boca Raton, 2010).

11. P. Groner, R. Meyer, A. Günter, H. Kühne and H. H. Günthard,"Far Infrared Spectrum of Nitroethane." *Chemical Physics* **5** (1), 136-141 (1974).

12. J. Ekkers, A. Bauder and H. H. Günthard,"Microwave spectrum and internal rotation of nitroethane." *Chemical Physics Letters* **22** (2), 249-252 (1973).

13. J. N. Bull, R. Maclagan and P. W. Harland,"On the Electron Affinity of Nitromethane (CH_3NO_2)." *Journal of Physical Chemistry A* **114** (10), 3622-3629 (2010).

14. M. J. Frisch, G. W. Trucks, H. B. Schlegel, G. E. Scuseria, M. A. Robb, J. R. Cheeseman, J. A. Montgomery, J. Vreven, T. , K. N. Kudin, J. C. Burant, J. M. Millam, S. S. Iyengar, J. Tomasi, V. Barone, B. Mennucci, M. Cossi, G. Scalmani, N. Rega, G. A. Petersson, H. Nakatsuji, M. Hada, M. Ehara, K. Toyota, R. Fukuda, J. Hasegawa, M. Ishida, T. Nakajima, Y. Honda, O. Kitao, H. Nakai, M. Klene, X. Li, J. E. Knox, H. P. Hratchian, J. B. Cross, V. Bakken, C. Adamo, J. Jaramillo, R. Gomperts, R. E. Stratmann, O. Yazyev, A. J. Austin, R. Cammi, C. Pomelli, J. W. Ochterski, P. Y. Ayala, K. Morokuma, G. A. Voth, P. Salvador, J. J. Dannenberg, V. G. Zakrzewski, S. Dapprich, A. D. Daniels, M. C. Strain, O. Farkas, D. K. Malick, A. D. Rabuck, K. Raghavachari, J. B. Foresman, J. V. Ortiz, Q. Cui, A. G. Baboul, S. Clifford, J. Cioslowski, B. B. Stefanov, G. Liu, A. Liashenko, P. Piskorz, I. Komaromi, R. L. Martin, D. J. Fox, T. Keith, M. A. Al-Laham, C. Y. Peng, A. Nanayakkara, M. Challacombe, P. M. W. Gill, B. Johnson, W. Chen, M. W. Wong, C. Gonzalez and J. A. Pople, Gaussian 03, Wallingford CT, 2004.

15. A. D. Becke,"Density-Functional Thermochemistry .3. The Role of Exact Exchange." *Journal of Chemical Physics* **98** (7), 5648-5652 (1993).

16. C. T. Lee, W. T. Yang and R. G. Parr,"Development of the Colle-Salvetti Correlation-Energy Formula into a Functional of the Electron-Density." *Physical Review B* **37** (2), 785-789 (1988).

17. K. M. Ervin, PESCAL, University of Nevada, Reno, 2008.

18. T. E. Sharp and H. M. Rosenstock,"Franck-Condon Factors for Polyatomic Molecules." *Journal of Chemical Physics* **41** (11), 3453-& (1964).

19. P. Chen, in *Unimolecular and Bimolecular Reaction Dynamics*, edited by C.-Y. Ng, T. Baer and I. Powis (John Wiley & Sons, Chichester, 1994), pp. 371.

20. P. Groner, R. Meyer and H. H. Günthard,"Matrix and gas infrared spectra of nitroethane isotopic species." *Chemical Physics* **11** (1), 63-85 (1975).

21. K. M. Ervin, FCFGaus03, University of Reno, Nevada, 2008.

22. L. H. Spangler,"Structural information from methyl internal rotation spectroscopy." *Annual Review of Physical Chemistry* **48**, 481-510 (1997).

23. K. M. Ervin, J. Ho and W. C. Lineberger,"Ultraviolet Photoelectron Spectrum of NO_2." *Journal of Physical Chemistry* **92** (19), 5405-5412 (1988).

24. S. J. Blanksby and G. B. Ellison,"Bond dissociation energies of organic molecules." *Accounts of Chemical Research* **36** (4), 255-263 (2003).

25. D. J. Goebbert, D. Khuseynov and A. Sanov,"Photodissociation of nitromethane cluster anions." *Journal of Chemical Physics* **133** (8) (2010).

26. K. J. Reed, A. H. Zimmerman, H. C. Andersen and J. I. Brauman,"Cross-Sections for Photodetachment of Electrons from Negative-Ions near Threshold." *Journal of Chemical Physics* **64** (4), 1368-1375 (1976).

27. E. P. Wigner,"On the Behavior of Cross Sections near Thresholds." *Physical Review* **73** (9), 1002-1009 (1948).

28. J. R. Smith, J. B. Kim and W. C. Lineberger,"High-resolution threshold photodetachment spectroscopy of OH^-." *Physical Review A* **55** (3), 2036-2043 (1997).

29. H. K. Gerardi, K. J. Breen, T. L. Guasco, G. H. Weddle, G. H. Gardenier, J. E. Laaser and M. A. Johnson,"Survey of Ar-Tagged Predissociation and Vibrationally Mediated Photodetachment Spectroscopies of the Vinylidene Anion, $C_2H_2^-$." *Journal of Physical Chemistry A* **114** (3), 1592-1601 (2010).

30. E. Surber and A. Sanov,"Photoelectron imaging spectroscopy of molecular and cluster anions: CS_2^- and $OCS^-(H_2O)_{1,2}$." *Journal of Chemical Physics* **116** (14), 5921-5924 (2002).

6 Photoelectron Spectroscopy of 1-Nitropropane and 1-Nitrobutane anions

6.1 Introduction

In a macroscopic system, the emission of an electron from hot, vibrationally excited matter is characterized as thermionic emission.[1, 2] As one moves to smaller systems, the emission becomes less statistical, necessitating a molecular description in which sufficient vibrational excitation facilitates a breakdown of the Born-Oppenheimer leading to vibrational autodetachment.[3] The nitroalkane anions are an intriguing group of molecules that possess sufficiently small adiabatic electron affinities (AEA) to undergo vibrational autodetachment following the excitation of a fundamental CH stretching mode.[4, 5] A photoelectron spectroscopy study used to monitor vibrational autodetachment from the simplest of these nitroalkane anions, nitromethane anion, revealed substantial non-statistical contributions to the photoelectron spectrum.[3] An expansion of this study to the larger nitroalkane anions is expected to tend towards electron emission modeled more accurately as a statistical process. A step-wise approach (adding one CH_2 at a time) can offer some insight into the boundaries of each theoretical description of the electron emission. An important property in the description within either theoretical description is the AEA. This has been determined for the smaller nitroalkanes, nitromethane and nitroethane.[6, 7] The focus of this chapter will be to determine the AEA of the larger nitroalkanes, 1-nitropropane (1-NP) and 1-nitrobutane (1-NB).

At present, there only a few studies performed on 1-NP and 1-NB. The infrared spectrum of 1-NP and 1-NB anions has been determined by Schneider *et al.*[5] and several studies infrared

studies of neutral 1-NP have been performed in the liquid phase.[8, 9] Each of these molecules is expected to have several stable conformers in the anion as well as the neutral.[5, 9] In this chapter, we will present photoelectron spectra for bare and argon solvated 1-NP and 1-NB anions which are used to determine the AEA of each neutral molecule. This will be followed by a discussion of the various stable conformers found using *ab initio* theory and their relative populations in the anion beam. Franck-Condon simulations are presented for the stable anion conformations in an attempt to identify the conformer that accounts for the majority of the Franck-Condon profile intensity. Finally, an anomalous feature appearing at a fixed kinetic energy in the bare photoelectron spectrum of both 1-NP and 1-NB anions is discussed.

6.2 Computational Details

6.2.1 *Ab Initio* Calculations

In both $CH_3(CH_2)_2NO_2^-$ and $CH_3(CH_2)_3NO_2^-$, a number of stable conformers, as well as their enantiomers, can be generated by internal rotations about the CN bond or various CC bonds. It is possible that in our experiment several of the conformers are present as the temperature of our ions is estimated to be approximately 250 K, as suggested by previous studies on nitromethane and nitroethane anions under very similar source conditions.[6, 7] Density functional theory (DFT) calculations were performed using the Becke-3-Lee-Yang-Parr (B3LYP) hybrid functional[10, 11] using the GAUSSIAN 03[12] software package. The 6-311++G(2*df*,2*p*)[13, 14] basis set was used for the anion and neutral of 1-NP while computations for the larger 1-NB utilized the 6-311+G(2*d*,*p*) basis set for the anion and neutral. Various stable conformers were found for both anionic species. The stability of several conformers, with

respect to isomerization from internal rotation about the CN bond, was established by carrying out relaxed scans, employing a 6-311++G(2*d*,*p*) basis set for 1-NP anions and a 6-311+G(2*d*,*p*) basis set for 1-NB anions. Each scan was performed by scanning the HCNX dihedral angle, where X is a vector perpendicular to the plane of the NO_2 group and H is one of the H atoms on the adjacent carbon, while allowing all other distances and angles to relax.

Franck-Condon profiles for 1-NP and 1-NB anions were simulated using the PESCAL program, developed by Ervin and coworkers.[15] All vibrational degrees of freedom corresponding to the hindered internal rotations were excluded from the Franck-Condon simulation as they are poorly represented in the harmonic oscillator approximation. The remaining vibrational degrees of freedom were treated as independent harmonic oscillators and used to generate Franck-Condon factors. Duschinsky rotation[16] was taken into account using the Sharp-Rosenstock-Chen[17, 18] recursion method as implemented by the FCFGAUS03 program, also developed by Ervin and coworkers.[19] The spectra were simulated as a function of electron velocity, and later converted to spectra as a function of kinetic or binding energy, with a velocity resolution of 5000 m/s.

6.4 Results and Discussion

6.4.1 Experimental Photoelectron Spectra

6.4.1.1 1-Nitropropane Anion

Several photon energies were used to capture the photoelectron spectrum of 1-NP anion: 273 meV (2200 cm^{-1}), 329 meV (2650 cm^{-1}), 368 meV (2968 cm^{-1}), 393 meV (3170 cm^{-1}) and 2.331 eV (532 nm). The higher photon energy PE spectrum was chosen to obtain the entire vibrational progression belonging to the electronic ground state of the neutral, while the spectra obtained at lower photon energies (and correspondingly high resolution) were used to identify any important vibrational bands and to measure the adiabatic electron affinity. It should be noted that the mid-infrared photon energies were chosen to avoid contributions from vibrational autodetachment resonances of the 1-NP anion.[5]

The spectrum taken at 2.331 eV, shown in Figure 6.1, reveals an unresolved vibrational progression extending to ~1.5 eV. The maximum of the spectrum, and therefore its vertical detachment energy, is found at (0.92 ± 0.05) eV. The origin of the vibrational progression cannot be determined from this spectrum. Some vibrational structure may be seen in the high binding energy region of the spectrum (which corresponds to relatively low kinetic energy where the resolution is best for the spectrometer); the features are roughly spaced by (420 ± 150) cm^{-1}, but in light of anharmonicity effects at high vibrational quantum numbers and the possibility that several vibrations could be contributing to the observed pattern, better resolution is needed to determine what vibrational modes are active.

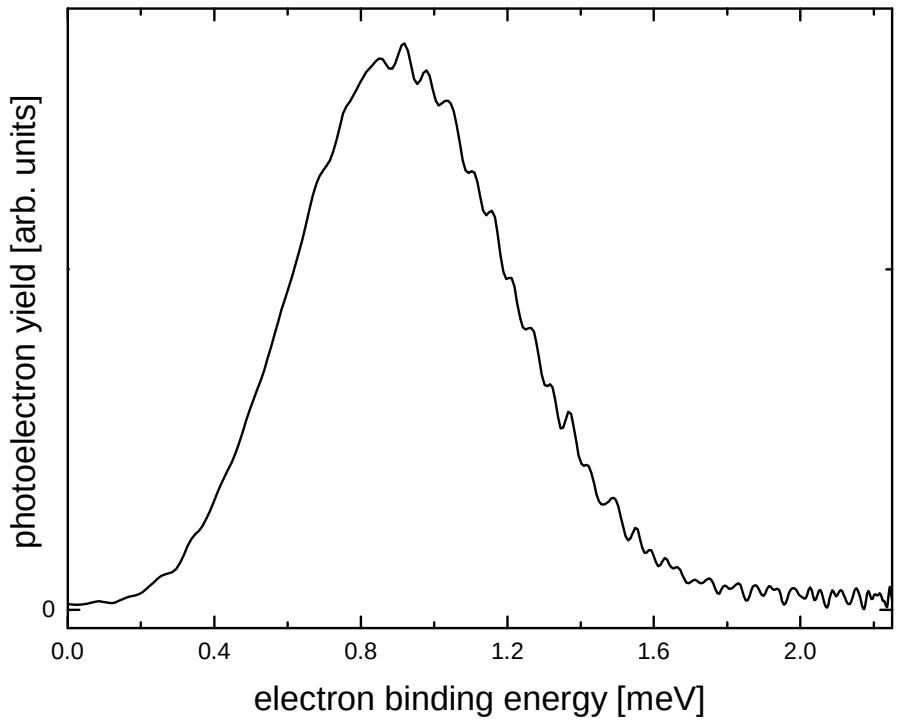

Figure 6.1 – Photoelectron spectrum of 1-NP anion obtained at a photon energy of 2.331 eV.

The low-energy photoelectron spectra are presented together in Figure 6.3 as functions of electron kinetic energy and electron binding energy. At binding energies above ~ 100 meV, all spectra exhibit a largely unresolved plateau. The first sharp peak common to all spectra (labeled "A" in Figure 6.3) is observed at a binding energy of (223 $\pm$ 6) meV with a second peak ("B") observed consistently at (296 $\pm$ 5 meV). The spacing between the first two features is (73 $\pm$ 7) meV or (589 $\pm$ 56) cm^{-1}.

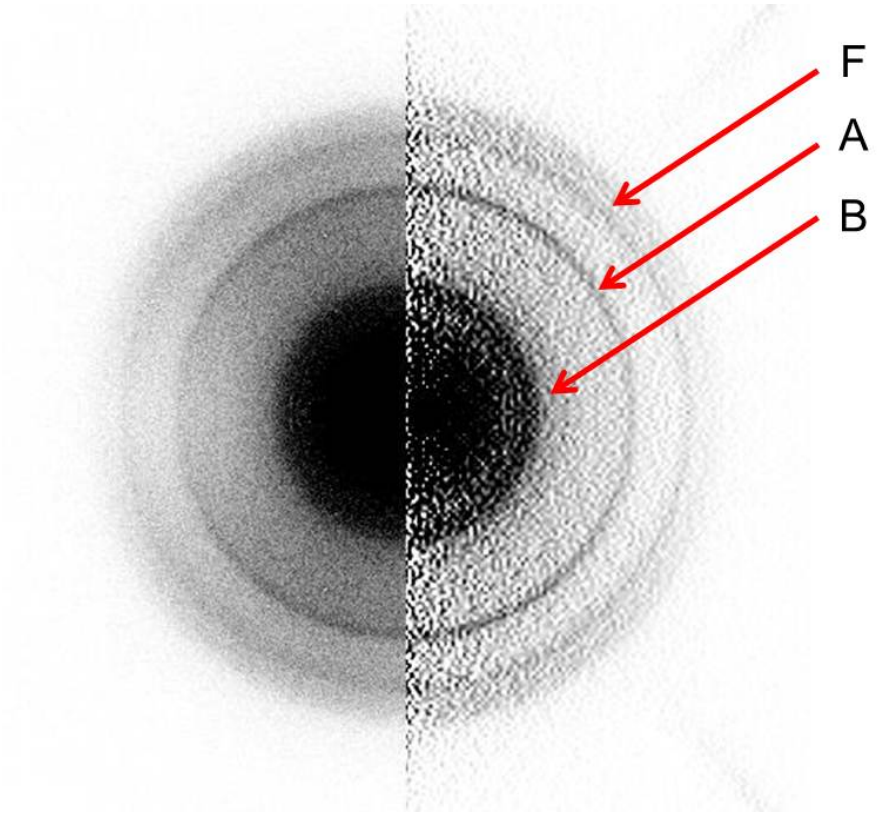

Figure 6.2 – Photoelectron image of 1-NP taken at a photon energy of 329 meV (2650 cm^{-1}). The labels "A" and "B" denote two features that are consistently observed at the same binding energy. The label "F" denotes a prominent feature found at a fixed kinetic energy in the spectra taken at photon energies of 329 meV (2650 cm^{-1}) and 368 meV (2968 cm^{-1}). See text for more details.

Curiously, an additional prominent feature ("F") appears at electron binding energies below 220 meV in the photoelectron spectra taken at 329 meV and 368 meV. The electron *binding* energy determined for this anomalous feature varies, but it shows a *kinetic* energy of (165 $\pm$ 5) meV in both spectra, i.e., independent of photon energy. Feature "F" is nearly coincident with feature "A" in the PE spectrum taken at 393 meV photon energy.

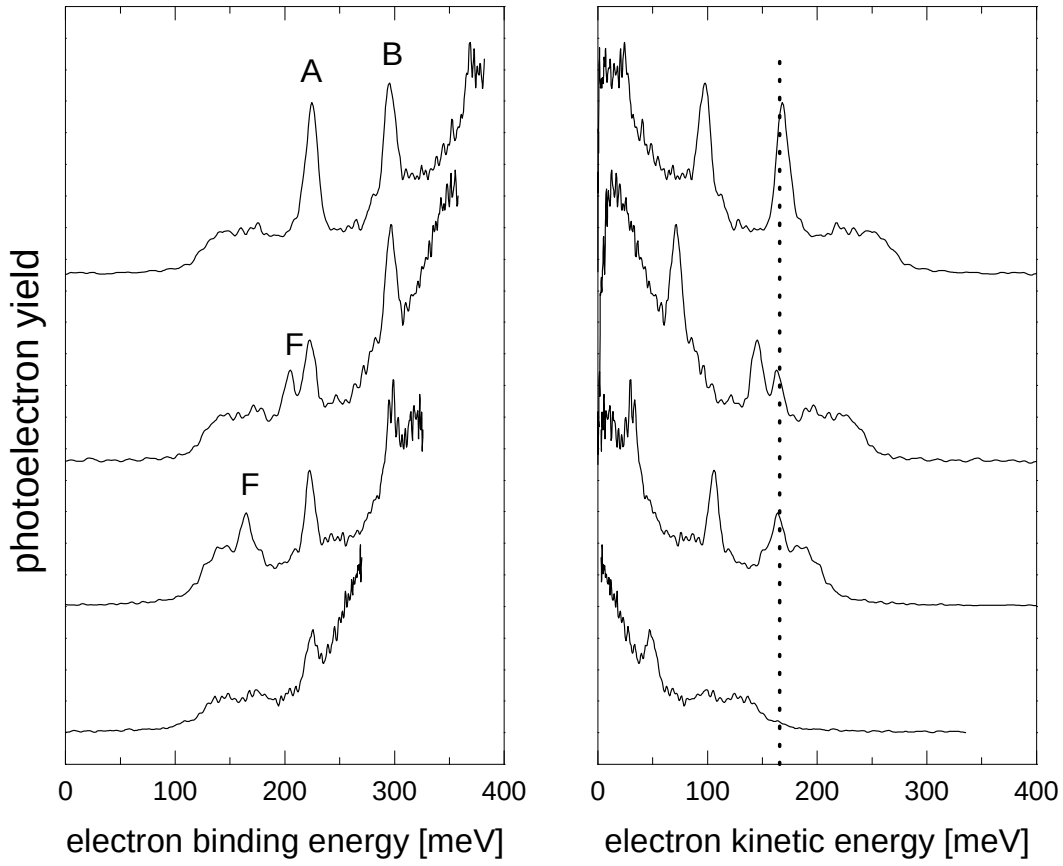

Figure 6.3 - Photoelectron spectra of 1-NP anion taken at photon energies of 393 meV (3170 cm^{-1}), 368 meV (2968 cm^{-1}), 329 meV (2650 cm^{-1}), and 273 meV (2200 cm^{-1}), from top to bottom. The spectra on the left are presented as a function of binding energy while the spectra on the right are graphed as a function of kinetic energy. The labels "A" and "B" denote two features that are consistently observed at the same binding energy. The label "F" denotes a prominent feature found at a "fixed" kinetic energy in the spectra taken at photon energies of 329 meV (2650 cm^{-1}) and 368 meV (2968 cm^{-1}). The dotted line in the spectra on the right indicates a kinetic energy of 165 meV (see text for further details).

The spectrum of $CH_3(CH_2)_2NO_2^- \cdot Ar$ obtained at a photon energy of 393 meV showed only two prominent features, as may be seen in Figure 6.4. The features on the low binding energy side of the bare $CH_3(CH_2)_2NO_2^-$ photoelectron spectrum have been strongly suppressed. We attribute the residual signal in that region to the feature observed at fixed kinetic energy, which also seems to have been suppressed in this case. The spacing of the two prominent features corresponds to the spacing of the two prominent features at in the bare PE spectrum.

Vibrational spectroscopy on liquid and solid 1-NP revealed bands at 580 cm^{-1} and at 602 cm^{-1} ,present in both phases, that have been identified as the out-of-plane bending vibration of the nitro group (or nitro wagging mode) for two different conformations.[9] This energy range is compatible with the spacing of the two prominent features at an energy of (589 ± 56) cm^{-1}. In view of the prior observation of this mode as a prominent Franck-Condon active mode in the PE spectra of smaller nitroalkane anions,[6, 20] we assign feature "A" to the $0 \leftarrow 0$ transition and "B" to the $1 \leftarrow 0$ transition of the nitro wagging mode in 1-NP. Features "A" and "B" are shifted by (56 ± 7) meV upon Ar solvation; we attribute this shift to the solvation energy of argon. It is in good agreement with the corresponding shifts observed in the PE spectra of nitromethane and nitroethane anions upon argon solvation.[6, 7] Identification of the Ar induced shift of the spectral features and the suppression of the hot bands in the PE spectrum of the Ar solvated anion corroborates the assignment of the feature located at (223 ± 6) meV to the $(0 \leftarrow 0)$ band.

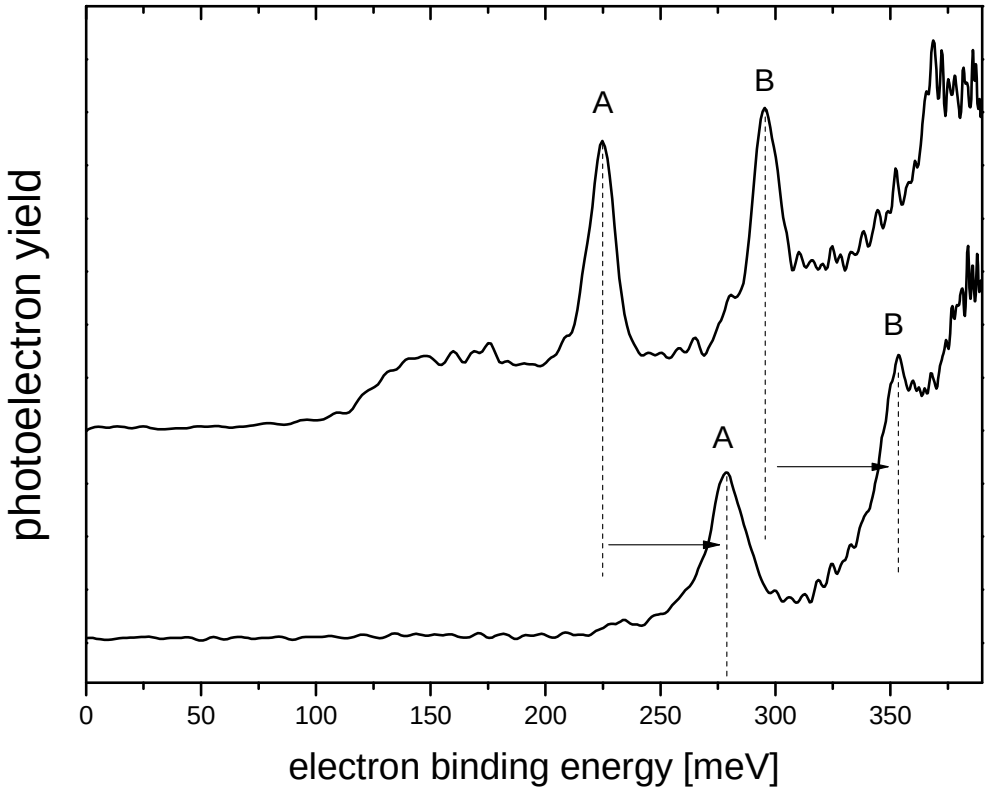

Figure 6.4 – Photoelectron spectra of bare 1-NP anion (upper curve) as well as argon-solvated 1-NP anion (lower curve) taken at a photon energy of 393 meV. The arrows represent the shift of the spectrum by an energy of (56 ± 7) meV upon argon solvation. The labels "A" and "B" denote two features that are consistently observed at the same binding energy in the bare 1-NP anion spectra.

6.4.1.2 1-Nitrobutane Anion

A similar protocol as described for 1-NP was followed for 1-NB anion with several photon energies chosen to capture the low binding energy portion as well as the entire the entire vibrational progression belonging to the electronic ground state of the neutral: 329 meV (2650 cm^{-1}), 384 meV (3100 cm^{-1}), 404 meV (3260 cm^{-1}), 424 meV (3420 cm^{-1}), 444 meV (3580cm^{-1}),

and 2.331 eV (532 nm). Again, all mid-IR photon energies were chosen to avoid influences from known vibrational autodetachment resonances.[5]

The photoelectron spectrum obtained at 2.331 eV, shown below in Figure 6.5, reveals an extended, vibrationally unresolved progression, similar to the case of 1-NP anion and nitroethane anion.[21] The vertical detachment energy is found at a binding energy of (0.88 $\pm$ 0.05) eV. At high binding energies, there are some irregular spaced features suggestive of vibrational structure. As in 1-NP anion, the ($0 \leftarrow 0$) transition cannot be unambiguously determined from the spectrum taken at high photon energy.

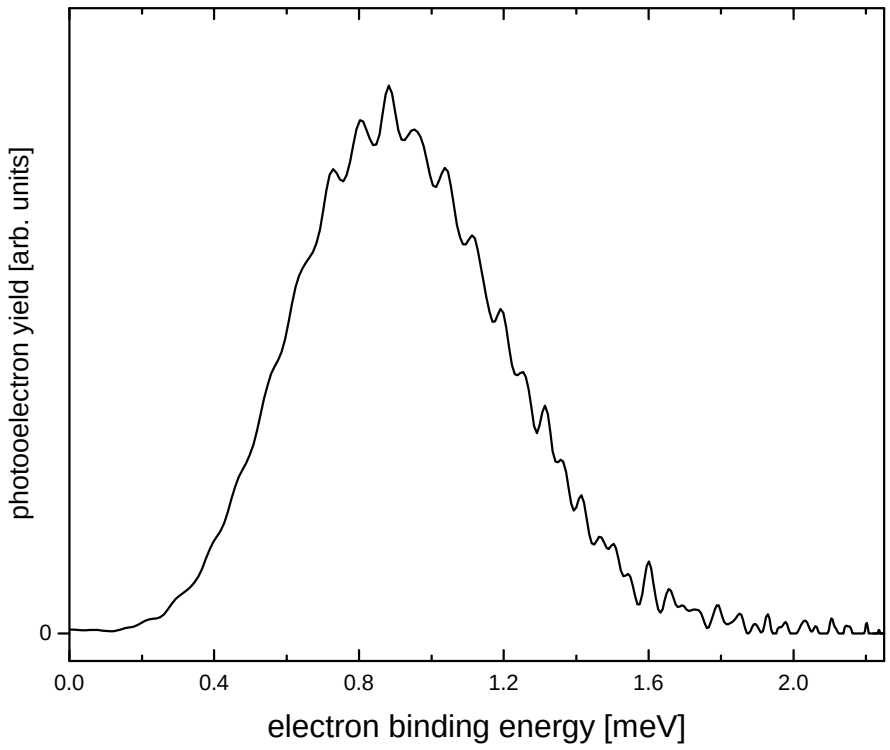

Figure 6.5 – Photoelectron spectra of 1-NB anion, obtained at a photon energy of 2.331 eV.

The low-energy, bare 1-NB anion photoelectron spectra are presented in Figure 6.6 as a function of both electron kinetic energy and electron binding energy. The spectra are remarkably

similar to the spectra of 1-NP anion with two prominent features at constant binding energies and an anomalous feature that appears at constant kinetic energy, all superimposed on a vibrationally unresolved background that extends down to approximately 125 meV binding energy. In the spectra of 1-NB anion the anomalous feature is clearly observed at all photon energies, always at a constant kinetic energy of (165 ± 5) meV (the same kinetic energy as the anomalous feature observed in 1-NP anion), as shown by the dotted line in Figure 6.6. The other two features are spaced by an energy of (74 ± 15) meV or (598 ± 120) cm^{-1} with the first feature located at a binding energy of (240 ± 6) meV. Again, based on the similarity of the photoelectron spectra of all of the 1-nitroalkane anions,[6] we assign the first two prominent bands to a vibration that is largely characterized by the nitro wagging mode in neutral 1-NB. The subject of the anomalous feature will be discussed below.

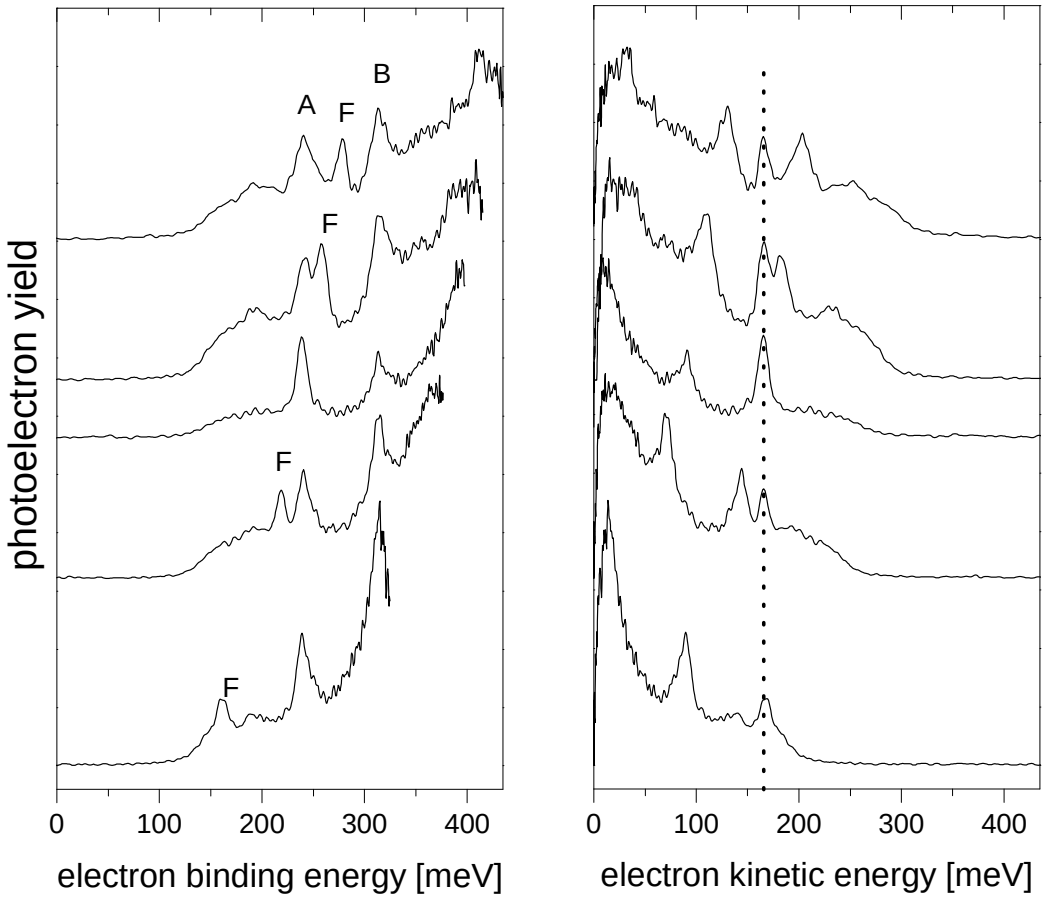

Figure 6.6 - Photoelectron spectra of 1-NB anion at photon energies of 444 meV (3580cm^{-1}), 424 meV (3420 cm^{-1}), 404 meV (3260 cm^{-1}), 384 meV (3100 cm^{-1}), 329 meV (2650 cm^{-1}), from top to bottom. The spectra on the left are presented as a function of binding energy while the spectra on the right are graphed as a function of kinetic energy. The labels "A" and "B" denote two features that are consistently observed at the same binding energy. The label "F" denotes a prominent feature found at a "fixed" kinetic energy in the spectra. The dotted line in the spectra on the right indicates a kinetic energy of 165 meV (see text for further details).

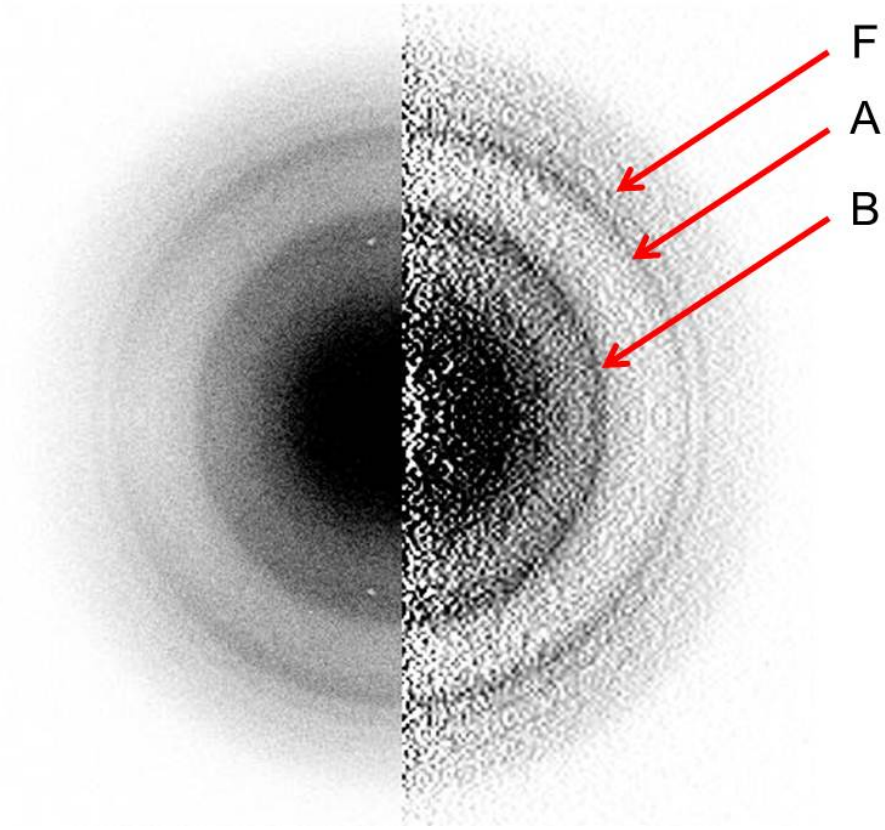

Figure 6.7 - – Photoelectron image of 1-NB taken at a photon energy of 384 meV (3100 cm^{-1}). The labels "A" and "B" denote two features that are consistently observed at the same binding energy. The label "F" denotes a prominent feature found at a fixed kinetic energy in the spectra. See text for more details.

A PE spectrum of $CH_3(CH_2)_3NO_2^- \cdot Ar$ was taken at a photon energy of 384 meV (3100 cm^{-1}), shown along with the bare 1-NB anion spectrum in Figure 6.8. The spectrum shows a strong suppression of the hot bands and only one prominent feature. The question is which of the features observed in the spectrum of the bare anion corresponds to the $(0 \leftarrow 0)$ transition. The argon solvation energy has been observed to be around 60 meV for the smaller 1-nitroalkane anions,[6] and it is reasonable to assume that this continues to be the case for 1-NB. In addition, the anomalous feature observed in the spectrum of 1-NP was suppressed upon Ar solvation. Based on these observations, we assign the feature observed at (240 ± 6) meV binding energy

in the spectrum of bare 1-NB anion to the ($0 \leftarrow 0$) transition. It is shifted by (57 ± 7) meV upon Ar solvation.

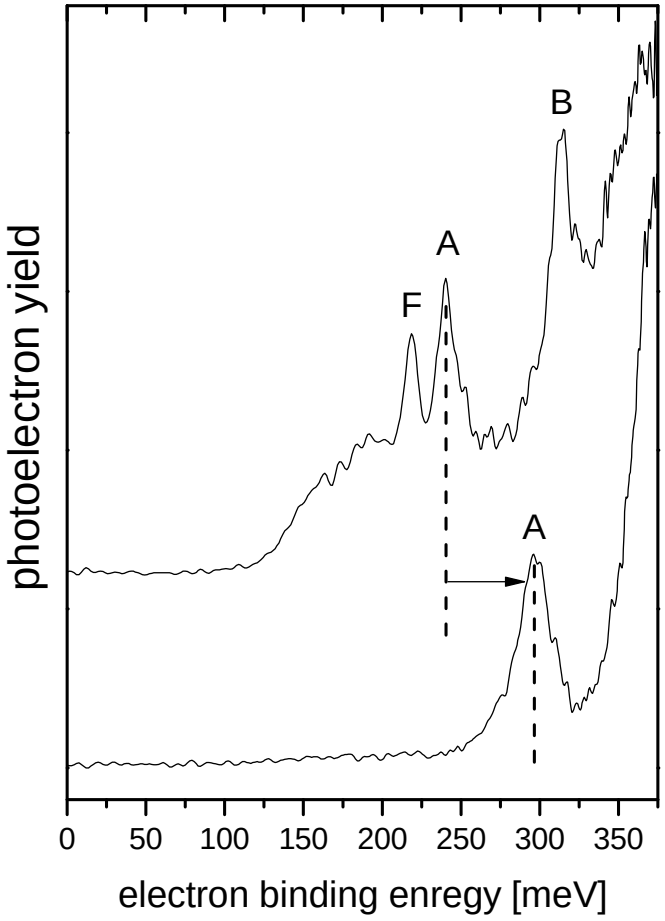

Figure 6.8 – The photoelectron spectrum of bare 1-NB anion (top curve) and argon-solvated 1-NB anion (bottom curve), taken at a photon energy of 384 meV. The arrow is used to illustrate the shift of the 0←0 feature. A "F" is placed above the anomalous feature and an "A" is placed above the feature corresponding to the 0←0 transition.

6.4.3 Stable Anionic Conformers

6.4.3.1 1-Nitropropane Anion

In order to perform FC simulations, we first have to determine which of the conformers of the anions under study are likely to be populated in the experiment. In 1-NP, five stable conformers were found as shown in Figure 6.9.

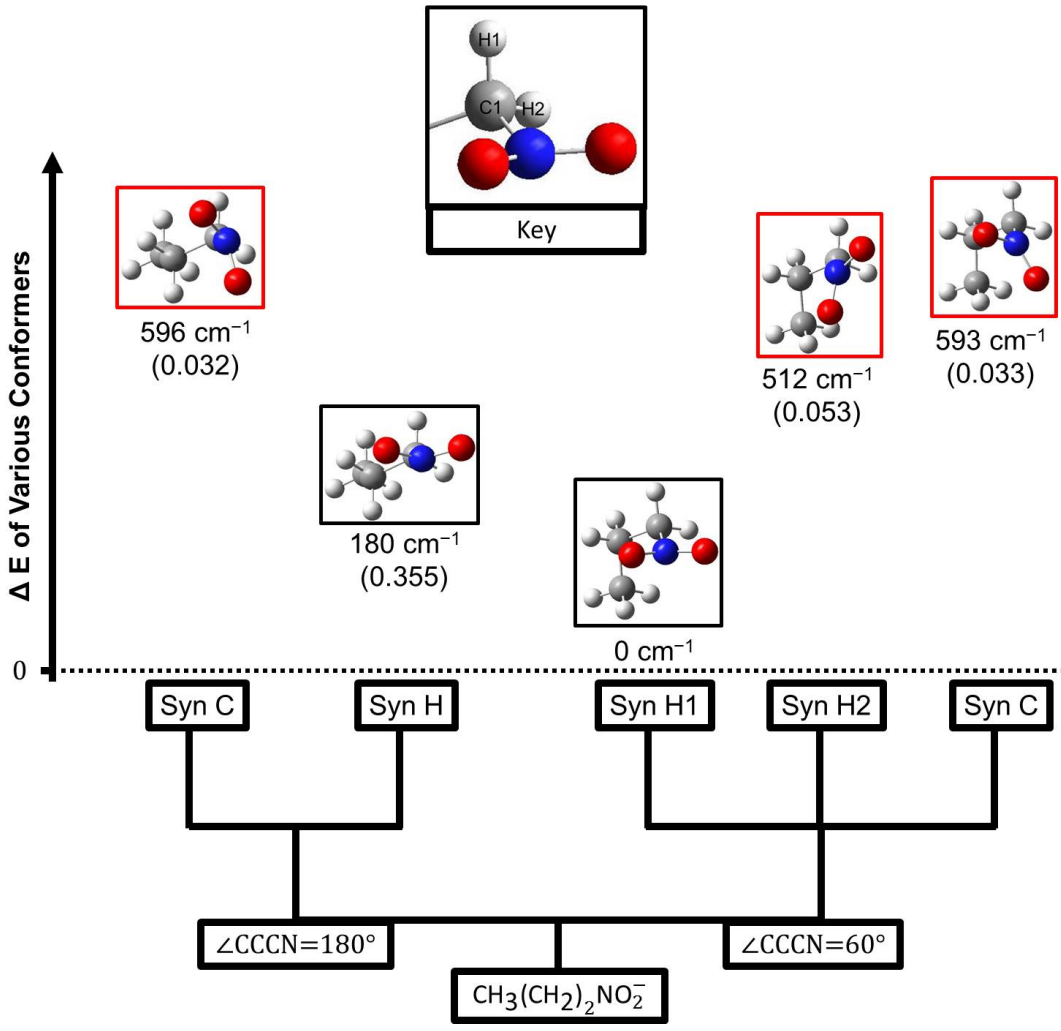

Figure 6.9 - Illustration of the various conformers of the 1-NP anion generated from rotations about the CN or central CC bond, their relative energies, and their population relative to the lowest energy conformer, according to a Boltzmann distribution. H1 and H2 are consistently defined but arbitrary designations to distinguish the hydrogens. The key at the top denotes the atoms H1 and H2. The conformers outlined in red are excluded in the Franck-Condon simulations, see discussion for more details.

The conformers can be characterized by the CCCN dihedral angle and further distinguished based upon the bond that is *syn* to the NO_2 group (C1H or C1C2). The relative populations, according to a Boltzmann distribution, are given for each conformation in Figure 6.9. These suggest that only the two lowest lying conformers are likely to be significantly populated in the beam. Additionally, calculations of the different conformers indicate that the excess electron in nitroalkane anions is stabilized by delocalization into the σ^* orbital of the CH or CC bond that is *syn* to the nitro group. For the conformer in which the CH bond is *syn* to the nitro group, this leads to a large red-shift in the CH stretching vibrational mode largely described by the motion of the destabilized CH bond. This effect has been both simulated and observed in the IR spectra of all the nitroalkane anions.[5] Importantly, calculations suggest that this shift will not be observed for any of the CH vibrational modes for the conformers in which the CC bond is *syn* to the nitro group. The spectra obtained by Schneider *et al.*[5] did not identify all of the bands in the IR spectrum of 1-NP anion, but any conformers with the CC bond *syn* to the nitro group would have a distinct vibrational band corresponding to the unshifted CH stretch. Upon sequential argon solvation the infrared spectrum remained relatively unchanged. The presence of the argon ensures that the temperature of the target cluster is low. The contribution of the two higher-energy conformers in which the CC bond is *syn* to the nitro group should be suppressed. Since no significant change was observed in the IR spectrum upon argon solvation, we find it safe to say that the two highest energy conformers are not present. The decision to exclude the conformer at a relative energy of 512 cm^{-1} was based upon relaxed scans (described in detail in section 6.2.1). These scans revealed a relatively small, ~100 cm^{-1} barrier to isomerisation to the lowest-energy conformer. We expect that within the ion source, upon electron attachment molecules in which the NCCC dihedral angle is initially 60° will readily isomerize to the lowest

energy conformation. On these grounds in addition to the low predicted population, we exclude this conformation from further analysis.

6.4.3.2 1-Nitrobutane Anion

The 1-NB anion has twelve stable conformations generated by internal rotations. Five of the higher-lying conformers, corresponding to the conformations in which the NO_2 group is *syn* to the CC bond, are not considered as they are not consistent with the infrared spectrum of 1-NB. The remaining seven conformations are illustrated in Figure 6.10 along with their relative energies and relative populations, according to a Boltzmann distribution.

Of the seven remaining conformers, the three highest energy conformers are excluded simply on the basis of their negligible populations according to the Boltzmann analysis. Relaxed scans (described in more detail in Section 6.2.1) indicated that the conformer at a relative energy of 410 cm^{-1} possesses a relatively small barrier of ~ 115 cm^{-1} to isomerisation to the lowest energy conformer. Based upon this we exclude this conformation as we expect this conformer will readily isomerize to the lowest-energy conformer.

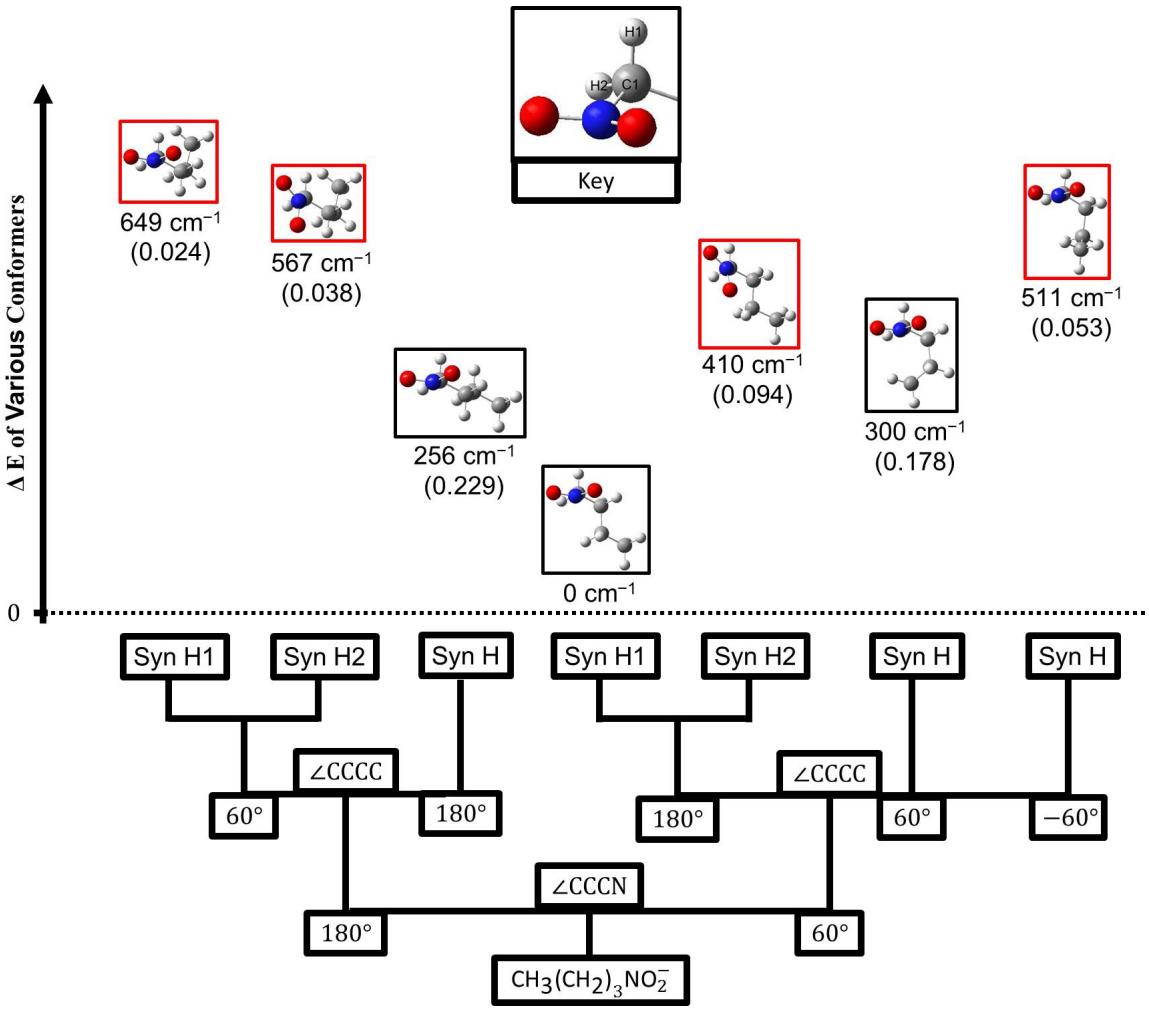

Figure 6.10 - Diagram of the stable conformers along with their relative energies, excluding the conformations in which the CC bond is *syn* to the NO_2 group. Their population relative to the lowest energy conformer, according to a Boltzmann distribution, is denoted in the parentheses. H1 and H2 are consistently defined but arbitrary designations to distinguish the hydrogens. The key at the top denotes the atoms H1 and H2. The conformers outlined in red are excluded in the Franck-Condon simulations, see discussion for more details.

6.4.4 Franck-Condon Simulations

Franck-Condon simulations were performed for the conformers of 1-NP and 1-NB anions (discussed above) that were assumed to potentially make significant contributions to the photoelectron spectra of the anions. The photoelectron spectra for both species, at low photon energies, have several features superimposed on a vibrationally unresolved and congested

background. To recover every detail of the spectrum would be exhaustive, if possible, and is not necessary to explain the experimental spectra. The purpose of these simulations is to identify which conformers best represent the experimental photoelectron spectra. Given that the photoelectron spectra of nitromethane and nitroethane anions were well represented with little to no adjustments of the displacements determined with similar calculations we assume the direct output of our simulations is sufficient for a first-order simulation.[6, 7] It should be mentioned that the entire band of the photoelectron spectrum was not fitted as the great number of active modes becomes too computationally expensive.

Calculations were also performed to identify the stable neutral conformers for each molecule. The number of neutral conformers decreases, relative to its anionic counterpart, since there is only one stable orientation for the nitro group about the CN bond. Two stable conformers were found for 1-NP and five were found for 1-NB. All of the stable neutral conformers, for each molecule, are separated by large barriers to internal rotation about the CC bonds. As the neutral conformers are well separated, each stable anion conformer will be simulated only with the neutral conformer with a matching geometry for the alkane chain.

6.4.4.1 1-Nitropropane Anion

Simulations were performed, using an anion temperature of 250 K, for the two calculated lowest energy conformers of 1-NP anion (see Section 6.2.1 for discussion), and compared to the experimental photoelectron spectrum of 1-NP anion taken at a photon energy of 368 meV (2968 cm^{-1}). The simulations were performed without the inclusion of the first four energetically low-lying vibrations as they all had significant character of the torsional modes. The nitro wagging

mode was adjusted to 589 cm^{-1} as this was the value extracted from the experimental PES. A threshold scaling factor of $E_K^{1/2}$,[22, 23] where E_K represents the electron's kinetic energy was used as it has been found to be necessary in previous near-threshold photoelectron spectroscopy studies of the smaller nitroalkane anions.[6] The simulations are shown in Figure 6.11 below along with the experimental photoelectron spectrum.

The Franck-Condon simulation of the lowest-energy conformer yields a very congested spectrum with little Franck-Condon intensity at the $0 \leftarrow 0$ transition or at lower binding energies. The simulation suggests that the unexpectedly intense and congested higher binding energy side of the experimental spectrum could be, in part, due to the presence of this conformer. However, the torsional mode around the CN bond axis has been observed in nitromethane and nitroethane anion to contribute significantly to spectral congestion and we expect this to be of similar importance here.

The simulation of the higher-energy conformer achieves a much better agreement with the prominent features of the experimental PES, as it has a substantial overlap with the experimentally identified $0 \leftarrow 0$ transition and the intensities of the two largest features are intense enough to be clearly observable through the congested background. Additionally, if the numerous combination bands with the torsional modes (not included in this simulation) were accounted for, it appears that the active transitions would serve as a reasonable manifold which could approach the shape of the observed PES. These simulations are a simplistic representation of a very complex and congested spectrum. We conclude that the simulations suggest that the conformer calculated to be at higher energy is responsible for the two prominent features in the photoelectron spectrum, and therefore is the conformer that gives rise to an AEA of (223 ± 6) meV.

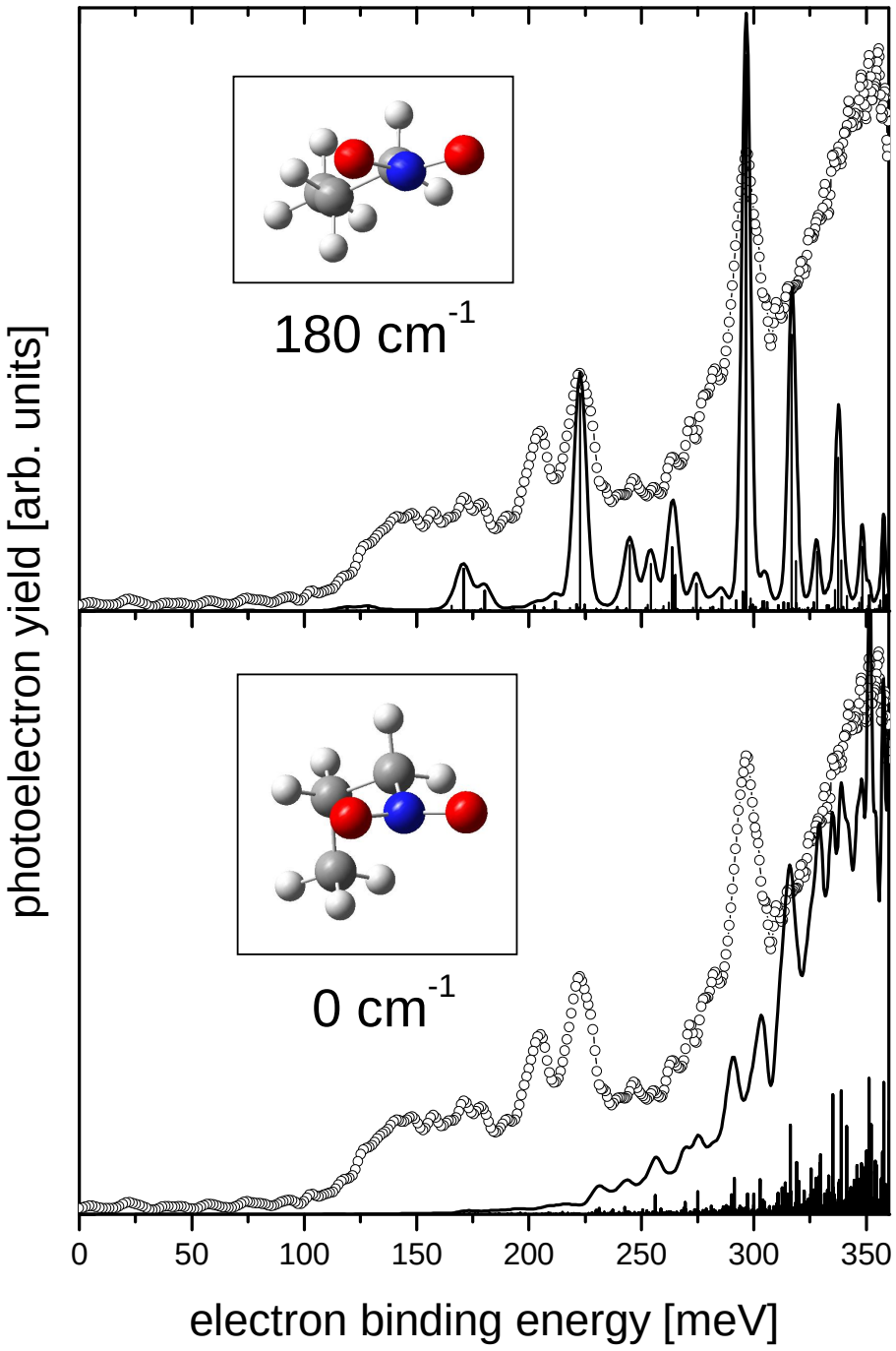

Figure 6.11 – The Franck-Condon simulations of the two lowest energy conformers of 1-NP anion, using an anion temperature of 250 K. An inset in each graph illustrates the 1-NP anion conformer along with its relative energy. The open circles, solid lines, and bars represent the observed, simulated curve, and the individual transitions.

6.4.4.2 1-Nitrobutane Anion

Franck-Condon simulations were performed using an anion temperature of 250 K for the three conformers discussed in Section 6.4.3.2. The nitro wagging mode was adjusted to the experimentally observed value of 598 cm^{-1} and the five lowest energy vibrational modes were excluded from the analysis as they are all strongly characterized by torsional motion. Just like for 1-NP, the simulations were all scaled by $E_K^{1/2}$. The simulation for each conformer is shown in Figure 10 alongside the experimental photoelectron spectrum obtained at a photon energy of 384 meV.

The Franck-Condon simulations of the 1-NB conformers results in both the lowest and highest energy conformers yielding congested spectra with little to no Franck-Condon intensity for the experimentally identified $0 \leftarrow 0$ transition. The conformer second lowest in energy best represents the experimental spectrum as it has a substantial in both the $0 \leftarrow 0$ transition and the $1 \leftarrow 0$ transition of the nitro wagging mode. As was the case in 1-NP, the assignment of the conformer responsible for the prominent features in the photoelectron spectrum is by no means definitive, given the simplifications employed in the analysis. With this in mind, the simulations indicate that the higher-energy conformer is responsible for the two prominent features in the photoelectron spectrum, and therefore is the conformer that gives rise to an AEA of (240 ± 6).

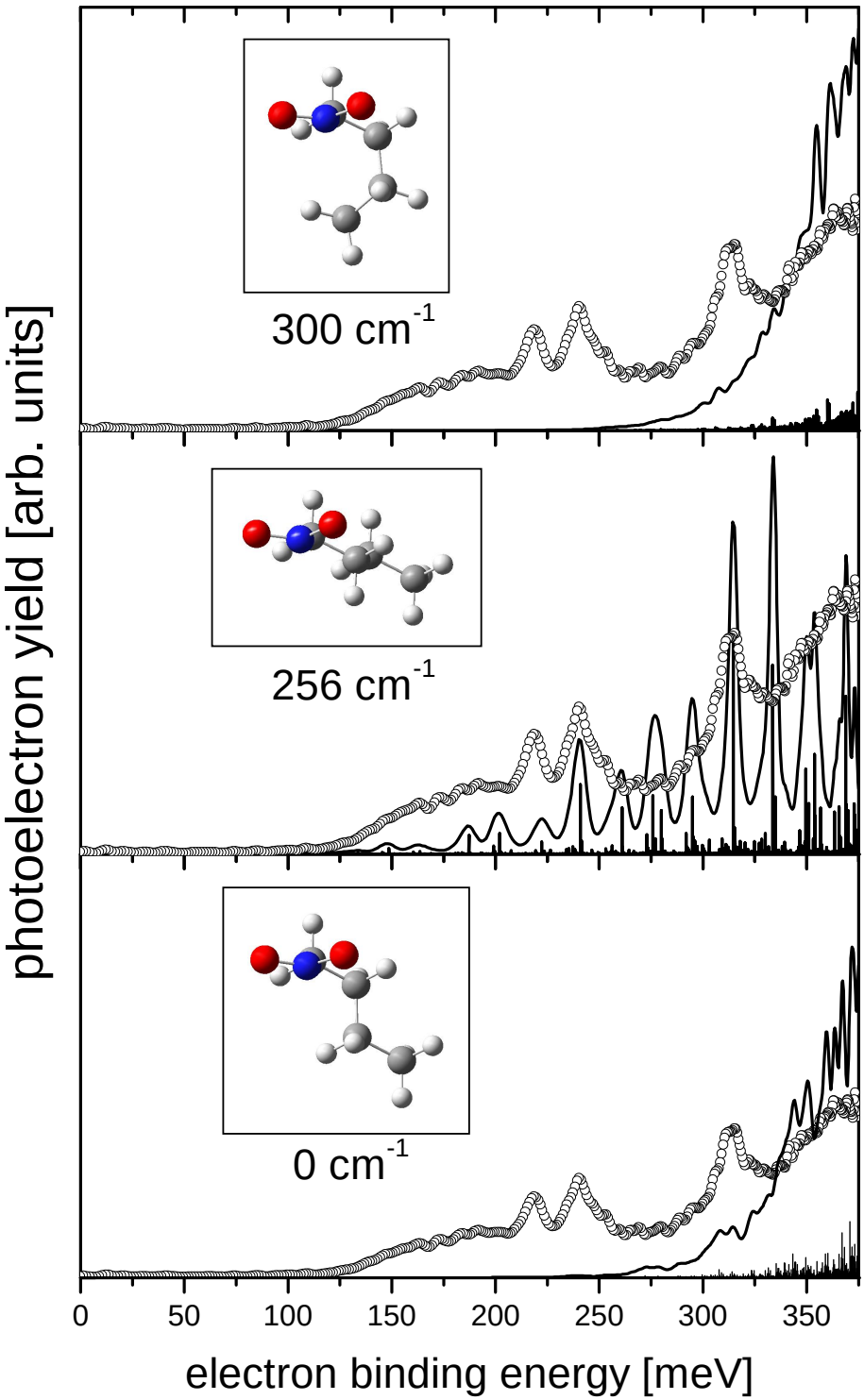

Figure 6.12 - The Franck-Condon simulations of the three lowest energy conformers of 1-NB anion, using an anion temperature of 250 K. An inset in each graph illustrates the 1-NP anion conformer along with its relative energy. The open circles, solid lines, and bars represent the observed, simulated curve, and the individual transitions.

6.4.5 Angular Distributions

The photoelectron angular distribution for single-photon detachment with linearly polarized light is described by the function[24, 25]

Equation 6.1

$$I(\theta) = \frac{\sigma}{4\pi}[1 + \beta P_2(\cos\theta)],$$

where θ is defined by the angle between the laser polarization and the emission angle, σ is the total photodetachment cross section, $P_2(\cos\theta)$ is the second-order Legendre polynomial, and β is the anisotropy parameter which varies from -1 to 2. The angular dependence is defined by β and is found by fitting Equation 6.1 to the reconstructed image over a desired range of radii.

While the anisotropy parameter β does not lend itself to a straightforward interpretation, in the case of photodetachment from anions, it carries the signature of the electronic nature of the detachment transition,[22] and features belonging to the same electronic transition usually exhibit a smooth behavior in β. Therefore, the anisotropy parameter β can hint at anomalous behavior in the electronic transition that leads to observed features in experimental PE spectra.

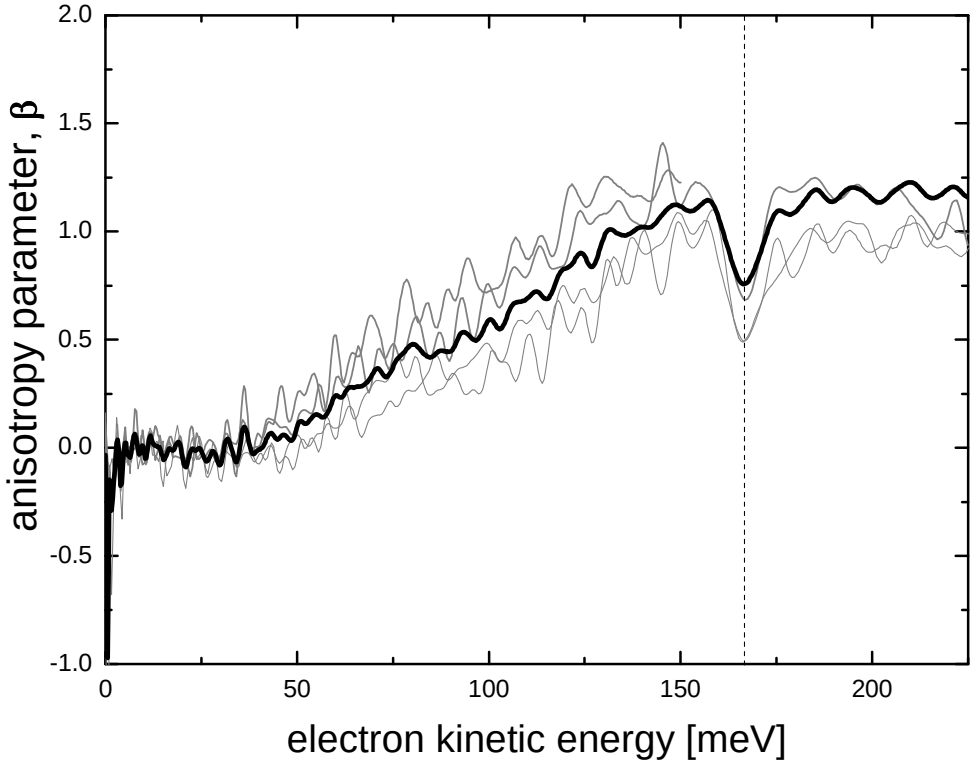

Figure 6.13 – Plot of the fitted anisotropy parameters, β, as a function of kinetic energy for the four different lower-energy photon wavelengths used in the study of 1-NP anion (gray lines) as well as their average (dark black line). The dashed line is located at a kinetic energy of 166 meV.

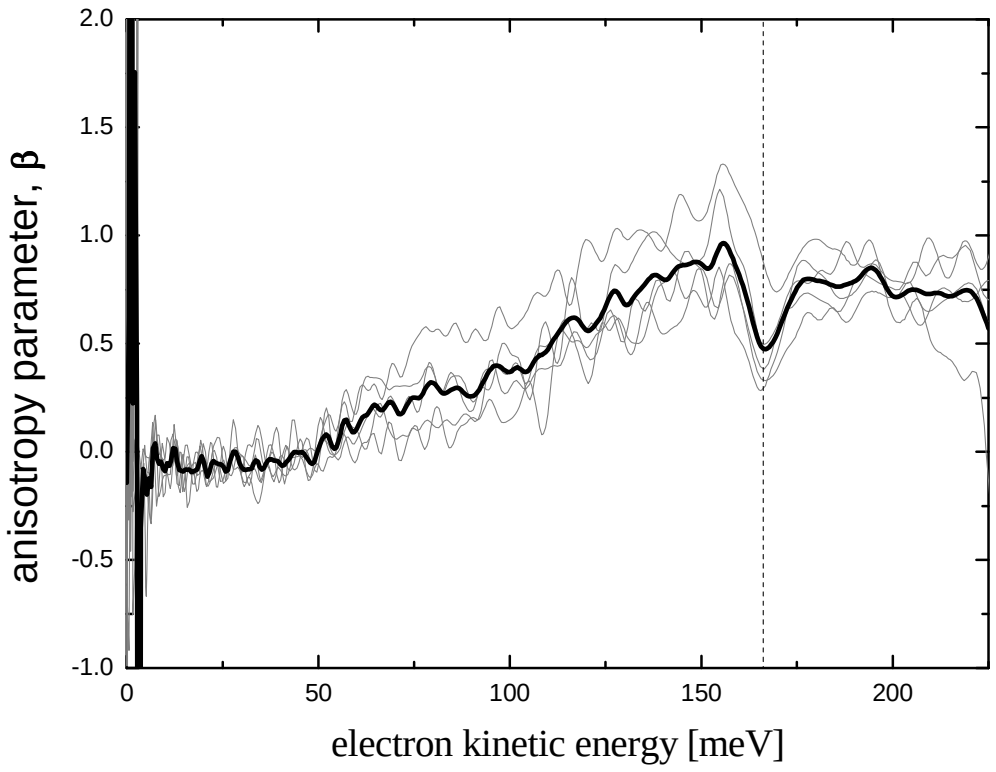

Figure 6.14 - Plot of the fitted anisotropy parameters, β, as a function of kinetic energy for the five different lower-energy photon wavelengths used in the study of 1-NB anion (gray lines) as well as their average (dark black line). The dashed line is located at a kinetic energy of 166 meV.

The plot of the anisotropy parameters is very similar for both 1-NP and 1-NB anions (see Figure 6.13 and Figure 6.14) and remains relatively stable with respect to the photodetaching energy. The beta parameter is insensitive to the two well-behaved peaks that appear at constant binding energy in all of the spectra. The angular distribution is nearly isotropic out to a kinetic energy of 50 meV at which point both plots exhibit a steady increase in the anisotropy parameter. At an energy of 166 meV, the anisotropy parameter exhibits a sharp decrease. This sharp deviation of the anisotropy parameter at a kinetic energy of 166 meV, which is coincident with the anomalous feature seen at fixed kinetic energies in all of the plots, strongly suggests that this feature is due to a different electronic detachment transition.

6.4.6 Remarks on the Anomalous Feature in Photodetachment from 1-nitropropane and 1-nitrobutane anions

The observation of an anomalous feature in photoelectron imaging of 1-nitropropane and 1-nitrobutane is puzzling. Naturally, the first suspicion one would have is that this feature is due to an experimental artifact, but we saw no such feature in the spectrum of nitromethane anion, which was often used to check the validity of the PE spectra during the present study. After a number of careful tests recording the known PE spectrum of nitromethane and reproducing the experiments on 1-NP and 1-NB on several different days, we are convinced that the anomalous feature in both spectra is not due to an experimental artifact. At the present time, we feel confident that this feature belongs to a detachment process distinctly different from that of direct photodetachment but our understanding of the origin of this feature is fairly rudimentary. As such, we will postpone further discussion of this feature until we are able to obtain a more detailed understanding of its origin.

6.5 Summary

We have studied the photoelectron spectra and angular distributions of the 1-NP and 1-NB anion at several photon energies. The relatively high-energy photoelectron studies were able to capture the entire vibrational progression corresponding to the electronic ground state of the neutral. From these, vertical detachment energies of $(0.92 \pm .05)$ eV and $(0.88 \pm .05)$ eV were established for 1-NP anion and 1-NB anion, respectively. We have determined a new value for the adiabatic electron affinity of 1-NP at (223 ± 6) meV and (240 ± 6) meV for 1-NB. We utilized *ab initio* calculations to establish the stable conformers of each anion and employed Franck-Condon simulations to identify what conformations could be responsible for the

empirically determined AEA's. Finally, an anomalous feature appearing at a constant kinetic energy was shown to have significantly different anisotropy parameter, indicating that it originates from a different electronic transition.

6.6 References for Chapter 6

1. E. E. B. Campbell and R. D. Levine,"Delayed ionization and fragmentation en route to thermionic emission: Statistics and dynamics." *Annual Review of Physical Chemistry* **51**, 65-98 (2000).

2. B. Climen, F. Pagliarulo, A. Ollagnier, B. Baguenard, B. Concina, M. A. Lebeault, F. Lepine and C. Bordas,"Threshold laws in delayed emission: an experimental approach." *European Physical Journal D* **43** (1-3), 85-89 (2007).

3. C. L. Adams, H. Schneider and J. M. Weber,"Vibrational Autodetachment – Intramolecular Vibrational Relaxation Translated Into Electronic Motion." *Journal of Physical Chemistry A* **114**, 4017-4030 (2010).

4. J. M. Weber, W. H. Robertson and M. A. Johnson,"Argon predissociation and electron autodetachment spectroscopy of size-selected $CH_3NO_2^-\cdot Ar_n$ clusters." *Journal of Chemical Physics* **115** (23), 10718-10723 (2001).

5. H. Schneider, K. M. Vogelhuber, F. Schinle, J. F. Stanton and J. M. Weber,"Vibrational spectroscopy of nitroalkane chains using electron autodetachment and Ar predissociation." *Journal of Physical Chemistry A* **112** (33), 7498-7506 (2008).

6. C. L. Adams, H. Schneider, K. M. Ervin and J. M. Weber,"Low-energy photoelectron imaging spectroscopy of nitromethane anions: Electron affinity, vibrational features, anisotropies and the dipole-bound state." *Journal of Chemical Physics* **130**, 074307-074301 - 074310 (2009).

7. C. L. Adams and J. M. Weber,"Photoelectron imaging spectroscopy of nitroethane anions." *J. Chem Phys.* **134** (24), 244301-244308 (2011).

8. D. C. Smith, C.-Y. Pan and J. R. Nielsen,"Vibrational Spectra of the Four Lowest Nitroparaffins." *The Journal of Chemical Physics* **18** (5), 706-712 (1950).

9. M. I. Shilina, V. M. Senyavin, G. M. Kuramshina, V. V. Smirnov and Y. A. Pentin,"Vibrational spectra, assignment, conformational stability and ab Initio/DFT calculations for 1-nitropropane." *Structural Chemistry* **14** (6), 559-573 (2003).

10. A. D. Becke,"Density-Functional Thermochemistry .3. The Role of Exact Exchange." *Journal of Chemical Physics* **98** (7), 5648-5652 (1993).

11. C. T. Lee, W. T. Yang and R. G. Parr,"Development of the Colle-Salvetti Correlation-Energy Formula into a Functional of the Electron-Density." *Physical Review B* **37** (2), 785-789 (1988).

12. M. J. Frisch, G. W. Trucks, H. B. Schlegel, G. E. Scuseria, M. A. Robb, J. R. Cheeseman, J. A. Montgomery, J. Vreven, T. , K. N. Kudin, J. C. Burant, J. M. Millam, S. S. Iyengar, J. Tomasi, V. Barone, B. Mennucci, M. Cossi, G. Scalmani, N. Rega, G. A. Petersson, H. Nakatsuji, M. Hada, M. Ehara, K. Toyota, R. Fukuda, J. Hasegawa, M. Ishida, T. Nakajima, Y. Honda, O. Kitao, H. Nakai, M. Klene, X. Li, J. E. Knox, H. P. Hratchian, J. B. Cross, V. Bakken, C. Adamo, J. Jaramillo, R. Gomperts, R. E. Stratmann, O. Yazyev, A. J. Austin, R. Cammi, C. Pomelli, J. W. Ochterski, P. Y. Ayala, K. Morokuma, G. A. Voth, P. Salvador, J. J. Dannenberg, V. G. Zakrzewski, S. Dapprich, A. D. Daniels, M. C. Strain, O. Farkas, D. K. Malick, A. D. Rabuck, K. Raghavachari, J. B. Foresman, J. V. Ortiz, Q. Cui, A. G. Baboul, S. Clifford, J. Cioslowski, B. B. Stefanov, G. Liu, A. Liashenko, P. Piskorz, I. Komaromi, R. L. Martin, D. J. Fox, T. Keith, M. A. Al-Laham, C. Y. Peng, A. Nanayakkara, M. Challacombe, P. M. W. Gill, B. Johnson, W. Chen, M. W. Wong, C. Gonzalez and J. A. Pople, Gaussian 03, Wallingford CT, 2004.

13. R. Krishnan, J. S. Binkley, R. Seeger and J. A. Pople,"Self-Consistent Molecular-Orbital Methods .20. Basis Set for Correlated Wave-Functions." *Journal of Chemical Physics* **72** (1), 650-654 (1980).

14. A. D. McLean and G. S. Chandler,"Contracted Gaussian-Basis Sets for Molecular Calculations .1. 2nd Row Atoms, Z=11-18." *Journal of Chemical Physics* **72** (10), 5639-5648 (1980).

15. K. M. Ervin, PESCAL, University of Nevada, Reno, 2008.

16. F. Duschinsky,"The importance of the electron spectrum in multi atomic molecules. concerning the Franck-Condon principle." *Acta Physicochimica URSS* **7** (4), 551-566 (1937).

17. T. E. Sharp and H. M. Rosenstock,"Franck-Condon Factors for Polyatomic Molecules." *Journal of Chemical Physics* **41** (11), 3453-3463 (1964).

18. P. Chen, in *Unimolecular and Bimolecular Reaction Dynamics*, edited by C.-Y. Ng, T. Baer and I. Powis (John Wiley & Sons, Chichester, 1994), pp. 371.

19. K. M. Ervin, FCFGaus03, University of Reno, Nevada, 2008.

20. R. N. Compton, H. S. Carman, C. Desfrancois, H. Abdoul-Carmine, J. P. Schermann, J. H. Hendricks, S. A. Lyapustina and K. H. Bowen,"On the binding of electrons to nitromethane: Dipole and valence bound anions." *Journal of Chemical Physics* **105** (9), 3472-3478 (1996).

21. S. T. Stokes, K. H. Bowen, T. Sommerfeld, S. Ard, N. Mirsaleh-Kohan, J. D. Steill and R. N. Compton,"Negative ions of nitroethane and its clusters." *Journal of Chemical Physics* **129** (6) (2008).

22. K. J. Reed, A. H. Zimmerman, H. C. Andersen and J. I. Brauman,"Cross-Sections for Photodetachment of Electrons from Negative-Ions near Threshold." *Journal of Chemical Physics* **64** (4), 1368-1375 (1976).

23. E. P. Wigner,"On the Behavior of Cross Sections near Thresholds." *Physical Review* **73** (9), 1002-1009 (1948).

24. C. N. Yang,"On the Angular Distribution in Nuclear Reactions and Coincidence Measurements." *Phys. Rev.* **74** (7), 764-772 (1948).

25. J. Cooper and R. N. Zare,"Angular Distribution of Photoelectrons." *Journal of Chemical Physics* **48** (2), 942-943 (1968).

7 Vibrational Autodetachment Photoelectron Spectroscopy of Nitromethane Anion

This chapter has been reproduced in part with permission from Adams, C.L., Schneider, H., and Weber, J.M., "Vibrational Autodetachment-Intramolecular Vibrational Relaxation Translated Into Electronic Motion." *Journal of Physical Chemistry A,* 2010. dx.doi.org/10.1021/jp105910s.

7.1 Overview of Vibrational Autodetachment

All chemical reactions are governed by the nuclear dynamics of molecules, in other words, their patterns of vibrational motion, and any predictive theoretical treatment of chemical reactions needs to describe these motions. Therefore, the way in which vibrational energy flows through and is redistributed in molecules after excitation has significant impact on the understanding of chemical reactions (see, e.g., refs 1 and 2). Moreover, energy flow through nanoscale systems is presently of much interest as technology utilizes progressively smaller electronic devices which can approach the destruction limit of energy density.[3, 4]

Consequently, there has been much work on intramolecular vibrational relaxation (IVR) processes during the last several decades. Much progress has been made, which has been documented in a number of excellent reviews of the field.[5-24] "Standard models" of IVR are in existence, which have been used with great success in the modeling of IVR in relatively small molecules.[7, 10, 25-28] However, the extension to larger systems is still a challenging and fertile area for experimental and theoretical investigation (see, e.g., refs 2, 15, 17, 23, and 29-44).

It is important to make a distinction between the relatively simple normal mode description of molecular vibration and the "true" eigenstates of the full molecular Hamiltonian. While providing a reasonable approximation at low vibrational energies, the "zero-order" normal mode description is based on the harmonic approximation and therefore neglects the coupling between different modes. In contrast, the eigenstates of the full Hamiltonian are the result of all forces in the molecule, including anharmonic contributions. They can be expanded in terms of the "zero-order" basis.

One important experimental access to studying IVR has been optical excitation. Since the transition dipole matrix for vibrational transitions from the ground state is effectively diagonal in the zero-order basis, only one of the zero-order basis states will carry significant transition strength from the ground state and couple efficiently to the exciting radiation field. This is the zero-order bright state (ZOBS), which is not a stationary state (since it is not an eigenstate of the system). In a one-photon excitation with narrow bandwidth (i.e., relatively long pulses or cw radiation), the spectrum consists of a series of molecular eigenstates. Since these molecular eigenstates can be represented in the zero-order basis, the intensity of the transition to a given eigenstate reflects the contribution of the ZOBS to that eigenstate.

Often, IVR processes are analyzed in terms of a tier model where the energy in the ZOBS is first transferred by strong, low-order anharmonic coupling to a "tier" of energetically close dark states (often called doorway states), from which the energy flows into states further removed (see, e.g., ref 7 for a review). The density of states becomes successively greater with each new tier. Another approach to describe energy flow in molecular systems is in a state space picture, representing normal mode basis states as lattice points in multidimensional quantum number space, where eigenstates typically delocalize over the lattice.[45, 46] In the condensed

phase, the energy eventually dissipates out of the molecule into the “bath” states of the solvent. In the case of a molecule in the gas phase under single collision conditions, the only pathways for relaxation are radiative cooling, electron emission, and dissociation, all of which can be neglected for nanosecond time scales and sufficiently low excitation energies. Therefore, the sum of rovibrational energy in the molecule is conserved and one can view the lowest frequency modes of the molecule (e.g., skeletal modes of a long alkane chain) as “bath modes”, if the molecule is large enough.

There is continued interest in IVR as new theoretical methods are developed and need to be tested with ever larger molecular species.[38, 40, 41, 47, 48] While IVR processes are in general qualitatively understood and the theory on small molecules has reached a reasonable level of predictive power, the complexity of anharmonic coupling in larger molecules makes these systems formidably difficult to understand.

Experiments at low vibrational energies seem like an obvious starting point, as the probability of accidental resonances between zero-order modes will be small. Moreover, quantum effects and “non-statistical” processes in IVR will be most important at low energies, while high energies often afford a description on the basis of statistical models. Many groups have obtained IVR time scales from the line width analysis of IR excitation (see, e.g., refs 7, 15-17, 25, and 49-62) and fluorescence (e.g., refs 63-67) resolution, these experiments primarily probe the time scales corresponding to the coupling of the various “tiers”. The multiple time scales involved can be extracted from hierarchical analysis of these frequency-resolved spectra. Another class of experiments on IVR on the ground state electronic surface employed pump-probe ultrafast spectroscopy, both in molecules and clusters (e.g., 31, 32, 68, 34, and 69-72), and

in liquids (e.g., refs 3, 24, 72-75). In these cases, the coupling time scales can be obtained from multi-exponential behavior of the molecular response.

One intriguing group of targets is anions which possess low adiabatic electron affinities in which a vibrational mode represents a ZOBS embedded in a continuum of dark states (the electron emission continuum). Vibrational autodetachment (VAD) can occur if the electron binding energy of the excess electron in an anion is comparable to or less than the energies of some of its vibrational modes.

The conceptual and theoretical foundation for auto-ionization in neutral molecules and autodetachment was laid as early as 1966 by Berry.[76] Theoretical studies of autodetachment from anions by Simons and co-workers[77, 78] followed some 15 years later, prompted by early studies of Brauman and co-workers[79-83] and Beauchamp and co-workers[84-86] on vibrational autodetachment from multiphoton excitation of anions. The VAD approach has not been widely used for spectroscopic purposes. One of the first spectroscopic studies investigating rovibrational autodetachment was performed by Lineberger and coworkers,[87] where the excess electron from NH^- was ejected after rovibrational excitation of the anion. They also studied the vibrational autodetachment spectrum of enolate via excitation of the dipole-bound state of CH_2CHO^-.[88] VAD has been employed with a (partial) focus on IVR a few years ago by Johnson and coworkers, in a study of bare and argon solvated nitromethane anions.[89] In addition, the same group applied VAD more recently to the water hexamer anion,[90] where they studied how different isomers of this cluster ion are responsible for different features in the photoelectron spectrum as the detachment laser is tuned through OH stretching resonances belonging to a particular isomer. This approach has been recently extended within our group to include many

more nitroalkane species where the excess electron has a lower binding energy than the energy of the CH stretching modes.[91]

The coupling of vibrational energy to electronic motion manifests itself in macroscopic systems, e.g., as thermionic emission, described by the Richardson equation.[92] In a molecular description, VAD constitutes a breakdown of the Born-Oppenheimer approximation, since it is a clear example of the coupling of electronic and nuclear motion. Its inverse process, vibration-mediated electron attachment, has long been studied by many groups and falls into a similar category (see, e.g., refs 93 and 94).

A simplifying assumption allowing a qualitative discussion of the underlying process is that VAD is primarily promoted along some reaction coordinate Q describing the concomitant change in molecular geometry. Q will, in general, not be a normal coordinate (except for a diatomic) but is likely a linear combination of several normal coordinates. In a photoelectron spectroscopy experiment, the normal modes belonging to these coordinates will have the most pronounced vibrational progressions, signifying the main geometry difference between anion and neutral. In a series of pioneering theoretical articles on VAD, Simons[77, 78] described several scenarios according to the behavior of the anionic and neutral potential energy curves along Q. He distinguished these scenarios based on whether or not the potential curves cross along Q, and, if so, whether crossing would occur at the limits of Q (i.e., some internuclear separation approaching zero or infinity) or at some intermediate configuration. Moreover, the rate of variation of the energy difference between the anionic and the neutral potential energy curves along Q is an important point, as is the energy difference between the anionic parent vibrational state and the neutral final state, i.e., the kinetic energy of the emitted electron. The latter is expected to be the dominant contribution to the electron emission rate constant, since the energy

difference appears in a “resonance denominator” in the expression governing the emission probability.

It should be pointed out that Franck-Condon factors are not governing the VAD process in the same way as in “regular” (i.e., nonresonant) photodetachment. Instead of the overlap between the vibrational wavefunction of the anion *prior* to excitation and of the neutral final state (nonresonant photodetachment), it is the overlap of the vibrational wavefunction of the anion and the neutral final state *after* vibrational excitation of the anion that will play a role. This overlap will critically depend on the evolution of the anion vibrational wavefunction during IVR and will therefore be time dependent. When VAD occurs after targeted excitation of a specific vibrational mode in the anion by infrared radiation, it encodes information on the IVR processes that take place between excitation and electron emission.

It should be noted that in the case where the anionic and neutral diabatic curves cross (which is the relevant scenario here), one can describe the transition of the excess electron from the bound to the continuum state as a Feshbach or shape resonance.[77, 78, 95] In this case, the factors governing the detachment rate from a vibrational state accessing the intersection are the overlap of the anionic and neutral vibrational wavefunctions at the “seam” of the diabatic potential energy curves and an electronic coupling term containing the resonance description, which does not necessarily involve large nonadiabatic terms. In this case, the description of the detachment process contains a mixture of electronic and nonadiabatic coupling. If the curves do not cross, there is no electronic coupling and the nonadiabatic coupling terms involved generate qualitatively different rate expressions.[96]

In the remainder of this chapter we will discuss some general considerations regarding vibrational autodetachment in $CH_3NO_2^-$ and present the photoelectron spectra of $CH_3NO_2^-$ obtained on vibrational resonances that lead to VAD. Then we will discuss the results in the context of several simple models before closing with a summary of open questions and an outlook toward future work.

7.2 Vibrational Autodetachment of Nitromethane Anion: General Considerations

As was discussed earlier in Chapter 4, the main geometry difference between the anion and the neutral geometries of CH_3NO_2 lies in angle between the ONO plane and the CN bond axis; the angle is nearly coplanar in the neutral molecule but is ~ 30° in the anion. Correspondingly, the NO_2 "wagging" mode, $w(NO_2)$ (note that we use the same labels for the vibrational modes of CH_3NO_2 as Gorse et al.[97]), in which the displacement is largely described by this angle, has an extended vibrational progression which accounts for the majority of the Franck-Condon activity in the photoelectron spectrum of $CH_3NO_2^-$.[98, 99] The remainder of the activity in the photoelectron spectrum is almost completely accounted for by four other normal modes. These are the CH_3 umbrella mode, $\delta_s(CH_3)$; the NO_2 symmetric stretch, $\nu_s(NO_2)$; the CH_3 rocking mode, $r_\perp(CH_3)$; and the CN stretch, $\nu(CN)$. Given that these modes all undergo a substantial displacement upon photodetachment, it is expected that a linear combination of the corresponding normal coordinates will largely define the detachment reaction coordinate, Q, in which the $w(NO_2)$ mode is expected to the most prominent. The strong geometry difference results in a crossing of the diabatic anionic and neutral potential curves along Q.[89, 95, 98]

In contrast to the modes largely characterized by displacement within the nitro group, the CH stretching normal coordinates do not seem to be important contributors to Q.[89, 99] In a greatly simplified picture, one could summarize the reaction coordinate Q as one coordinate and a generalized CH stretching coordinate as a second coordinate orthogonal to Q. The resulting potential energy surfaces of the anion and the neutral in these two coordinates is depicted in Figure 7.1.

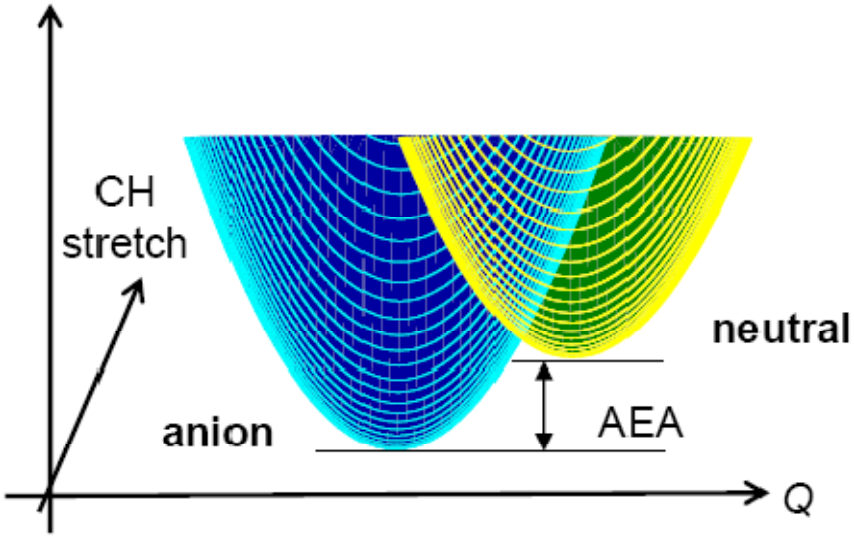

Figure 7.1 – Schematic drawing of the diabatic anionic and neutral potential energy surfaces of nitromethane. The anionic surface is connected to that of the neutral along the detachment coordinate *Q*. In contrast, the CH stretching modes are not connecting the two surfaces and excitation of one quantum of a CH stretching vibration will not lead to immediate detachment. VAD will only occur after sufficient energy has been redistributed into *Q*.

A very interesting aspect of nitromethane is that it can bind an excess electron in two fundamentally different ways. In one form of $CH_3NO_2^-$, the excess electron is contained in a valence orbital (see Figure 7.2); the other is a state where the excess electron is bound in the dipole field of the molecule, where the average distance of the electron from the molecular frame is typically on the order of several 10 Å (see e.g., refs 95, 98, 100). The molecular geometry belonging to the dipole-bound state is practically the same as for the neutral. In the context of

vibrational autodetachment, the dipole-bound state can be seen as a "doorway" between the valence anion and the neutral. The actual coupling between the two states has been explored by Sommerfeld using multi-reference configuration interaction.[95] He describes the valence anion in the geometry of the neutral, i.e., in the "crossing region" of the diabatic curves, as a shape resonance with a width of 0.25 eV, corresponding to a lifetime of a few femtoseconds.

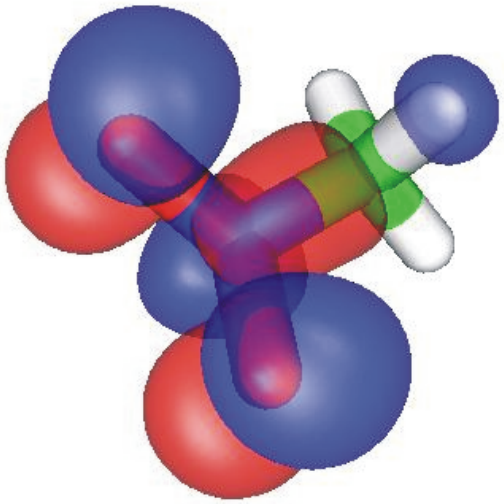

Figure 7.2 – Highest occupied molecular orbital (HOMO) of the nitromethane valence anion.

Upon absorption of an IR photon in a CH stretching vibrational mode, the absorbed energy is redistributed in the molecule. If enough energy is transferred to vibrational modes that promote electron emission, the excess electron leaves[89] (see Figure 7.1). The absorption bands of the CH stretching vibrations in the hydrocarbon serve as zero-order bright states, while the nitro group serves as a localized energy acceptor.

Nitromethane has an adiabatic electron affinity of (168 ± 6) meV or ~ 1355 cm^{-1},[99] well below the excitation energies for CH stretching modes and is therefore an excellent model system to study VAD.

7.3 Photoelectron Imaging Results

Figure 7.3 shows a comparison of photoelectron images obtained off-resonance (3200 cm^{-1}, a photon energy that is free of any contributions from vibrational autodetachment) and on the VAD resonance belonging to the totally symmetric $\nu_s(CH_3)$. There are substantial differences between the two images. We observe that all anisotropy is lost and that new bands appear in the VAD image, together with an accentuation of the inner part of the image, which corresponds to low-energy electrons.

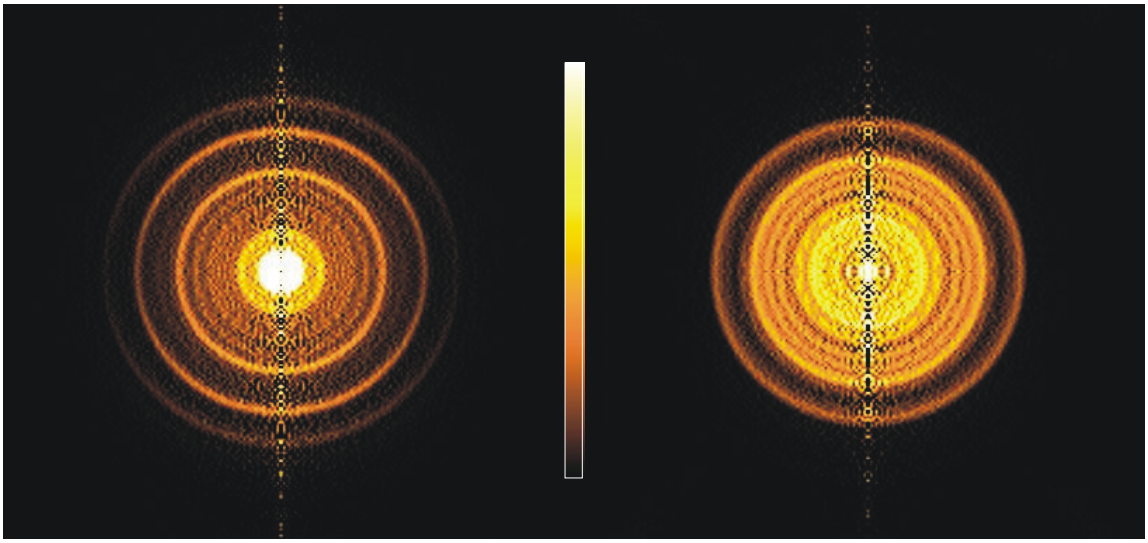

Figure 7.3 – Comparison of BASEX transformed photoelectron images of $CH_3NO_2^-$. The image on the left panel is taken off-resonance at an energy of 3200 cm^{-1}. The image on the right panel is taken on the vibrational resonance of the totally symmetric $\nu_s(CH_3)$ at 2777 cm^{-1}.

We note that the VAD photoelectron spectra contain some contributions from direct photoemission. In order to extract the VAD photoelectron yield, one must subtract the off-resonance photoelectron spectrum from the VAD photoelectron spectrum. The contribution from direct photoemission may be subtracted if one considers the photoelectron spectrum taken at a vibrational resonance to be the composite of a direct detachment process as well as a vibrational autodetachment process,

Equation 7.1

$$I_{M,h\nu}(E_K) = \chi_{VAD,h\nu} \cdot I_{VAD,h\nu}(E_K) + \chi_{DD,h\nu} \cdot I_{DD,h\nu}(E_K)$$

where $I_{h\nu}(E_K)$ is the intensity profile at a photon energy, $h\nu$, as a function of electron kinetic energy, E_K, and the additional subscripts of M, DD, and VAD represent the measured, direct detachment and vibrational autodetachment spectra, respectively. The terms $\chi_{h\nu}$ represent the relative weighting of the two profiles. From previous studies of direct detachment of nitromethane anion[99] (See Chapter 4), we observed that the photoelectron spectrum is well-characterized by,

Equation 7.2

$$I_{DD,h\nu}(E_{KE}) = FCF(E_{KE}) \cdot f_{thr}(E_{KE})$$

where FCF are the simulated Franck-Condon factors and f_{thr} is a threshold function necessary to recover the experimental spectra. A comparison of the Franck-Condon simulations and the direct off-resonance photoelectron imaging spectroscopy results seems to indicate the threshold effects involve mainly s-wave detachment with a small admixture of p-wave detachment given by

Equation 7.3

$$f_{thr}(E_{KE}) = E_{KE}^{1/2} + 5 \times 10^{-3} \cdot E_{KE}^{3/2}$$

where the first term contains the s-wave contribution and the second a small p-wave term. Since we now have an approximation for the threshold function, we may reconstruct the intensity profile of the direct-detachment, $I_{DD,h\nu}(E_{KE})$ at the photon energy coincident with the vibrational resonance. The last detail necessary to construct $I_{VAD,h\nu}$ is the relative weighting of the direct-

detachment to the total photoelectron detachment. This can be found using the vibrational autodetachment IR spectra obtained by Schneider *et al.*, where the IR spectra sits on a smooth background of photoelectrons from direct-detachment. Equation 7.1 may now be rearranged to give $I_{VAD,hv}$.

We note that the weakness of this analysis lies primarily in the threshold function, which is likely too simple to describe the actual detachment cross-section (see Chapter 4 for a more thorough discussion on the threshold function).[99] As a precaution, photon energies as close as possible (< 5 meV) to the vibrational resonances were used to avoid any problems arising from the threshold function. In addition, this approach assumes that there is no interference between the direct detachment channel and the VAD channel.

7.4 Modeling

In order to describe the process of VAD in the present case, we start with several assumptions. Ignoring rotational degrees of freedom, we describe the vibrational states of the anion upon vibrational excitation in a normal mode basis within the harmonic approximation, i.e., as 15-tuple of quantum numbers $(n_1, n_2, \cdots, n_{15})$. If the molecule is in its vibrational ground state prior to excitation, then there is one quantum in the ZOBS upon excitation, while all other quantum numbers are zero. As IVR sets in, vibrational energy is transferred to other vibrational states in the molecule through low-order anharmonic coupling. As soon as sufficient energy is coupled into vibrational modes that connect the anionic and neutral potential energy surfaces, electron emission can occur. If we assume that the main difference between the anion and the neutral geometries is the angle between the CN bond axis and the ONO plane, the main “emission

active" vibrational mode is the NO_2 "wagging" mode, $w(NO_2)$, and its normal coordinate is the detachment coordinate Q. This mode has the largest Franck-Condon factors in the photoelectron spectra[99] and we assume that electron emission will occur on a time scale of a few femtoseconds as soon as sufficient energy is pooled in this mode. On the basis of this simple idea, the population of vibrational states in the neutral will provide a rough map of how energy was distributed in the anion just prior to electron loss.

While many of the vibrational modes of the neutral and the anion are similar, the methyl torsion changes quite drastically upon electron loss.[99] In the anion, the interaction between the CH group *syn* to the NO_2 leads to structural stabilization of the methyl group, making the methyl torsion a hindered internal rotation. In contrast, the calculated potential for methyl torsion in neutral nitromethane has no significant barrier ($\sim$2 cm^{-1}), resulting in a free internal rotor. A detailed treatment of the internal rotors can be found in Chapter 4 along with their energy levels.

There are altogether 390 vibrational and torsional states of neutral CH_3NO_2 within the first 200 meV of the ground state. Even if we assume only relatively low-order coupling to the hindered rotor states with $|J| > 8$, we still count 326 states in this energy range (we will give a justification for this "cutoff" below). This means that it will not be meaningful to try to fit the VAD spectrum to individual final states of the neutral, since the number of states makes an unambiguous assignment without restrictions through other assumptions and modeling impossible. However, the VAD spectra can be modeled in different ways, and we will discuss several of them below using the VAD photoelectron spectrum of $CH_3NO_2^-$ at 2777 cm^{-1} as a case study. We chose this state for particular attention because the relative intensity of the contribution of VAD to direct detachment is highest for this state. The models discussed below

are based on a separation of the free internal rotor states, and the other vibrational degrees of freedom. The intensity distribution of the VAD spectrum $I_{VAD}(E)$ can be written as

Equation 7.4

$$I_{VAD}(E) = f_{thr}(E) \cdot \sum_{v,J} a_{v,J} \cdot I_0(E - E_{v,J})$$

where v and J denote the vibrational and free internal rotor quantum states, respectively. The coefficients $a_{v,J}$ represent the intensities of the final states with vibrational quantum number v, torsional quantum number J, and the corresponding energies $E_{v,J}$. The experimental response function, $I_0(E - E_{v,J})$, is represented by a Gauss function corresponding to the experimental resolution. The sum over all vibrational and internal rotor states is weighted with a threshold law $f_{thr}(E)$ (see Equation 7.3) determined from the off-resonance behavior at 3200 cm^{-1}. Each model described below will make some assumptions about the coefficients $a_{v,J}$, and we compare the resulting model curves with the experimental VAD spectrum. While this represents a reasonably objective route for the lower energy range up to ~ 120 meV, we stress that some ambiguity remains for higher energies due to the high density of states there.

7.4.1 "No Torsion" Model

A very simple approach to the problem is to assume that torsional modes do not play a role at all. This means that the coefficients $a_{v,J}$ are zero for $|J| > 0$. This assumption could in principle be justified by the argument that the $\nu_s(CH_3)$ vibrational mode and indeed all CH stretching modes are so much higher in energy than the torsion in the anion that coupling between these modes will be rather ineffective, since it would be of high order. However,

several examples from the IVR literature indicate that methyl torsion plays an important role in IVR for other, related systems.[6, 7, 26-28, 101] Figure 7.4 shows a fit of this model without internal rotor excitation of neutral CH_3NO_2 to the VAD spectrum. While some states at higher binding energies are rather well represented by this model, the lower energy region of the spectrum is not recovered by the simulation, and neither is the feature at 100 meV. Moreover, the valleys between most of the features are too deep, suggesting that the zero-torsion states are too "insular" to represent the more congested structure of the VAD spectrum, 8 states are above 120 meV. Therefore, the good agreement at high energies can simply be an effect of a sufficient number of states in this region (even without internal rotor excitation) to reach a good description of the spectrum.

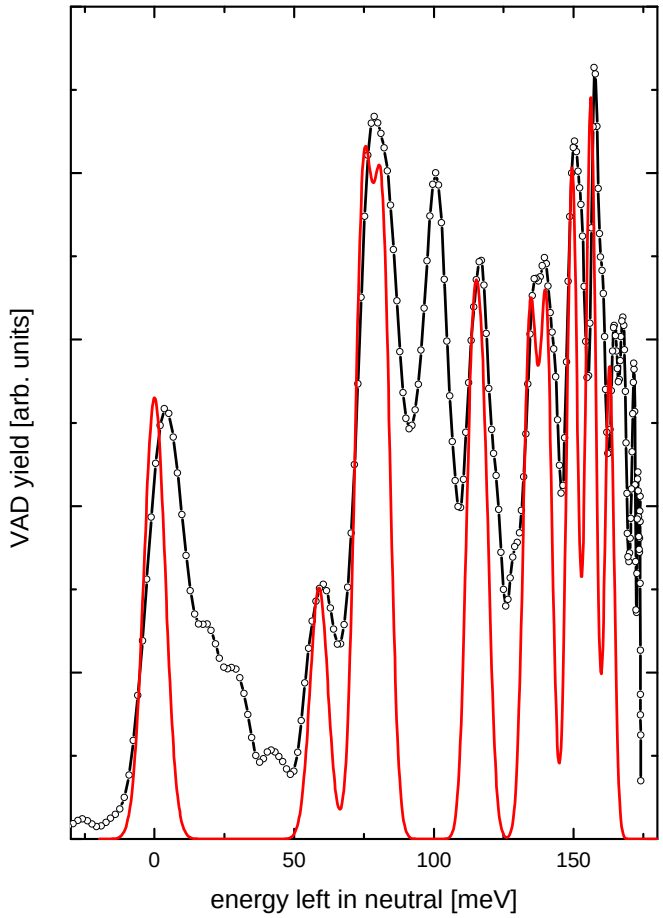

Figure 7.4 – Comparison of the experimental VAD spectrum (connected open circles) of $CH_3NO_2^-$ on the $\nu_s(CH_3)$ resonance (symmetric methyl stretch) with the "no torsion" model (full line, see text). The contribution of each vibrational state was weighted to yield the best fit of the model to the experimental data.

7.4.2 Energy Randomization Model

If the energy is completely randomized in the molecule before electron emission occurs, one should be able to describe the VAD yield with the density of states (DOS) in the neutral molecule. Since an anharmonic calculation for the DOS of the neutral molecule is not available to us at the time of this writing, we represent the DOS within the harmonic approximation, using the experimentally known values for the vibrational fundamental transitions[99] and the free

internal rotor levels described above. In other words, $a_{v,J} = 1$ for all v and J and the $a_{v,J}$ are the statistical weights of the individual states. Note that each internal rotor energy level except the ground state is doubly degenerate, since J and $-J$ have the same energy.

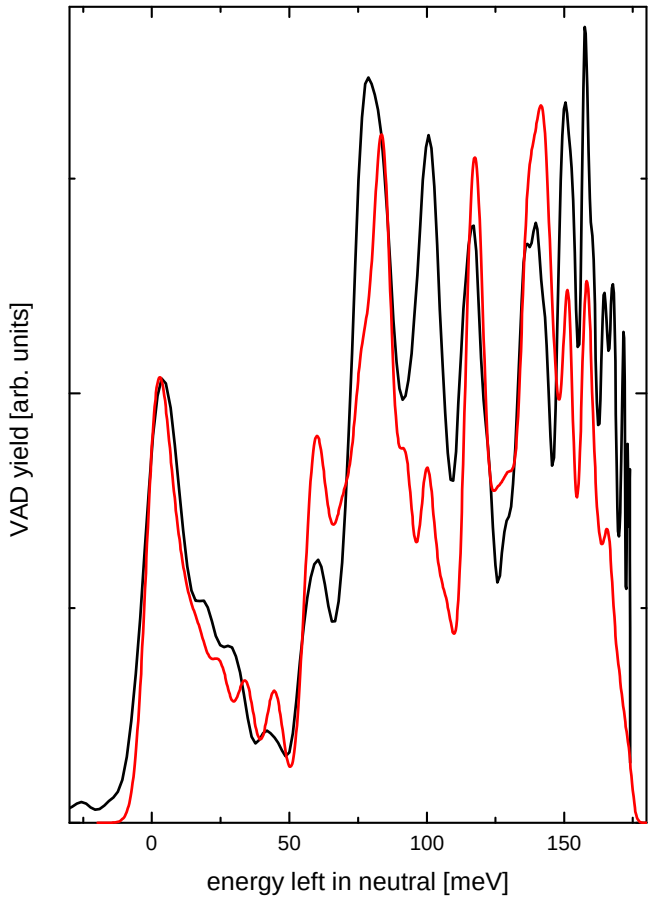

Figure 7.5 – Comparison of the experimental VAD spectrum (solid black line) of $CH_3NO_2^-$ on the $\nu_s(CH_3)$ resonance (symmetric methyl stretch) with the energy randomization model (solid red line, see text). The model has been normalized to the experimental data at the 0-eV feature.

Figure 7.5 shows a comparison of the VAD photoelectron yield on the resonance belonging to the symmetric methyl stretch, $\nu_s(\mathrm{CH_3})$, with the DOS in neutral $\mathrm{CH_3NO_2}$. One can clearly see at lower energies that the experimental VAD spectrum shows a close resemblance to

the DOS. At higher energies (above 50 meV), the simulation recovers many of the peak positions but the intensities are either over- or underestimated.

The feature located in the lower energy region (up to 50 meV) of the spectrum is particularly interesting, since it is due to pure free internal rotor excitations without contributions from other vibrational modes. Figure 7.6 shows this feature in more detail. The model curve is based only on the statistical weight of each internal rotor energy level, where the ground state is nondegenerate, while each excited energy level is doubly degenerate. The agreement with the experimental curve is nearly quantitative. The main difference is that the contribution of $|J| = 8$ overestimates the experimental curve. As a result, we will keep the statistical weight as a basis for the internal rotor distribution in the model described below for low $|J|$ but ignore all states with $|J| > 8$, i.e., $a_{v,J} = 0$ for $|J| > 8$.

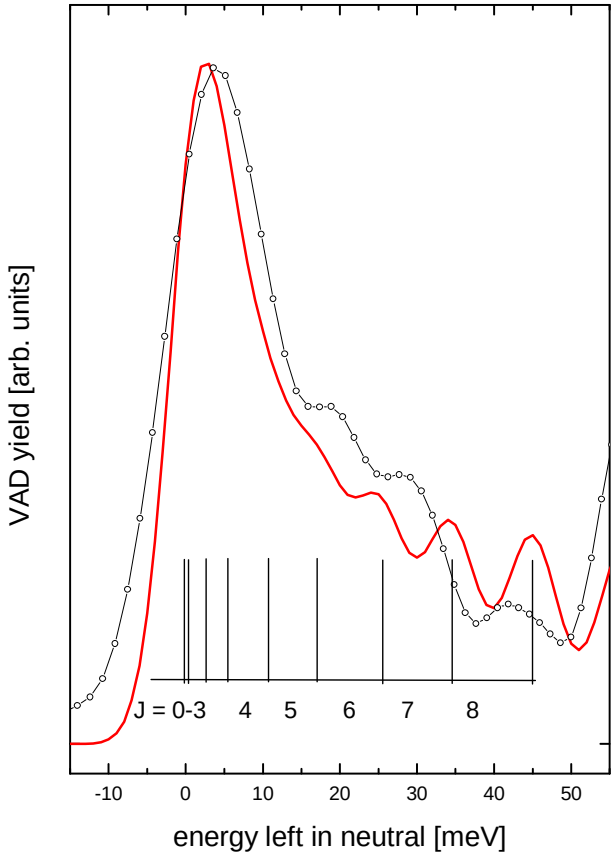

Figure 7.6 – Comparison of the experimental VAD spectrum (connected open circles) of $CH_3NO_2^-$ on the $\nu_s(CH_3)$ resonance (symmetric methyl stretch) with the density of states (full line) in neutral CH_3NO_2. The DOS has been normalized to the experimental data at the 0-eV feature.

7.4.3 Partial Randomization Model

The idea of using the DOS without any modification as a model for the VAD photoelectron spectrum as described above is fundamentally flawed, since it does not take into account any differences in the coupling between the anionic and neutral potential surfaces for different final vibrational states. Since we cannot assume that this coupling is uniform, it makes sense to allow intensity variations for each vibrational state to obtain a better fit. Moreover, if only partial randomization occurs prior to electron emission, fitting the intensities of the vibrational modes

can also take these differences into account. Although we cannot distinguish between these two effects, it is appropriate to speak of a "partial randomization model", as will become apparent below.

Since we vary the contribution of each vibrational final state while keeping the internal rotor intensity distribution the same for each vibrational state, this corresponds to writing the coefficients $a_{v,J}$ as a product

Equation 7.5

$$a_{v,J} = b_v \cdot c_J$$

with $c_J = 1$ for all $|J| \leq 8$, $c_J = 0$ otherwise, but varying the coefficients b_v to obtain the best agreement with the experimental VAD curve.

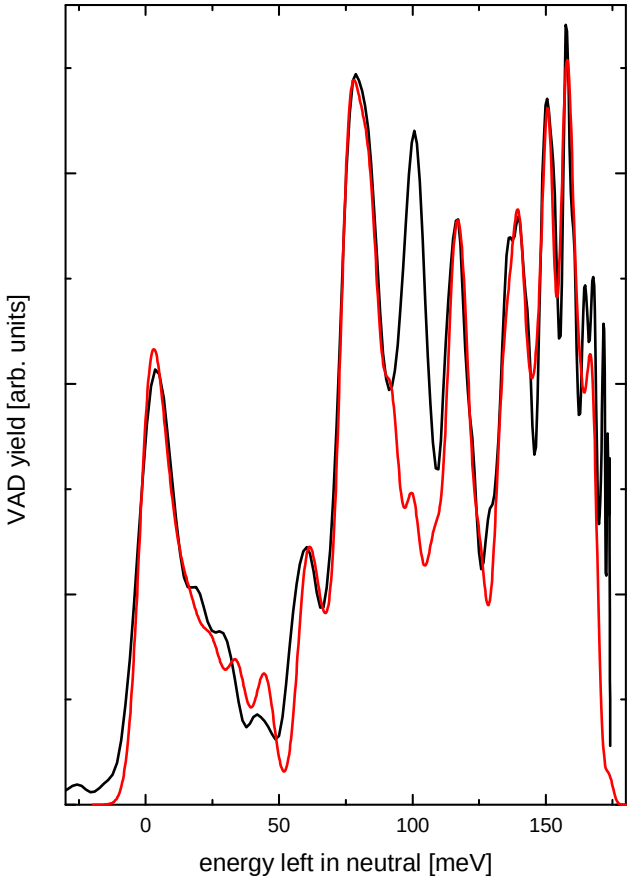

Figure 7.7 – Comparison of the experimental VAD spectrum (solid black line) of $CH_3NO_2^-$ on the $\nu_s(CH_3)$ resonance (symmetric methyl stretch) with the partial randomization model (solid red line). The model has been normalized to the experimental data at the 0-eV feature.

Figure 7.7 shows the result of this simulation. The agreement of the energy randomization model with the experimental data is excellent, with the exception of the feature at 100 meV.

This "missing" feature is interesting in that it seems to be caused by a special final state that is particularly well coupled to one or more partner states in the anion. There are only two levels in the neutral that are candidates for this feature. One is a combination band of the nitro wagging mode (a' symmetry) and the free internal rotor state with $|J| = 6$ (100 meV). The other is a combination band of the NO_2 bending mode (a' symmetry) and the free internal rotor state

with $|J| = 5$ (99 meV). At this time, we refrain from speculation concerning the special significance of these states.

7.4.4 Application to VAD PE for the Symmetric and Antisymmetric Methylene Stretching Modes

We will now compare the results of the energy randomization model with the VAD photoelectron spectra of the other two CH stretching modes in $CH_3NO_2^-$, the symmetric $\nu_s'(CH_3)$ and antisymmetric $\nu_a(CH_3)$ methylene stretching modes. Figure 7.8 shows the results for these two modes. Each of the experimental VAD spectra can be fitted by the partial randomization model, although the quality of the simulations of these spectra is not as high for the $\nu_s(CH_3)$ mode. This is mainly due to the lower VAD cross section of these modes, compared to the cross sections for direct detachment. The subtraction of the direct detachment contribution results in an error in the VAD spectra, which grows with the relative importance of direct detachment, even though the data quality of the actual photoelectron spectra (which contain both the VAD and direct detachment contributions) is similar for all ZOBS under study. This is especially true for the $\nu_a(CH_3)$ mode, where the VAD contribution is in fact smaller than that from direct detachment. Nevertheless, we can use the partial randomization model to describe the VAD spectra.

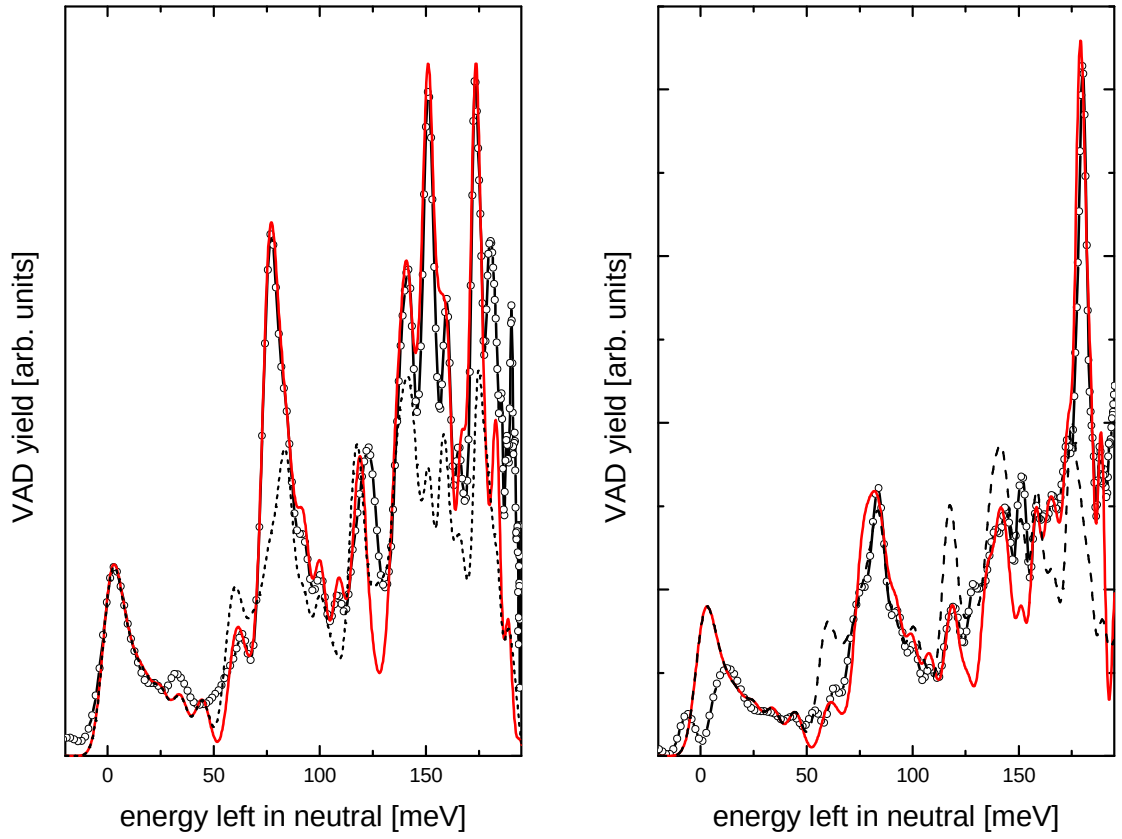

Figure 7.8 – Comparison of the experimental VAD photoelectron spectra (connected open circles) belonging to the $\nu'_s(CH_3)$ (symmetric methylene stretch, left panel) and $\nu_a(CH_3)$ (antisymmetric methylene stretch, right panel) modes of $CH_3NO_2^-$ with the partial randomization model (full lines). The dashed line in both spectra is a representation of the full energy randomization model. The models have been normalized to the experimental data at the 0-eV feature for each spectrum.

Interestingly, the intense peak at 100 meV energy, which showed very clearly in the $\nu_s(CH_3)$ VAD spectrum, does not appear. It is important to note that the intensity distribution in the neutral final states is different for each ZOBS studied here; i.e., the coefficients b_v depend on the ZOBS. Since the coupling efficiency between anion and neutral states should not depend on which ZOBS has been excited, the difference between the intensity distributions is most likely due to different populations in the parent anion vibrational states prior to photoemission, justifying the term "partial randomization model".

7.4.5 Critical Discussion of the Modeling

Despite our partial success in modeling the VAD spectra from nitromethane anions, it seems appropriate to discuss the limitations common to the model discussed above. The model description so far is purely empirical. It has no predictive character, and we can only extract very limited information on the dynamics of IVR and VAD processes involved. It is based on a rather crude idea of how VAD occurs, and it cannot distinguish between effects based on the coupling between the anionic and neutral vibrational states and the energy distribution in the anion prior to electron loss. It treats threshold effects in electron emission only in an approximate, averaged way, and it contains no vibration-rotation coupling.

Moreover, while the lower energy states up to ~ 120 meV are reasonably well separated to allow unambiguous assignment of vibrational features, the description of higher energy states is difficult because of the high DOS, even if the internal rotor substructure of each vibrational band is fixed. As an example, even though the combination band of the $w(NO_2)$ mode with the $r(NO_2)$ mode at 134 meV and the fundamental of the $r_{\parallel}(CH_3)$ mode at 136 meV can barely be distinguished on the basis of the photoelectron band contours, the $r_{\perp}(CH_3)$ fundamental and the combination band of the $\delta(NO_2)$ and $r(NO_2)$ modes are both at 140 meV and cannot be distinguished in the experimental spectrum. Assignments of the vibrational features at higher energies and their relative intensities therefore carry some ambiguity.

Without losing sight of the limitations of the description, we can nevertheless extract some interesting information from the VAD photoelectron spectra and the ideas discussed above. Obviously, VAD cannot be described merely on the basis of the density of the available states of the neutral. Also, as expected, the clear differences of the off-resonance and on-resonance photoelectron spectra indicate that the Franck-Condon factors that dictate the profile of the

direct- detachment photoelectron spectrum do not play the most crucial role in the description of the VAD spectra.

The intensity distribution in the free internal rotor states is rather interesting. It seems not to be subject to any restriction by symmetry, at least if one argues that the parent anion is in its vibrational ground state prior to infrared excitation. However, this is probably not the case, since the ion temperature is of the order of 250 K, based on Franck-Condon simulations of the off-resonance photoelectron spectrum under typical experimental conditions.[99] The lowest three hindered rotor states for the anion are nearly triply degenerate. As a result, we have to assume significant population of states with torsional excitation. Moreover, if the process of populating detaching states is sufficiently slow, vibration-rotation coupling can relax the symmetry requirements. Our discussion implies that the main role of the methyl torsion is in the IVR process leading up to VAD. We note, however, that the role of the methyl torsion in the VAD process itself is unclear, especially in light of its dramatic change upon electron loss.

The difference between the intensity distributions in VAD spectra coming from different ZOBS excitations indicates that even if there is some degree of randomization among the low $|J|$ torsional degrees of freedom, there is no complete randomization in the population of the vibrational states. This is a significant observation, since it highlights the fact that purely statistical theoretical approaches will likely fail to describe VAD time scales. Even more importantly, it shows that there is a clear dependence of the VAD process in the $CH_3NO_2^-$ on which ZOBS is excited in the beginning of the process.

From the relative intensities of the vibrational modes in the VAD photoelectron spectra, we can try to infer which modes are of particular importance as populated final states. The states

that are populated higher than average for all ZOBS are the fundamentals of $r(NO_2)$, $w(NO_2)$, $r_{\parallel}(CH_3)$ and the higher-order states $r(NO_2) + w(NO_2)$ and $2 \times w(NO_2)$. The fundamental of $\delta(CH_3)$ is important for the VAD spectra belonging to both $v_s'(CH_3)$ and $v_a(CH_3)$ but is energetically inaccessible via $v_s(CH_3)$ as a ZOBS.

As mentioned above, there is a feature in the $v_s(CH_3)$ VAD spectrum that is underestimated or unrecovered in the models. This feature can be traced to either the $[w(NO_2) + (|J| = 6)]$ or the $[\delta(NO_2) + (|J| = 5)]$ combination bands. Other such "special states" have not been observed. Ideally, one would like to be able to map the final states of the neutral onto the anionic parent states. However, the VAD coupling efficiency for the parent anion states would have to be characterized on the basis of suitable theoretical approach, such as that of Simons,[77, 102, 103] before this is possible.

7.5 Open Questions and Future Challenges

In summary, we have presented one of the first VAD photoelectron spectroscopy studies of a polyatomic molecular anion. This approach opens up new and exciting avenues into the investigation of VAD and the underlying IVR problem of how the energy deposited into a ZOBS by IR excitation is transferred into the vibrational modes facilitating electron emission. There are many open questions that require a better theoretical treatment.

As mentioned above, one important unresolved aspect is the description of the coupling between the anionic and neutral potential energy curve as a function of the anionic vibrational state. This could potentially be achieved by applying the strategy outlined by Simons[77, 103, 104] to the specific molecules in question. The results from such a calculation would be instrumental to

map the neutral final state distribution observed in a VAD photoelectron spectrum onto the anionic precursor vibrational states. Are the normal modes that are not involved in the VAD reaction coordinate Q spectators during electron loss? What is the role of the methyl torsion in the IVR?

Another, separate problem is a good description of IVR in the parent anion. It will be problematic to tackle this problem by molecular dynamics simulations, since the quantum mechanical character of the methyl rotor and of the CH stretching ZOBS will probably not be well described that way. A lattice model for the vibrational state space would probably do more justice to this situation. For such an approach, one needs cubic and–if affordable–quartic force constants for the molecular system under study, which is feasible for small molecules (e.g., CH_3NO_2) but very expensive for larger systems. In this context, the mutual interaction between the torsional motion and the other vibrational degrees of freedom is of particular importance because of the obvious impact of the methyl torsion on the VAD spectra.

While the partial randomization model described above seems to recover most of the details of the VAD spectra, it is an open question whether it recovers even in broad strokes the physics involved in the IVR/VAD process. If so, what is the special significance of the spectral features that deviate from the partial randomization model? Do the anionic precursor states that map onto these neutral states play the roles of doorway states in the IVR?

Future experimental developments could include ultrafast pump-probe spectroscopy, where a mid-infrared pump pulse $\hbar\omega_1$ excites a CH stretching mode and the near-infrared probe pulse $\hbar\omega_2$ detaches the electron. The resulting photoelectron spectra would show the temporal evolution from a regular photoelectron spectrum ($\hbar\omega_2$ before $\hbar\omega_1$) through developing

vibrational hot bands ($\hbar\omega_2$ after $\hbar\omega_1$ but before VAD) to a VAD spectrum ($\hbar\omega_2$ after VAD). In this way, one could determine time scales for both IVR (monitoring the vibrational hot bands) and VAD separately.

7.6 References

1. F. F. Crim,"Making energy count." *Science* **316** (5832), 1707-1708 (2007).

2. D. Weidinger, M. F. Engel and M. Gruebele,"Freezing Vibrational Energy Flow: A Fitness Function for Interchangeable Computational and Experimental Control." *Journal of Physical Chemistry A* **113** (16), 4184-4191 (2009).

3. Z. H. Wang, J. A. Carter, A. Lagutchev, Y. K. Koh, N. H. Seong, D. G. Cahill and D. D. Dlott,"Ultrafast flash thermal conductance of molecular chains." *Science* **317** (5839), 787-790 (2007).

4. B. Cretin, S. Gomes, N. Trannoy and P. Vairac, in *Microscale and Nanoscale Heat Transfer* (2007), Vol. 107, pp. 181-238.

5. F. F. Crim,"Vibrationally Mediated Photodissociation - Exploring Excited-State Surfaces and Controlling Decomposition Pathways." *Annual Review of Physical Chemistry* **44**, 397-428 (1993).

6. K. K. Lehmann, G. Scoles and B. H. Pate,"Intramolecular Dynamics from Eigenstate-Resolved Infrared-Spectra." *Annual Review of Physical Chemistry* **45**, 241-274 (1994).

7. D. J. Nesbitt and R. W. Field,"Vibrational energy flow in highly excited molecules: Role of intramolecular vibrational redistribution." *Journal of Physical Chemistry* **100** (31), 12735-12756 (1996).

8. D. Boyall and K. L. Reid,"Modern studies of intramolecular vibrational energy redistribution." *Chemical Society Reviews* **26** (3), 223-232 (1997).

9. H. Ueba,"Vibrational relaxation and pump-probe spectroscopies of adsorbates on solid surfaces." *Progress in Surface Science* **55** (2), 115-179 (1997).

10. M. Gruebele and R. Bigwood,"Molecular vibrational energy flow: beyond the Golden Rule." *International Reviews in Physical Chemistry* **17** (2), 91-145 (1998).

11. J. C. Keske and B. H. Pate,"Decoding the dynamical information embedded in highly mixed quantum states." *Annual Review of Physical Chemistry* **51**, 323-353 (2000).

12. J. Assmann, M. Kling and B. Abel,"Watching photoinduced chemistry and molecular energy flow in solution in real time." *Angewandte Chemie-International Edition* **42** (20), 2226-2246 (2003).

13. A. Stolow,"Time-resolved photoelectron spectroscopy: Non-adiabatic dynamics in polyatomic molecules." *International Reviews in Physical Chemistry* **22** (2), 377-405 (2003).

14. A. Sanov and W. C. Lineberger,"Cluster anions: Structure, interactions, and dynamics in the sub-nanoscale regime." *Physical Chemistry Chemical Physics* **6** (9), 2018-2032 (2004).

15. H. S. Yoo, M. J. DeWitt and B. H. Pate,"Vibrational dynamics of terminal acetylenes: II. Pathway for vibrational relaxation in gas and solution." *Journal of Physical Chemistry A* **108** (8), 1365-1379 (2004).

16. H. S. Yoo, M. J. DeWitt and B. H. Pate,"Vibrational dynamics of terminal acetylenes: I. Comparison of the intramolecular vibrational energy redistribution rate of gases and the total relaxation rate of dilute solutions at room temperature." *Journal of Physical Chemistry A* **108** (8), 1348-1364 (2004).

17. H. S. Yoo, D. A. McWhorter and B. H. Pate,"Vibrational dynamics of terminal acetylenes: III. Comparison of the acetylenic C-H stretch intramolecular vibrational-energy redistribution rates in ultracold molecular beams, room-temperature gases, and room-temperature dilute solutions." *Journal of Physical Chemistry A* **108** (8), 1380-1387 (2004).

18. B. K. Carpenter,"Nonstatistical dynamics in thermal reactions of polyatomic molecules." *Annual Review of Physical Chemistry* **56**, 57-89 (2005).

19. A. Chakraborty, D. Seth, P. Setua and N. Sarkar,"Dynamics of solvent and rotational relaxation of glycerol in the nanocavity of reverse micelles." *Journal of Physical Chemistry B* **110** (11), 5359-5366 (2006).

20. C. G. Elles and F. F. Crim,"Connecting chemical dynamics in gases and liquids." *Annual Review of Physical Chemistry* **57**, 273-302 (2006).

21. K. Giese, M. Petkovic, H. Naundorf and O. Kuhn,"Multidimensional quantum dynamics and infrared spectroscopy of hydrogen bonds." *Physics Reports-Review Section of Physics Letters* **430** (4), 211-276 (2006).

22. I. V. Hertel and W. Radloff,"Ultrafast dynamics in isolated molecules and molecular clusters." *Reports on Progress in Physics* **69** (6), 1897-2003 (2006).

23. D. M. Leitner, M. Havenith and M. Gruebele,"Biomolecule large-amplitude motion and solvation dynamics: modelling and probes from THz to X-rays." *International Reviews in Physical Chemistry* **25** (4), 553-582 (2006).

24. Y. Pang, J. C. Deak, W. T. Huang, A. Lagutchev, A. Pakoulev, J. E. Patterson, T. D. Sechler, Z. H. Wang and D. D. Dlott,"Vibrational energy in molecules probed with high time and space resolution." *International Reviews in Physical Chemistry* **26** (1), 223-248 (2007).

25. D. S. Perry,"Random Matrix Treatment of Intramolecular Vibrational Redistribution .1. Methodology and Anharmonic Interactions in 1-Butyne." *Journal of Chemical Physics* **98** (9), 6665-6677 (1993).

26. X. L. Wang and D. S. Perry,"An internal coordinate model of coupling between the torsion and C-H vibrations in methanol." *Journal of Chemical Physics* **109** (24), 10795-10805 (1998).

27. A. Chirokolava, D. S. Perry, O. V. Boyarkin, M. Schmid and T. R. Rizzo,"Rotational and torsional analysis of the OH-stretch third overtone in (CH_3OH)-C-13." *Journal of Molecular Spectroscopy* **211** (2), 221-227 (2002).

28. T. N. Clasp and D. S. Perry,"Torsion-vibration coupling in methanol: The adiabatic approximation and intramolecular vibrational redistribution scaling." *Journal of Chemical Physics* **125** (10), art. no. 104313 (2006).

29. L. Lespade, D. Cavagnat and P. Asselin,"A new way for IVR induced by fast internal motion as revealed by a jet-cooled spectrum of cyclopentene." *Journal of Physical Chemistry A* **106** (41), 9451-9459 (2002).

30. Y. J. Hu, B. Hadas, M. Davidovitz, B. Balta and C. Lifshitz,"Does IVR take place prior to peptide ion dissociation?" *J. Phys. Chem. A* **107** (34), 6507-6514 (2003).

31. Y. Yamada, T. Ebata, M. Kayano and N. Mikami,"Picosecond IR-UV pump-probe spectroscopic study of the dynamics of the vibrational relaxation of jet-cooled phenol. I. Intramolecular vibrational energy redistribution of the OH and CH stretching vibrations of bare phenol." *Journal of Chemical Physics* **120** (16), 7400-7409 (2004).

32. M. Kayano, T. Ebata, Y. Yamada and N. Mikami,"Picosecond IR-UV pump-probe spectroscopic study of the dynamics of the vibrational relaxation of jet-cooled phenol. II. Intracluster vibrational energy redistribution of the OH stretching vibration of hydrogen-bonded clusters." *Journal of Chemical Physics* **120** (16), 7410-7417 (2004).

33. U. S. Tasic and C. S. Parmenter,"Test of a chemical timing method for measuring absolute vibrational relaxation rate constants for S_1 p-difluorobenzene." *Journal of Physical Chemistry B* **109** (17), 8297-8303 (2005).

34. Y. Yamada, J. Okano, N. Mikami and T. Ebata,"Picosecond IR-UV pump-probe spectroscopic study on the intramolecular vibrational energy redistribution of NH_2 and CH stretching vibrations of jet-cooled aniline." *Journal of Chemical Physics* **123** (12) (2005).

35. Y. Yamada, M. Kayano, N. Mikami and T. Ebata,"Picosecond IR-UV pump-probe study on the vibrational relaxation of phenol-ethylene hydrogen-bonded cluster: Difference of relaxation route/rate between the donor and the acceptor site excitations." *Journal of Physical Chemistry A* **110** (19), 6250-6255 (2006).

36. D. Gerbasi, A. S. Sanz, P. S. Christopher, M. Shapiro and P. Brumer,"Overlapping resonances in the control of intramolecular vibrational redistribution." *Journal of Chemical Physics* **126** (12) (2007).

37. Y. Yamada, Y. Katsumoto and T. Ebata,"Picosecond IR-UV pump-probe spectroscopic study on the vibrational energy flow in isolated molecules and clusters." *Physical Chemistry Chemical Physics* **9** (10), 1170-1185 (2007).

38. M. Gruebele and P. G. Wolynes,"Vibrational energy flow and chemical reactions." *Accounts of Chemical Research* **37** (4), 261-267 (2004).

39. P. D. Chowdary and M. Gruebele,"Size and Energy Scaling of Nonstatistical Vibrational Quantum States." *Physical Review Letters* **101** (25) (2008).

40. D. M. Leitner and M. Gruebele,"Quantum model of restricted vibrational energy flow on the way to the transition state in unimolecular reactions." *Molecular Physics* **106** (2-4), 433-442 (2008).

41. S. S. Iyengar and J. Jakowski,"Quantum wave packet ab initio molecular dynamics: An approach to study quantum dynamics in large systems." *Journal of Chemical Physics* **122** (11) (2005).

42. I. Sumner and S. S. Iyengar,"Quantum wavepacket ab initio molecular dynamics: An approach for computing dynamically averaged vibrational spectra including critical nuclear quantum effects." *Journal of Physical Chemistry A* **111** (41), 10313-10324 (2007).

43. P. Ortoleva and S. S. Iyengar,"Multiscale theory of collective and quasiparticle modes in quantum nanosystems." *Journal of Chemical Physics* **128** (16) (2008).

44. I. Sumner and S. S. Iyengar,"Combining quantum wavepacket ab initio molecular dynamics with QM/MM and QM/QM techniques: Implementation blending ONIOM and empirical valence bond theory." *Journal of Chemical Physics* **129** (5) (2008).

45. S. A. Schofield and P. G. Wolynes,"Rate Theory and Quantum Energy-Flow in Molecules - Modeling the Effects of Anisotropic Diffusion and of Dephasing." *Journal of Physical Chemistry* **99** (9), 2753-2763 (1995).

46. V. Wong and M. Gruebele,"How does vibrational energy flow fill the molecular state space?" *Journal of Physical Chemistry A* **103** (49), 10083-10092 (1999).

47. J. K. Agbo, D. M. Leitner, E. M. Myshakin and K. D. Jordan,"Quantum energy flow and the kinetics of water shuttling between hydrogen bonding sites on trans-formanilide." *Journal of Chemical Physics* **127** (6) (2007).

48. D. M. Leitner and P. G. Wolynes,"Quantum theory of enhanced unimolecular reaction rates below the ergodicity threshold." *Chemical Physics* **329** (1-3), 163-167 (2006).

49. A. M. Desouza, D. Kaur and D. S. Perry,"Vibrational-State Mixing of Individual Rotational Levels in 1-Butyne near 3333 cm^{-1}." *Journal of Chemical Physics* **88** (8), 4569-4578 (1988).

50. A. McIlroy and D. J. Nesbitt,"High-Resolution, Slit Jet Infrared-Spectroscopy of Hydrocarbons - Quantum State Specific Mode Mixing in CH Stretch-Excited Propyne." *Journal of Chemical Physics* **91** (1), 104-113 (1989).

51. M. A. Suhm, J. T. Farrell, S. H. Ashworth and D. J. Nesbitt,"High-Resolution Infrared-Spectroscopy of Df Trimer - a Cyclic Ground-State Structure and DF Stretch Induced Intramolecular Vibrational Coupling." *Journal of Chemical Physics* **98** (7), 5985-5989 (1993).

52. A. McIlroy and D. J. Nesbitt,"Large-Amplitude Skeletal Isomerization as a Promoter of Intramolecular Vibrational-Relaxation in Ch Stretch Excited Hydrocarbons." *Journal of Chemical Physics* **101** (5), 3421-3435 (1994).

53. A. McIlroy, D. J. Nesbitt, E. R. T. Kerstel, B. H. Pate, K. K. Lehmann and G. Scoles,"Sub-Doppler, Infrared-Laser Spectroscopy of the Propyne $2\nu_1$ Band - Evidence of Z-Axis Coriolis Dominated Intramolecular State Mixing in the Acetylenic CH Stretch Overtone." *Journal of Chemical Physics* **100** (4), 2596-2611 (1994).

54. M. Farnik, S. Davis and D. J. Nesbitt,"High-resolution IR studies of hydrogen bonded clusters: Large amplitude dynamics in $(HCl)_n$." *Faraday Discussions* **118**, 63-78 (2001).

55. K. K. Lehmann, B. H. Pate and G. Scoles,"Statistical Intramolecular Vibrational-Relaxation and Its Hindrance - the Fundamentals of $(CH_3)_3C$-C=CH and $(CH_3)_3Si$-C=CH." *Journal of Chemical Physics* **93** (3), 2152-2153 (1990).

56. J. E. Gambogi, R. Z. Pearson, X. M. Yang, K. K. Lehmann and G. Scoles,"Intramolecular Vibrational Dynamics of Diacetylene and Diacetylene-D(1) Via Eigenstate-Resolved Overtone Spectroscopy." *Chemical Physics* **190** (2-3), 191-205 (1995).

57. J. E. Gambogi, K. K. Lehmann, B. H. Pate, G. Scoles and X. M. Yang,"The Rate of Intramolecular Vibrational-Energy Relaxation of the Fundamental C-H Stretch in $(CF_3)_3C$-CC-H." *Journal of Chemical Physics* **98** (2), 1748-1749 (1993).

58. B. H. Pate, K. K. Lehmann and G. Scoles,"The Onset of Intramolecular Vibrational-Energy Redistribution and Its Intermediate Case - the ν_1 and $2\nu_1$ Molecular-Beam,

Optothermal Spectra of Trifluoropropyne." *Journal of Chemical Physics* **95** (6), 3891-3916 (1991).

59. D. Green, S. Hammond, J. Keske and B. H. Pate,"Intramolecular vibrational energy redistribution and conformational isomerization in vibrationally excited 2-fluoroethanol: High-resolution, microwave-infrared double-resonance spectroscopy investigation of the asymmetric -CH_2(F) stretch near 2980 cm^{-1}." *Journal of Chemical Physics* **110** (4), 1979-1989 (1999).

60. D. A. McWhorter, E. Hudspeth and B. H. Pate,"The rotational spectra of single molecular eigenstates of 2-fluoroethanol: Measurement of the conformational isomerization rate at 2980 cm^{-1}." *Journal of Chemical Physics* **110** (4), 2000-2009 (1999).

61. B. C. Dian, G. G. Brown, K. O. Douglass, F. S. Rees, J. E. Johns, P. Nair, R. D. Suenram and B. H. Pate,"Conformational isomerization kinetics of pent-1-en-4-yne with 3,330 cm(-1) of internal energy measured by dynamic rotational spectroscopy." *Proceedings of the National Academy of Sciences of the United States of America* **105** (35), 12696-12700 (2008).

62. G. T. Fraser, B. H. Pate, G. A. Bethardy and D. S. Perry,"Frequency-Resolved Measurement of Fast Intramolecular Vibrational-Energy Redistribution (IVR) in the O-H Stretch of Gas-Phase Ethanol." *Chemical Physics* **175** (1), 223-236 (1993).

63. T. K. Minton, H. L. Kim, S. A. Reid and J. D. McDonald,"High-Resolution Infrared-Laser Induced Fluorescence Study of State Mixing in Methyl Formate." *Journal of Chemical Physics* **89** (10), 6550-6552 (1988).

64. T. J. Kulp, H. L. Kim and J. D. McDonald,"Rotational Effects on Intramolecular Vibrational-Relaxation in Dimethyl Ether and 1,4 Dioxane." *Journal of Chemical Physics* **85** (1), 211-220 (1986).

65. T. Kulp, R. S. Ruoff and J. D. McDonald,"Limits on the Lifetimes of Intramolecular Rovibrational Relaxation." *Journal of Chemical Physics* **82** (5), 2175-2179 (1985).

66. G. M. Stewart and J. D. McDonald,"Intramolecular Vibrational-Relaxation from C-H Stretch Fundamentals." *Journal of Chemical Physics* **78** (6), 3907-3915 (1983).

67. J. D. McDonald,"Creation and Disposal of Vibrational Energy in Polyatomic-Molecules." *Annual Review of Physical Chemistry* **30**, 29-50 (1979).

68. Y. Yamada, N. Mikami and T. Ebata,"Real-time detection of doorway states in the intramolecular vibrational energy redistribution of the OH/OD stretch vibration of phenol." *Journal of Chemical Physics* **121** (23), 11530-11534 (2004).

69. T. Ebata, A. Iwasaki and N. Mikami,"Vibrational relaxation of OH and OD stretching vibrations of phenol and its clusters studied by IR-UV pump-probe spectroscopy." *Journal of Physical Chemistry A* **104** (34), 7974-7979 (2000).

70. R. Yamamoto, S. Ishikawa, T. Ebata and N. Mikami,"Vibrational spectra and relaxation of benzonitrile and its clusters using time-resolved stimulated Raman-UV double resonance spectroscopy." *Journal of Raman Spectroscopy* **31** (4), 295-304 (2000).

71. M. L. Hause, Y. H. Yoon, A. S. Case and F. F. Crim,"Dynamics at conical intersections: The influence of O-H stretching vibrations on the photodissociation of phenol." *Journal of Chemical Physics* **128** (10) (2008).

72. F. F. Crim,"Chemical dynamics of vibrationally excited molecules: Controlling reactions in gases and on surfaces." *Proceedings of the National Academy of Sciences of the United States of America* **105** (35), 12654-12661 (2008).

73. X. Y. Hong, S. Chen and D. D. Dlott,"Ultrafast Mode-Specific Intermolecular Vibrational-Energy Transfer to Liquid Nitromethane." *Journal of Physical Chemistry* **99** (22), 9102-9109 (1995).

74. Z. H. Wang, Y. S. Pang and D. D. Dlott,"Hydrogen-bond disruption by vibrational excitations in water." *Journal of Physical Chemistry A* **111** (17), 3196-3208 (2007).

75. S. Shigeto, Y. Pang, Y. Fang and D. D. Dlott,"Vibrational relaxation of normal and deuterated liquid nitromethane." *Journal of Physical Chemistry B* **112** (2), 232-241 (2008).

76. R. S. Berry,"Ionization of Molecules at Low Energies." *Journal of Chemical Physics* **45** (4), 1228-& (1966).

77. J. Simons,"Propensity Rules for Vibration-Induced Electron Detachment of Anions." *Journal of the American Chemical Society* **103** (14), 3971-3976 (1981).

78. P. K. Acharya, R. A. Kendall and J. Simons,"Vibration-Induced Electron Detachment in Molecular Anions." *Journal of the American Chemical Society* **106** (12), 3402-3407 (1984).

79. F. K. Meyer, J. M. Jasinski, R. N. Rosenfeld and J. I. Brauman,"Infrared Multi-Photon Photodetachment of Negative-Ions in the Gas-Phase." *Journal of the American Chemical Society* **104** (3), 663-667 (1982).

80. R. N. Rosenfeld, J. M. Jasinski and J. I. Brauman,"Infrared Multi-Photon Electron Detachment from the Benzyl Anion." *Journal of Chemical Physics* **71** (2), 1030-1031 (1979).

81. R. F. Foster, W. Tumas and J. I. Brauman,"Unimolecular Decomposition and Vibrationally Induced Electron Autodetachment of Acetone Enolate Ion." *Journal of Chemical Physics* **79** (9), 4644-4646 (1983).

82. W. Tumas, K. E. Salomon and J. I. Brauman,"Dimethylsilanone Enolate Anion - Competitive Fragmentation and Electron Autodetachment of Vibrationally Excited Siloxide Anions in the Gas-Phase." *Journal of the American Chemical Society* **108** (10), 2541-2546 (1986).

83. C. C. Han and J. I. Brauman,"Dissociation and Vibration-Induced Electron Autodetachment of 3-Fluoronitrobenzene Radical-Anion by Infrared Multiple Photon Excitation." *Journal of Physical Chemistry* **94** (9), 3403-3415 (1990).

84. C. A. Wight and J. L. Beauchamp,"Infrared-Spectra of Butenyl Anions - Multiphoton Electron Detachment as a Photochemical Probe of Isomeric Structures of Gas-Phase Anions." *International Journal of Mass Spectrometry and Ion Processes* **100**, 445-455 (1990).

85. C. A. Wight and J. L. Beauchamp,"Infrared-Spectra of Gas-Phase Ions and Their Use in Elucidating Reaction-Mechanisms - Identification of $C_7H_7^-$ Structural Isomers by Multi-Photon Electron Detachment Using a Low-Power Infrared-Laser." *Journal of the American Chemical Society* **103** (21), 6499-6501 (1981).

86. C. A. Wight and J. L. Beauchamp,"Multiphoton Electron Detachment Studies of $C_7H_7^-$ Using a Low-Power Infrared-Laser - Competition of Radiative and Collisional Relaxation with Vibrational-Excitation." *Chemical Physics* **134** (2-3), 375-384 (1989).

87. D. M. Neumark, K. R. Lykke, T. Andersen and W. C. Lineberger,"Infrared-Spectrum and Autodetachment Dynamics of NH^-." *Journal of Chemical Physics* **83** (9), 4364-4373 (1985).

88. A. S. Mullin, K. K. Murray, C. P. Schulz, D. M. Szaflarski and W. C. Lineberger,"Autodetachment Spectroscopy of Vibrationally Excited Acetaldehyde Enolate Anion, Ch2cho." *Chemical Physics* **166** (1-2), 207-213 (1992).

89. J. M. Weber, W. H. Robertson and M. A. Johnson,"Argon predissociation and electron autodetachment spectroscopy of size-selected $CH_3NO_2^-\cdot Ar_n$ clusters." *Journal of Chemical Physics* **115** (23), 10718-10723 (2001).

90. B. M. Elliott, L. R. McCunn and M. A. Johnson,"Photoelectron imaging study of vibrationally mediated electron autodetachment in the type I isomer of the water hexamer anion." *Chemical Physics Letters* **467** (1-3), 32-36 (2008).

91. H. Schneider, K. M. Vogelhuber, F. Schinle, J. F. Stanton and J. M. Weber,"Vibrational spectroscopy of nitroalkane chains using electron autodetachment and Ar predissociation." *Journal of Physical Chemistry A* **112** (33), 7498-7506 (2008).

92. O. W. Richardson, *The Emission of Electricity from Hot Bodies*. (Longmans Green and Company, London, 1921).

93. I. I. Fabrikant and H. Hotop,"Low-energy behavior of exothermic dissociative electron attachment." *Physical Review A* **6302** (2) (2001).

94. H. Hotop, M. W. Ruf, M. Allan and Fabrikant, II, in *Advances in Atomic Molecular, and Optical Physics, Vol 49* (2003), Vol. 49, pp. 85-216.

95. T. Sommerfeld,"Coupling between dipole-bound and valence states: the nitromethane anion." *Physical Chemistry Chemical Physics* **4** (12), 2511-2516 (2002).

96. G. Chalasinski, R. A. Kendall, H. Taylor and J. Simons,"Propensity Rules for Vibration Rotation-Induced Electron Detachment of Diatomic Anions - Application to Nh--]Nh+E." *Journal of Physical Chemistry* **92** (11), 3086-3091 (1988).

97. D. Gorse, D. Cavagnat, M. Pesquer and C. Lapouge,"Theoretical and Spectroscopic Study of Asymmetric Methyl Rotor Dynamics in Gaseous Partially Deuterated Nitromethanes." *Journal of Physical Chemistry* **97** (17), 4262-4269 (1993).

98. R. N. Compton, H. S. Carman, C. Desfrancois, H. Abdoul-Carmine, J. P. Schermann, J. H. Hendricks, S. A. Lyapustina and K. H. Bowen,"On the binding of electrons to nitromethane: Dipole and valence bound anions." *Journal of Chemical Physics* **105** (9), 3472-3478 (1996).

99. C. L. Adams, H. Schneider, K. M. Ervin and J. M. Weber,"Low-energy photoelectron imaging spectroscopy of nitromethane anions: Electron affinity, vibrational features, anisotropies and the dipole-bound state." *Journal of Chemical Physics* **130**, 074307-074301 - 074310 (2009).

100. G. L. Gutsev and R. J. Bartlett,"A theoretical study of the valence- and dipole-bound states of the nitromethane anion." *Journal of Chemical Physics* **105** (19), 8785-8792 (1996).

101. C. S. Parmenter and B. M. Stone,"The Methyl Rotor as an Accelerating Functional-Group for IVR." *Journal of Chemical Physics* **84** (8), 4710-4711 (1986).

102. J. Simons,"Semiquantum expressions for electronically nonadiabatic electron ejection rates." *Journal of Physical Chemistry A* **102** (29), 6035-6042 (1998).

103. J. Simons,"An analytical model for vibrational non-Born-Oppenheimer induced electron ejection in molecular anions." *Journal of Chemical Physics* **117** (20), 9124-9132 (2002).

104. J. Simons,"Time-domain and tunneling pictures of nonadiabatic induced electron ejection in molecular anions." *Journal of Physical Chemistry A* **103** (47), 9408-9416 (1999).

8 Bibliography

P. K. Acharya, R. A. Kendall and J. Simons,"Vibration-Induced Electron Detachment in Molecular Anions." *Journal of the American Chemical Society* **106** (12), 3402-3407 (1984).

C. L. Adams, H. Schneider, K. M. Ervin and J. M. Weber,"Low-energy photoelectron imaging spectroscopy of nitromethane anions: Electron affinity, vibrational features, anisotropies and the dipole-bound state." *Journal of Chemical Physics* **130**, 074307-074301 - 074310 (2009).

C. L. Adams, H. Schneider and J. M. Weber,"Vibrational Autodetachment – Intramolecular Vibrational Relaxation Translated Into Electronic Motion." *Journal of Physical Chemistry A* **114**, 4017-4030 (2010).

C. L. Adams and J. M. Weber,"Photoelectron imaging spectroscopy of nitroethane anions." *J. Chem Phys.* **134** (24), 244301-244308 (2011).

J. K. Agbo, D. M. Leitner, E. M. Myshakin and K. D. Jordan,"Quantum energy flow and the kinetics of water shuttling between hydrogen bonding sites on trans-formanilide." *Journal of Chemical Physics* **127** (6) (2007).

E. Alizadeh, F. F. da Silva, F. Zappa, A. Mauracher, A. Probst, S. Denifl, A. Bacher, T. D. Mark, P. Limao-Vieira and P. Scheier,"Dissociative electron attachment to nitromethane." *International Journal of Mass Spectrometry* **271** (1-3), 15-21 (2008).

J. Assmann, M. Kling and B. Abel,"Watching photoinduced chemistry and molecular energy flow in solution in real time." *Angewandte Chemie-International Edition* **42** (20), 2226-2246 (2003).

A. D. Becke,"Density-Functional Thermochemistry .3. The Role of Exact Exchange." *Journal of Chemical Physics* **98** (7), 5648-5652 (1993).

R. S. Berry,"Ionization of Molecules at Low Energies." *Journal of Chemical Physics* **45** (4), 1228-& (1966).

S. J. Blanksby and G. B. Ellison,"Bond dissociation energies of organic molecules." *Accounts of Chemical Research* **36** (4), 255-263 (2003).

D. Boyall and K. L. Reid,"Modern studies of intramolecular vibrational energy redistribution." *Chemical Society Reviews* **26** (3), 223-232 (1997).

J. N. Bull, R. Maclagan and P. W. Harland,"On the Electron Affinity of Nitromethane (CH_3NO_2)." *Journal of Physical Chemistry A* **114** (10), 3622-3629 (2010).

R. Campargue,"Aerodynamic Separation Effect on Gas and Isotope Mixtures Induced by Invasion of Free Jet Shock Wave Structure." *Journal of Chemical Physics* **52** (4), 1795 (1970).

E. E. B. Campbell and R. D. Levine,"Delayed ionization and fragmentation en route to thermionic emission: Statistics and dynamics." *Annual Review of Physical Chemistry* **51**, 65-98 (2000).

B. K. Carpenter,"Nonstatistical dynamics in thermal reactions of polyatomic molecules." *Annual Review of Physical Chemistry* **56**, 57-89 (2005).

A. Chakraborty, D. Seth, P. Setua and N. Sarkar,"Dynamics of solvent and rotational relaxation of glycerol in the nanocavity of reverse micelles." *Journal of Physical Chemistry B* **110** (11), 5359-5366 (2006).

G. Chalasinski, R. A. Kendall, H. Taylor and J. Simons,"Propensity Rules for Vibration Rotation-Induced Electron Detachment of Diatomic Anions - Application to Nh--]Nh+E." *Journal of Physical Chemistry* **92** (11), 3086-3091 (1988).

P. Chen, in *Unimolecular and Bimolecular Reaction Dynamics*, edited by C.-Y. Ng, T. Baer and I. Powis (John Wiley & Sons, Chichester, 1994), pp. 371.

A. Chirokolava, D. S. Perry, O. V. Boyarkin, M. Schmid and T. R. Rizzo,"Rotational and torsional analysis of the OH-stretch third overtone in (CH_3OH)-C-13." *Journal of Molecular Spectroscopy* **211** (2), 221-227 (2002).

P. D. Chowdary and M. Gruebele,"Size and Energy Scaling of Nonstatistical Vibrational Quantum States." *Physical Review Letters* **101** (25) (2008).

T. N. Clasp and D. S. Perry,"Torsion-vibration coupling in methanol: The adiabatic approximation and intramolecular vibrational redistribution scaling." *Journal of Chemical Physics* **125** (10), art. no. 104313 (2006).

B. Climen, F. Pagliarulo, A. Ollagnier, B. Baguenard, B. Concina, M. A. Lebeault, F. Lepine and C. Bordas,"Threshold laws in delayed emission: an experimental approach." *European Physical Journal D* **43** (1-3), 85-89 (2007).

W. B. Clodius, R. M. Stehman and S. B. Woo,"Zero-Core-Contribution Calculation of a Polyatomic Photodetachment Cross-Section - NO_2." *Physical Review A* **28** (2), 760-765 (1983).

R. N. Compton, H. S. Carman, C. Desfrancois, H. Abdoul-Carmine, J. P. Schermann, J. H. Hendricks, S. A. Lyapustina and K. H. Bowen,"On the binding of electrons to nitromethane: Dipole and valence bound anions." *Journal of Chemical Physics* **105** (9), 3472-3478 (1996).

J. Cooper and R. N. Zare,"Angular Distribution of Photoelectrons." *Journal of Chemical Physics* **48** (2), 942-943 (1968).

B. Cretin, S. Gomes, N. Trannoy and P. Vairac, in *Microscale and Nanoscale Heat Transfer* (2007), Vol. 107, pp. 181-238.

F. F. Crim,"Vibrationally Mediated Photodissociation - Exploring Excited-State Surfaces and Controlling Decomposition Pathways." *Annual Review of Physical Chemistry* **44**, 397-428 (1993).

F. F. Crim,"Making energy count." *Science* **316** (5832), 1707-1708 (2007).

F. F. Crim,"Chemical dynamics of vibrationally excited molecules: Controlling reactions in gases and on surfaces." *Proceedings of the National Academy of Sciences of the United States of America* **105** (35), 12654-12661 (2008).

A. M. Desouza, D. Kaur and D. S. Perry,"Vibrational-State Mixing of Individual Rotational Levels in 1-Butyne near 3333 cm^{-1}." *Journal of Chemical Physics* **88** (8), 4569-4578 (1988).

B. C. Dian, G. G. Brown, K. O. Douglass, F. S. Rees, J. E. Johns, P. Nair, R. D. Suenram and B. H. Pate,"Conformational isomerization kinetics of pent-1-en-4-yne with 3,330 cm(-1) of internal energy measured by dynamic rotational spectroscopy." *Proceedings of the National Academy of Sciences of the United States of America* **105** (35), 12696-12700 (2008).

V. Dribinski, A. Ossadtchi, V. A. Mandelshtam and H. Reisler,"Reconstruction of abel-transformable images: The Gaussian basis-set expansion abel transform method." *Review of Scientific Instruments* **73** (7), 2634-2642 (2002).

F. Duschinsky,"The importance of the electron spectrum in multi atomic molecules. concerning the Franck-Condon principle." *Acta Physicochimica URSS* **7** (4), 551-566 (1937).

A. L. L. East and L. Radom,"Ab initio statistical thermodynamical models for the computation of third-law entropies." *Journal of Chemical Physics* **106** (16), 6655-6674 (1997).

T. Ebata, A. Iwasaki and N. Mikami,"Vibrational relaxation of OH and OD stretching vibrations of phenol and its clusters studied by IR-UV pump-probe spectroscopy." *Journal of Physical Chemistry A* **104** (34), 7974-7979 (2000).

J. Ekkers, A. Bauder and H. H. Günthard,"Microwave spectrum and internal rotation of nitroethane." *Chemical Physics Letters* **22** (2), 249-252 (1973).

J. H. D. Eland,"Molecular Photoelectron Spectroscopy." *Journal of Physics E-Scientific Instruments* **11** (10), 969-977 (1978).

C. G. Elles and F. F. Crim,"Connecting chemical dynamics in gases and liquids." *Annual Review of Physical Chemistry* **57**, 273-302 (2006).

B. M. Elliott, L. R. McCunn and M. A. Johnson,"Photoelectron imaging study of vibrationally mediated electron autodetachment in the type I isomer of the water hexamer anion." *Chemical Physics Letters* **467** (1-3), 32-36 (2008).

P. C. Engelking,"Strong Electron-Dipole Coupling in Photodetachment of Molecular Negative-Ions - Anomalous Rotational Thresholds." *Physical Review A* **26** (2), 740-745 (1982).

A. Eppink and D. H. Parker,"Velocity map imaging of ions and electrons using electrostatic lenses: Application in photoelectron and photofragment ion imaging of molecular oxygen." *Review of Scientific Instruments* **68** (9), 3477-3484 (1997).

K. M. Ervin, J. Ho and W. C. Lineberger,"Ultraviolet Photoelectron Spectrum of NO_2." *Journal of Physical Chemistry* **92** (19), 5405-5412 (1988).

K. M. Ervin and W. C. Lineberger, in *Advances in Gas Phase Ion Chemistry*, edited by N. G. Adams and L. M. Babcock (JAI, Greenwich, CT, 1992), pp. 121.

K. M. Ervin, T. M. Ramond, G. E. Davico, R. L. Schwartz, S. M. Casey and W. C. Lineberger,"Naphthyl radical: Negative ion photoelectron spectroscopy, Franck-Condon simulation, and thermochemistry." *Journal of Physical Chemistry A* **105** (48), 10822-10831 (2001).

K. M. Ervin, I. Anusiewicz, P. Skurski, J. Simons and W. C. Lineberger,"The Only Stable State of O_2^- Is the X $^2\Pi_g$ Ground State and It (Still!) Has an Adiabatic Electron Detachment Energy of 0.45 eV." *The Journal of Physical Chemistry A* **107** (41), 8521-8529 (2003).

K. M. Ervin, FCFGaus03, University of Reno, Nevada, 2008.

K. M. Ervin, PESCAL, University of Nevada, Reno, 2008.

S. N. Eustis, D. Radisic, K. H. Bowen, R. A. Bachorz, M. Haranczyk, G. K. Schenter and M. Gutowski,"Electron-driven acid-base chemistry: Proton transfer from hydrogen chloride to ammonia." *Science* **319** (5865), 936-939 (2008).

I. I. Fabrikant and H. Hotop,"Low-energy behavior of exothermic dissociative electron attachment." *Physical Review A* **6302** (2) (2001).

M. Farnik, S. Davis and D. J. Nesbitt,"High-resolution IR studies of hydrogen bonded clusters: Large amplitude dynamics in $(HCl)_n$." *Faraday Discussions* **118**, 63-78 (2001).

R. F. Foster, W. Tumas and J. I. Brauman,"Unimolecular Decomposition and Vibrationally Induced Electron Autodetachment of Acetone Enolate Ion." *Journal of Chemical Physics* **79** (9), 4644-4646 (1983).

G. T. Fraser, B. H. Pate, G. A. Bethardy and D. S. Perry,"Frequency-Resolved Measurement of Fast Intramolecular Vibrational-Energy Redistribution (IVR) in the O-H Stretch of Gas-Phase Ethanol." *Chemical Physics* **175** (1), 223-236 (1993).

M. J. Frisch, G. W. Trucks, H. B. Schlegel, G. E. Scuseria, M. A. Robb, J. R. Cheeseman, J. A. Montgomery, J. Vreven, T. , K. N. Kudin, J. C. Burant, J. M. Millam, S. S. Iyengar, J. Tomasi, V. Barone, B. Mennucci, M. Cossi, G. Scalmani, N. Rega, G. A. Petersson, H. Nakatsuji, M. Hada, M. Ehara, K. Toyota, R. Fukuda, J. Hasegawa, M. Ishida, T. Nakajima, Y. Honda, O. Kitao, H. Nakai, M. Klene, X. Li, J. E. Knox, H. P. Hratchian, J.

B. Cross, V. Bakken, C. Adamo, J. Jaramillo, R. Gomperts, R. E. Stratmann, O. Yazyev, A. J. Austin, R. Cammi, C. Pomelli, J. W. Ochterski, P. Y. Ayala, K. Morokuma, G. A. Voth, P. Salvador, J. J. Dannenberg, V. G. Zakrzewski, S. Dapprich, A. D. Daniels, M. C. Strain, O. Farkas, D. K. Malick, A. D. Rabuck, K. Raghavachari, J. B. Foresman, J. V. Ortiz, Q. Cui, A. G. Baboul, S. Clifford, J. Cioslowski, B. B. Stefanov, G. Liu, A. Liashenko, P. Piskorz, I. Komaromi, R. L. Martin, D. J. Fox, T. Keith, M. A. Al-Laham, C. Y. Peng, A. Nanayakkara, M. Challacombe, P. M. W. Gill, B. Johnson, W. Chen, M. W. Wong, C. Gonzalez and J. A. Pople, Gaussian 03, Wallingford CT, 2004.

J. E. Gambogi, K. K. Lehmann, B. H. Pate, G. Scoles and X. M. Yang,"The Rate of Intramolecular Vibrational-Energy Relaxation of the Fundamental C-H Stretch in $(CF_3)_3C$-CC-H." *Journal of Chemical Physics* **98** (2), 1748-1749 (1993).

J. E. Gambogi, R. Z. Pearson, X. M. Yang, K. K. Lehmann and G. Scoles,"Intramolecular Vibrational Dynamics of Diacetylene and Diacetylene-D(1) Via Eigenstate-Resolved Overtone Spectroscopy." *Chemical Physics* **190** (2-3), 191-205 (1995).

E. Garand, J. Zhou, D. E. Manolopoulos, M. H. Alexander and D. M. Neumark,"Nonadiabatic interactions in the $Cl+H_2$reaction probed by ClH_2^- and ClD_2^- photoelectron imaging." *Science* **319** (5859), 72-75 (2008).

H. K. Gerardi, K. J. Breen, T. L. Guasco, G. H. Weddle, G. H. Gardenier, J. E. Laaser and M. A. Johnson,"Survey of Ar-Tagged Predissociation and Vibrationally Mediated Photodetachment Spectroscopies of the Vinylidene Anion, $C_2H_2^-$." *Journal of Physical Chemistry A* **114** (3), 1592-1601 (2010).

D. Gerbasi, A. S. Sanz, P. S. Christopher, M. Shapiro and P. Brumer,"Overlapping resonances in the control of intramolecular vibrational redistribution." *Journal of Chemical Physics* **126** (12) (2007).

K. Giese, M. Petkovic, H. Naundorf and O. Kuhn,"Multidimensional quantum dynamics and infrared spectroscopy of hydrogen bonds." *Physics Reports-Review Section of Physics Letters* **430** (4), 211-276 (2006).

D. J. Goebbert, D. Khuseynov and A. Sanov,"Photodissociation of nitromethane cluster anions." *Journal of Chemical Physics* **133** (8) (2010).

D. Gorse, D. Cavagnat, M. Pesquer and C. Lapouge,"Theoretical and Spectroscopic Study of Asymmetric Methyl Rotor Dynamics in Gaseous Partially Deuterated Nitromethanes." *Journal of Physical Chemistry* **97** (17), 4262-4269 (1993).

D. Green, S. Hammond, J. Keske and B. H. Pate,"Intramolecular vibrational energy redistribution and conformational isomerization in vibrationally excited 2-fluoroethanol: High-resolution, microwave-infrared double-resonance spectroscopy investigation of the asymmetric -CH_2(F) stretch near 2980 cm^{-1}." *Journal of Chemical Physics* **110** (4), 1979-1989 (1999).

C. H. Greene,"Manifestation of Dynamically Unfavored Transitions in the Angular-Distribution of Photofragments." *Physical Review Letters* **44** (13), 869-871 (1980).

P. Groner, R. Meyer, A. Günter, H. Kühne and H. H. Günthard,"Far Infrared Spectrum of Nitroethane." *Chemical Physics* **5** (1), 136-141 (1974).

P. Groner, R. Meyer and H. H. Günthard,"Matrix and gas infrared spectra of nitroethane isotopic species." *Chemical Physics* **11** (1), 63-85 (1975).

M. Gruebele and R. Bigwood,"Molecular vibrational energy flow: beyond the Golden Rule." *International Reviews in Physical Chemistry* **17** (2), 91-145 (1998).

M. Gruebele and P. G. Wolynes,"Vibrational energy flow and chemical reactions." *Accounts of Chemical Research* **37** (4), 261-267 (2004).

M. Gutowski, P. Skurski, A. I. Boldyrev, J. Simons and K. D. Jordan,"Contribution of electron correlation to the stability of dipole-bound anionic states." *Physical Review A* **54** (3), 1906 (1996).

G. L. Gutsev and R. J. Bartlett,"A theoretical study of the valence- and dipole-bound states of the nitromethane anion." *Journal of Chemical Physics* **105** (19), 8785-8792 (1996).

G. L. Gutsev, P. Jena and R. J. Bartlett,"Thermodynamical stability of CH_3ONO and CH_3ONO^-: A coupled-cluster and Hartree-Fock-density-functional-theory study." *Journal of Chemical Physics* **110** (1), 403-411 (1999).

J. L. Hall and M. W. Siegel,"Angular Dependence of the Laser Photodetachment of the Negative Ions of Carbon, Ozygen, and Hydrogen." *Journal of Chemical Physics* **48** (2), 943 (1968).

C. C. Han and J. I. Brauman,"Dissociation and Vibration-Induced Electron Autodetachment of 3-Fluoronitrobenzene Radical-Anion by Infrared Multiple Photon Excitation." *Journal of Physical Chemistry* **94** (9), 3403-3415 (1990).

D. C. Harris, & Bertolucci, M.D., *Symmetry and Spectroscopy: An Introduction to Vibrational and Electronic Spectroscopy*. (New York: Oxford University Press, 1978).

M. L. Hause, Y. H. Yoon, A. S. Case and F. F. Crim,"Dynamics at conical intersections: The influence of O-H stretching vibrations on the photodissociation of phenol." *Journal of Chemical Physics* **128** (10) (2008).

W. M. Haynes, *CRC Handbook of Chemistry and Physics*, 91 ed. (CRC Press, Boca Raton, 2010).

I. V. Hertel and W. Radloff,"Ultrafast dynamics in isolated molecules and molecular clusters." *Reports on Progress in Physics* **69** (6), 1897-2003 (2006).

X. Y. Hong, S. Chen and D. D. Dlott,"Ultrafast Mode-Specific Intermolecular Vibrational-Energy Transfer to Liquid Nitromethane." *Journal of Physical Chemistry* **99** (22), 9102-9109 (1995).

H. Hotop and W. C. Lineberger,"Binding-Energies in Atomic Negative-Ions .2." *Journal of Physical and Chemical Reference Data* **14** (3), 731-750 (1985).

H. Hotop, M. W. Ruf, M. Allan and Fabrikant, II, in *Advances in Atomic Molecular, and Optical Physics, Vol 49* (2003), Vol. 49, pp. 85-216.

Y. J. Hu, B. Hadas, M. Davidovitz, B. Balta and C. Lifshitz,"Does IVR take place prior to peptide ion dissociation?" *J. Phys. Chem. A* **107** (34), 6507-6514 (2003).

T. Ichino, S. W. Wren, K. M. Vogelhuber, A. J. Gianola, W. C. Lineberger and J. F. Stanton,"The vibronic level structure of the cyclopentadienyl radical." *Journal of Chemical Physics* **129** (8) (2008).

K. C. Ingham and Strickle.Sj,"Hindered Rotation in Ground and Excited Electronic States of Ortho-Xylene." *Journal of Chemical Physics* **53** (11), 4313-& (1970).

S. S. Iyengar and J. Jakowski,"Quantum wave packet ab initio molecular dynamics: An approach to study quantum dynamics in large systems." *Journal of Chemical Physics* **122** (11) (2005).

C. Q. Jiao, C. A. DeJoseph and A. Garscadden,"Formation of positive and negative ions in CH3NO2." *Journal of Physical Chemistry A* **107** (42), 9040-9044 (2003).

M. A. Johnson and W. C. Lineberger, in *Techniques for the Study of Gas-Phase Ion Molecule Reactions*, edited by J. M. Farrar and W. Saunders (Wiley, New York, 1988), pp. 591.

M. Kayano, T. Ebata, Y. Yamada and N. Mikami,"Picosecond IR-UV pump-probe spectroscopic study of the dynamics of the vibrational relaxation of jet-cooled phenol. II. Intracluster vibrational energy redistribution of the OH stretching vibration of hydrogen-bonded clusters." *Journal of Chemical Physics* **120** (16), 7410-7417 (2004).

J. C. Keske and B. H. Pate,"Decoding the dynamical information embedded in highly mixed quantum states." *Annual Review of Physical Chemistry* **51**, 323-353 (2000).

C. E. Klots,"Evaporative Cooling." *Journal of Chemical Physics* **83** (11), 5854-5860 (1985).

C. E. Klots,"The evaporative ensemble." *Zeitschrift für Physik D Atoms, Molecules and Clusters* **5** (1), 83-89 (1987).

R. Krishnan, J. S. Binkley, R. Seeger and J. A. Pople,"Self-Consistent Molecular-Orbital Methods .20. Basis Set for Correlated Wave-Functions." *Journal of Chemical Physics* **72** (1), 650-654 (1980).

T. Kulp, R. S. Ruoff and J. D. McDonald,"Limits on the Lifetimes of Intramolecular Rovibrational Relaxation." *Journal of Chemical Physics* **82** (5), 2175-2179 (1985).

T. J. Kulp, H. L. Kim and J. D. McDonald,"Rotational Effects on Intramolecular Vibrational-Relaxation in Dimethyl Ether and 1,4 Dioxane." *Journal of Chemical Physics* **85** (1), 211-220 (1986).

F. Lecomte, S. Carles, C. Desfrancois and M. A. Johnson,"Dipole bound and valence state coupling in argon-solvated nitromethane anions." *Journal of Chemical Physics* **113** (24), 10973-10977 (2000).

C. T. Lee, W. T. Yang and R. G. Parr,"Development of the Colle-Salvetti Correlation-Energy Formula into a Functional of the Electron-Density." *Physical Review B* **37** (2), 785-789 (1988).

K. K. Lehmann, B. H. Pate and G. Scoles,"Statistical Intramolecular Vibrational-Relaxation and Its Hindrance - the Fundamentals of $(CH_3)_3C$-C=CH and $(CH_3)_3Si$-C=CH." *Journal of Chemical Physics* **93** (3), 2152-2153 (1990).

K. K. Lehmann, G. Scoles and B. H. Pate,"Intramolecular Dynamics from Eigenstate-Resolved Infrared-Spectra." *Annual Review of Physical Chemistry* **45**, 241-274 (1994).

D. M. Leitner, M. Havenith and M. Gruebele,"Biomolecule large-amplitude motion and solvation dynamics: modelling and probes from THz to X-rays." *International Reviews in Physical Chemistry* **25** (4), 553-582 (2006).

D. M. Leitner and P. G. Wolynes,"Quantum theory of enhanced unimolecular reaction rates below the ergodicity threshold." *Chemical Physics* **329** (1-3), 163-167 (2006).

D. M. Leitner and M. Gruebele,"Quantum model of restricted vibrational energy flow on the way to the transition state in unimolecular reactions." *Molecular Physics* **106** (2-4), 433-442 (2008).

L. Lespade, D. Cavagnat and P. Asselin,"A new way for IVR induced by fast internal motion as revealed by a jet-cooled spectrum of cyclopentene." *Journal of Physical Chemistry A* **106** (41), 9451-9459 (2002).

W. Li, S. D. Chambreau, S. A. Lahankar and A. G. Suits,"Megapixel ion imaging with standard video." *Review of Scientific Instruments* **76** (6) (2005).

R. Mabbs, E. R. Grumbling, K. Pichugin and A. Sanov,"Photoelectron imaging: an experimental window into electronic structure." *Chemical Society Reviews* **38** (8), 2169-2177 (2009).

H. W. W. Massey, *Negative Ions*. (Cambridge Press, Cambridge, 1976).

J. D. McDonald,"Creation and Disposal of Vibrational Energy in Polyatomic-Molecules." *Annual Review of Physical Chemistry* **30**, 29-50 (1979).

A. McIlroy and D. J. Nesbitt,"High-Resolution, Slit Jet Infrared-Spectroscopy of Hydrocarbons - Quantum State Specific Mode Mixing in CH Stretch-Excited Propyne." *Journal of Chemical Physics* **91** (1), 104-113 (1989).

A. McIlroy and D. J. Nesbitt,"Large-Amplitude Skeletal Isomerization as a Promoter of Intramolecular Vibrational-Relaxation in Ch Stretch Excited Hydrocarbons." *Journal of Chemical Physics* **101** (5), 3421-3435 (1994).

A. McIlroy, D. J. Nesbitt, E. R. T. Kerstel, B. H. Pate, K. K. Lehmann and G. Scoles,"Sub-Doppler, Infrared-Laser Spectroscopy of the Propyne $2\nu_1$ Band - Evidence of Z-Axis Coriolis Dominated Intramolecular State Mixing in the Acetylenic CH Stretch Overtone." *Journal of Chemical Physics* **100** (4), 2596-2611 (1994).

A. D. McLean and G. S. Chandler,"Contracted Gaussian-Basis Sets for Molecular Calculations .1. 2nd Row Atoms, Z=11-18." *Journal of Chemical Physics* **72** (10), 5639-5648 (1980).

D. A. McWhorter, E. Hudspeth and B. H. Pate,"The rotational spectra of single molecular eigenstates of 2-fluoroethanol: Measurement of the conformational isomerization rate at 2980 cm^{-1}." *Journal of Chemical Physics* **110** (4), 2000-2009 (1999).

F. K. Meyer, J. M. Jasinski, R. N. Rosenfeld and J. I. Brauman,"Infrared Multi-Photon Photodetachment of Negative-Ions in the Gas-Phase." *Journal of the American Chemical Society* **104** (3), 663-667 (1982).

T. K. Minton, H. L. Kim, S. A. Reid and J. D. McDonald,"High-Resolution Infrared-Laser Induced Fluorescence Study of State Mixing in Methyl Formate." *Journal of Chemical Physics* **89** (10), 6550-6552 (1988).

A. Modelli and M. Venuti,"Empty level structure and dissociative electron attachment in gas-phase nitro derivatives." *International Journal of Mass Spectrometry* **205** (1-3), 7-16 (2001).

A. S. Mullin, K. K. Murray, C. P. Schulz, D. M. Szaflarski and W. C. Lineberger,"Autodetachment Spectroscopy of Vibrationally Excited Acetaldehyde Enolate Anion, Ch2cho." *Chemical Physics* **166** (1-2), 207-213 (1992).

D. J. Nesbitt and R. W. Field,"Vibrational energy flow in highly excited molecules: Role of intramolecular vibrational redistribution." *Journal of Physical Chemistry* **100** (31), 12735-12756 (1996).

D. M. Neumark, K. R. Lykke, T. Andersen and W. C. Lineberger,"Infrared-Spectrum and Autodetachment Dynamics of NH^-." *Journal of Chemical Physics* **83** (9), 4364-4373 (1985).

P. Ortoleva and S. S. Iyengar,"Multiscale theory of collective and quasiparticle modes in quantum nanosystems." *Journal of Chemical Physics* **128** (16) (2008).

C. Pan, A. F. Starace and C. H. Greene,"Parallels between High Doubly-Excited State Spectra in H^- and Li^- Photodetachment." *Journal of Physics B-Atomic Molecular and Optical Physics* **27** (8), L137-L142 (1994).

Y. Pang, J. C. Deak, W. T. Huang, A. Lagutchev, A. Pakoulev, J. E. Patterson, T. D. Sechler, Z. H. Wang and D. D. Dlott,"Vibrational energy in molecules probed with high time and space resolution." *International Reviews in Physical Chemistry* **26** (1), 223-248 (2007).

D. H. Parker and A. Eppink,"Photoelectron and photofragment velocity map imaging of state-selected molecular oxygen dissociation/ionization dynamics." *Journal of Chemical Physics* **107** (7), 2357-2362 (1997).

C. S. Parmenter and B. M. Stone,"The Methyl Rotor as an Accelerating Functional-Group for IVR." *Journal of Chemical Physics* **84** (8), 4710-4711 (1986).

B. H. Pate, K. K. Lehmann and G. Scoles,"The Onset of Intramolecular Vibrational-Energy Redistribution and Its Intermediate Case - the ν_1 and $2\nu_1$ Molecular-Beam, Optothermal Spectra of Trifluoropropyne." *Journal of Chemical Physics* **95** (6), 3891-3916 (1991).

D. S. Perry,"Random Matrix Treatment of Intramolecular Vibrational Redistribution .1. Methodology and Anharmonic Interactions in 1-Butyne." *Journal of Chemical Physics* **98** (9), 6665-6677 (1993).

J. A. Pople, M. Head-Gordon and K. Raghavachari,"Quadratic Configuration-Interaction - a General Technique for Determining Electron Correlation Energies." *Journal of Chemical Physics* **87** (10), 5968-5975 (1987).

K. J. Reed, A. H. Zimmerman, H. C. Andersen and J. I. Brauman,"Cross-Sections for Photodetachment of Electrons from Negative-Ions near Threshold." *Journal of Chemical Physics* **64** (4), 1368-1375 (1976).

O. W. Richardson, *The Emission of Electricity from Hot Bodies*. (Longmans Green and Company, London, 1921).

W. H. Robertson, J. A. Kelley and M. A. Johnson,"A pulsed supersonic entrainment reactor for the rational preparation of cold ionic complexes." *Review of Scientific Instruments* **71** (12), 4431-4434 (2000).

R. N. Rosenfeld, J. M. Jasinski and J. I. Brauman,"Infrared Multi-Photon Electron Detachment from the Benzyl Anion." *Journal of Chemical Physics* **71** (2), 1030-1031 (1979).

W. Sailer, A. Pelc, S. Matejcik, E. Illenberger, P. Scheier and T. D. Mark,"Dissociative electron attachment study to nitromethane." *Journal of Chemical Physics* **117** (17), 7989-7994 (2002).

A. Sanov and W. C. Lineberger,"Dynamics of cluster anions: a detailed look at condensed-phase interactions." *Physchemcomm*, 165-177 (2002).

A. Sanov and W. C. Lineberger,"Cluster anions: Structure, interactions, and dynamics in the sub-nanoscale regime." *Physical Chemistry Chemical Physics* **6** (9), 2018-2032 (2004).

H. Schneider, K. M. Vogelhuber, F. Schinle, J. F. Stanton and J. M. Weber,"Vibrational spectroscopy of nitroalkane chains using electron autodetachment and Ar predissociation." *Journal of Physical Chemistry A* **112** (33), 7498-7506 (2008).

S. A. Schofield and P. G. Wolynes,"Rate Theory and Quantum Energy-Flow in Molecules - Modeling the Effects of Anisotropic Diffusion and of Dephasing." *Journal of Physical Chemistry* **99** (9), 2753-2763 (1995).

T. E. Sharp and H. M. Rosenstock,"Franck-Condon Factors for Polyatomic Molecules." *Journal of Chemical Physics* **41** (11), 3453-3463 (1964).

S. Shigeto, Y. Pang, Y. Fang and D. D. Dlott,"Vibrational relaxation of normal and deuterated liquid nitromethane." *Journal of Physical Chemistry B* **112** (2), 232-241 (2008).

M. I. Shilina, V. M. Senyavin, G. M. Kuramshina, V. V. Smirnov and Y. A. Pentin,"Vibrational spectra, assignment, conformational stability and ab Initio/DFT calculations for 1-nitropropane." *Structural Chemistry* **14** (6), 559-573 (2003).

M. W. Siegel, R. J. Celotta, J. L. Hall, J. Levine and R. A. Bennett,"Molecular Photodetachment Spectrometry. I. The Electron Affinity of Nitric Oxide and the Molecular Constants of NO." *Physical Review A* **6** (2), 607 (1972).

J. Simons,"Propensity Rules for Vibration-Induced Electron Detachment of Anions." *Journal of the American Chemical Society* **103** (14), 3971-3976 (1981).

J. Simons,"Semiquantum expressions for electronically nonadiabatic electron ejection rates." *Journal of Physical Chemistry A* **102** (29), 6035-6042 (1998).

J. Simons,"Time-domain and tunneling pictures of nonadiabatic induced electron ejection in molecular anions." *Journal of Physical Chemistry A* **103** (47), 9408-9416 (1999).

J. Simons,"An analytical model for vibrational non-Born-Oppenheimer induced electron ejection in molecular anions." *Journal of Chemical Physics* **117** (20), 9124-9132 (2002).

D. C. Smith, C.-Y. Pan and J. R. Nielsen,"Vibrational Spectra of the Four Lowest Nitroparaffins." *The Journal of Chemical Physics* **18** (5), 706-712 (1950).

J. R. Smith, J. B. Kim and W. C. Lineberger,"High-resolution threshold photodetachment spectroscopy of OH^-." *Physical Review A* **55** (3), 2036-2043 (1997).

T. Sommerfeld,"Coupling between dipole-bound and valence states: the nitromethane anion." *Physical Chemistry Chemical Physics* **4** (12), 2511-2516 (2002).

L. H. Spangler and D. W. Pratt,"Laser-Induced Phosphorescence Spectroscopy in Supersonic Jets - the Lowest Triplet-States of Glyoxal, Methylglyoxal, and Biacetyl." *Journal of Chemical Physics* **84** (9), 4789-4796 (1986).

L. H. Spangler,"Structural information from methyl internal rotation spectroscopy." *Annual Review of Physical Chemistry* **48**, 481-510 (1997).

R. M. Stehman and S. B. Woo,"Zero-Core-Contribution Calculation of Photodetachment Cross-Sections of O_2^- and S_2." *Physical Review A* **23** (6), 2866-2876 (1981).

G. M. Stewart and J. D. McDonald,"Intramolecular Vibrational-Relaxation from C-H Stretch Fundamentals." *Journal of Chemical Physics* **78** (6), 3907-3915 (1983).

S. T. Stokes, K. H. Bowen, T. Sommerfeld, S. Ard, N. Mirsaleh-Kohan, J. D. Steill and R. N. Compton,"Negative ions of nitroethane and its clusters." *Journal of Chemical Physics* **129** (6) (2008).

A. Stolow,"Time-resolved photoelectron spectroscopy: Non-adiabatic dynamics in polyatomic molecules." *International Reviews in Physical Chemistry* **22** (2), 377-405 (2003).

L. Suess, R. Parthasarathy and F. B. Dunning,"Rydberg electron transfer to CH_3NO_2: Lifetimes and characteristics of the product $CH_3NO_2^-$ ions." *Journal of Chemical Physics* **119** (18), 9532-9537 (2003).

M. A. Suhm, J. T. Farrell, S. H. Ashworth and D. J. Nesbitt,"High-Resolution Infrared-Spectroscopy of Df Trimer - a Cyclic Ground-State Structure and DF Stretch Induced Intramolecular Vibrational Coupling." *Journal of Chemical Physics* **98** (7), 5985-5989 (1993).

I. Sumner and S. S. Iyengar,"Quantum wavepacket ab initio molecular dynamics: An approach for computing dynamically averaged vibrational spectra including critical nuclear quantum effects." *Journal of Physical Chemistry A* **111** (41), 10313-10324 (2007).

I. Sumner and S. S. Iyengar,"Combining quantum wavepacket ab initio molecular dynamics with QM/MM and QM/QM techniques: Implementation blending ONIOM and empirical valence bond theory." *Journal of Chemical Physics* **129** (5) (2008).

E. Surber and A. Sanov,"Photoelectron imaging spectroscopy of molecular and cluster anions: CS_2^- and $OCS^-(H_2O)_{1,2}$." *Journal of Chemical Physics* **116** (14), 5921-5924 (2002).

J. T. H. Dunning,"Gaussian basis sets for use in correlated molecular calculations. I. The atoms boron through neon and hydrogen." *The Journal of Chemical Physics* **90** (2), 1007-1023 (1989).

U. S. Tasic and C. S. Parmenter,"Test of a chemical timing method for measuring absolute vibrational relaxation rate constants for S_1 p-difluorobenzene." *Journal of Physical Chemistry B* **109** (17), 8297-8303 (2005).

W. Tumas, K. E. Salomon and J. I. Brauman,"Dimethylsilanone Enolate Anion - Competitive Fragmentation and Electron Autodetachment of Vibrationally Excited Siloxide Anions in the Gas-Phase." *Journal of the American Chemical Society* **108** (10), 2541-2546 (1986).

H. Ueba,"Vibrational relaxation and pump-probe spectroscopies of adsorbates on solid surfaces." *Progress in Surface Science* **55** (2), 115-179 (1997).

I. C. Walker and M. A. D. Fluendy,"Spectroscopy and dynamics of nitromethane (CH3NO2) and its anionic states." *International Journal of Mass Spectrometry* **205** (1-3), 171-182 (2001).

X. L. Wang and D. S. Perry,"An internal coordinate model of coupling between the torsion and C-H vibrations in methanol." *Journal of Chemical Physics* **109** (24), 10795-10805 (1998).

Z. H. Wang, J. A. Carter, A. Lagutchev, Y. K. Koh, N. H. Seong, D. G. Cahill and D. D. Dlott,"Ultrafast flash thermal conductance of molecular chains." *Science* **317** (5839), 787-790 (2007).

Z. H. Wang, Y. S. Pang and D. D. Dlott,"Hydrogen-bond disruption by vibrational excitations in water." *Journal of Physical Chemistry A* **111** (17), 3196-3208 (2007).

J. M. Weber, W. H. Robertson and M. A. Johnson,"Argon predissociation and electron autodetachment spectroscopy of size-selected $CH_3NO_2^-\cdot Ar_n$ clusters." *Journal of Chemical Physics* **115** (23), 10718-10723 (2001).

D. Weidinger, M. F. Engel and M. Gruebele,"Freezing Vibrational Energy Flow: A Fitness Function for Interchangeable Computational and Experimental Control." *Journal of Physical Chemistry A* **113** (16), 4184-4191 (2009).

P. G. Wenthold, D. A. Hrovat, W. T. Borden and W. C. Lineberger,"Transition-state spectroscopy of cyclooctatetraene." *Science* **272** (5267), 1456-1459 (1996).

P. G. Wenthold and W. C. Lineberger,"Negative ion photoelectron spectroscopy studies of organic reactive intermediates." *Accounts of Chemical Research* **32** (7), 597-604 (1999).

C. T. Wickham-Jones, K. M. Ervin, G. B. Ellison and W. C. Lineberger,"NH_2 Electron-Affinity." *Journal of Chemical Physics* **91** (4), 2762-2763 (1989).

C. A. Wight and J. L. Beauchamp,"Infrared-Spectra of Gas-Phase Ions and Their Use in Elucidating Reaction-Mechanisms - Identification of $C_7H_7^-$ Structural Isomers by Multi-Photon Electron Detachment Using a Low-Power Infrared-Laser." *Journal of the American Chemical Society* **103** (21), 6499-6501 (1981).

C. A. Wight and J. L. Beauchamp,"Multiphoton Electron Detachment Studies of $C_7H_7^-$ Using a Low-Power Infrared-Laser - Competition of Radiative and Collisional Relaxation with Vibrational-Excitation." *Chemical Physics* **134** (2-3), 375-384 (1989).

C. A. Wight and J. L. Beauchamp,"Infrared-Spectra of Butenyl Anions - Multiphoton Electron Detachment as a Photochemical Probe of Isomeric Structures of Gas-Phase Anions." *International Journal of Mass Spectrometry and Ion Processes* **100**, 445-455 (1990).

E. P. Wigner,"On the Behavior of Cross Sections near Thresholds." *Physical Review* **73** (9), 1002-1009 (1948).

W. C. Wiley and I. H. McLaren,"Time-of-Flight Mass Spectrometer with Improved Resolution." *Review of Scientific Instruments* **26** (12), 1150-1157 (1955).

V. Wong and M. Gruebele,"How does vibrational energy flow fill the molecular state space?" *Journal of Physical Chemistry A* **103** (49), 10083-10092 (1999).

Y. Yamada, T. Ebata, M. Kayano and N. Mikami,"Picosecond IR-UV pump-probe spectroscopic study of the dynamics of the vibrational relaxation of jet-cooled phenol. I. Intramolecular vibrational energy redistribution of the OH and CH stretching vibrations of bare phenol." *Journal of Chemical Physics* **120** (16), 7400-7409 (2004).

Y. Yamada, N. Mikami and T. Ebata,"Real-time detection of doorway states in the intramolecular vibrational energy redistribution of the OH/OD stretch vibration of phenol." *Journal of Chemical Physics* **121** (23), 11530-11534 (2004).

Y. Yamada, J. Okano, N. Mikami and T. Ebata,"Picosecond IR-UV pump-probe spectroscopic study on the intramolecular vibrational energy redistribution of NH_2 and CH stretching vibrations of jet-cooled aniline." *Journal of Chemical Physics* **123** (12) (2005).

Y. Yamada, M. Kayano, N. Mikami and T. Ebata,"Picosecond IR-UV pump-probe study on the vibrational relaxation of phenol-ethylene hydrogen-bonded cluster: Difference of relaxation route/rate between the donor and the acceptor site excitations." *Journal of Physical Chemistry A* **110** (19), 6250-6255 (2006).

Y. Yamada, Y. Katsumoto and T. Ebata,"Picosecond IR-UV pump-probe spectroscopic study on the vibrational energy flow in isolated molecules and clusters." *Physical Chemistry Chemical Physics* **9** (10), 1170-1185 (2007).

R. Yamamoto, S. Ishikawa, T. Ebata and N. Mikami,"Vibrational spectra and relaxation of benzonitrile and its clusters using time-resolved stimulated Raman-UV double resonance spectroscopy." *Journal of Raman Spectroscopy* **31** (4), 295-304 (2000).

C. N. Yang,"On the Angular Distribution in Nuclear Reactions and Coincidence Measurements." *Phys. Rev.* **74** (7), 764-772 (1948).

K. Yokoyama, G. W. Leach, J. B. Kim and W. C. Lineberger,"Autodetachment spectroscopy and dynamics of dipole bound states of negative ions: $^2A_1$-$^2B_1$ transitions of H_2CCC^-." *Journal of Chemical Physics* **105** (24), 10696-10705 (1996).

H. S. Yoo, M. J. DeWitt and B. H. Pate,"Vibrational dynamics of terminal acetylenes: II. Pathway for vibrational relaxation in gas and solution." *Journal of Physical Chemistry A* **108** (8), 1365-1379 (2004).

H. S. Yoo, M. J. DeWitt and B. H. Pate,"Vibrational dynamics of terminal acetylenes: I. Comparison of the intramolecular vibrational energy redistribution rate of gases and the total relaxation rate of dilute solutions at room temperature." *Journal of Physical Chemistry A* **108** (8), 1348-1364 (2004).

H. S. Yoo, D. A. McWhorter and B. H. Pate,"Vibrational dynamics of terminal acetylenes: III. Comparison of the acetylenic C-H stretch intramolecular vibrational-energy redistribution rates in ultracold molecular beams, room-temperature gases, and room-temperature dilute solutions." *Journal of Physical Chemistry A* **108** (8), 1380-1387 (2004).